Study on Diagnostic Techniques for Detecting Degradation of Underground Transmission Cables using Chemical Analysis Methods

November 2018

杉　本　　修

Table of Contents

Chapter 1 Introduction

1.1 Background of this study

1.1.1 Situation of underground transmission cables [1]

Underground power transmission cables used to carry more than 66 kV in Japan are mainly of two types: cross-linked polyethylene insulated vinyl sheath cable (CV Cable) and oil-filled cable (OF cable). The total length of the cables was approximately 17,790 km･cct as of the end of fiscal year 2010. The length of CV cables was approximately 13,170 km･cct, and nearly 74 % of the span. The length of OF cables was approximately 4,620 km･cct, and nearly 26 % of the span.

CV cables were introduced in the 1970s and have become mainstream after the 1990s. The use of OF cables increased until the 1980s but has been decreasing since 2000. However, OF cables designed to carry 110 kV or more are still mainstream.

In addition, CV cables exceeding 30 years of design life are approximately 4 % (490 km･cct) of the span, and OF cables that exceed are approximately 62 % (2,380 km･cct) of the span. Therefore, the increase in aged CV cables exceeding 30 years can be assumed in future, and most OF cables are aged cables exceeding 30 years.

1.1.2 Causes and states of cable accidents

Fig 1.1 shows the classification of degradation and defects that cause insulation breakdowns [1]. The degradation and defects presumed through aged cables are mainly long-term degradation ((4) in Fig 1.1) and natural degradation ((5) in Fig 1.1). The factors causing long-term and natural degradation are water trees and chemical deposits in CV cables, and core shift and the overlap of oil gap in OF cables [1]. The difference between long-term degradation and natural degradation is the presence or absence of initial defects (the “presence” of initial defects is “long-term degradation”). Contaminations at the time of manufacture and traumas at the time of laying are examples of initial defects.

Insulation breakdowns due to water trees occur several times every year throughout the year at 66 kV or more [1]; however, the occurrence of this type of breakdown has been decreasing in recent years. One of the reasons for this decreasing trend is the stability of quality achieved owing to the technical improvements in the design and manufacture of cables. In addition, CV cables manufactured after 1985 are formed with an impervious layer to suppress the generation of water trees [1]. Nevertheless, water trees continue to be one of the major degradation factors because the CV cables with the impervious layer used are less at less than 66 kV.

The insulation breakdowns due to long-term and natural degradation caused by factors other than water trees have hardly occurred in both CV and OF cables [1]. However, a possibility exists that insulation breakdowns due to never-before factors occur in the future because of the increase in aged cables.

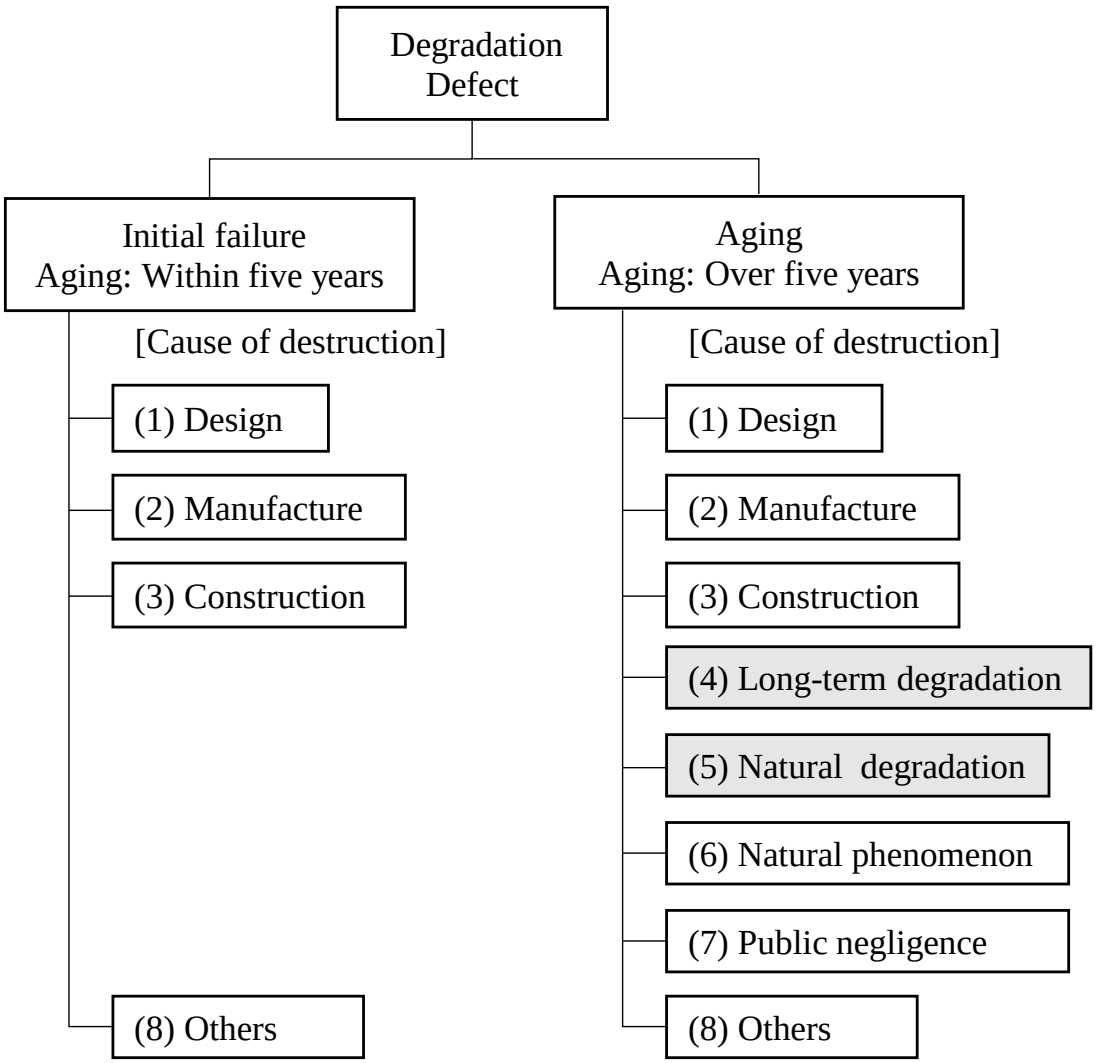

Fig 1.1 Classification of degradation and defects that cause insulation breakdowns [1]

1.1.3 Status of study on long-term and natural degradation

(1) CV Cables

a. Water tree degradation

A water tree is generated in cross-linked polyethylene (XLPE), which is an insulating material, due to the presence of electric field and water, and the progress of time [2]. The factors that influence the growth of water trees include voltage, frequency, time, temperature, amount of moisture, water quality, and solvents [2]. Water trees formed in underground power transmission cables adversely affect the insulation performance of insulating materials and subsequently cause insulation breakdown [2]. Water trees are classified as an inner tree, an outer tree, and a bow-tie tree, that based on the origin. Fig 1.2 shows an example of each water tree type. The water tree structure, generation/growth process, electrical characteristics, and the insulation breakdown process have been studied since the 1970s, and the basic course of treeing degradation in polymer insulation materials has been published [3]. However, water tree degradation is a complicated process due to the combined effect of various factors. The basic course points out that the elucidation of the process is insufficient [3].

(a) Inner tree

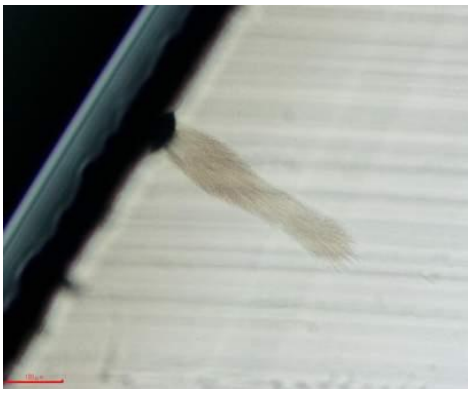

(b) Outer tree

(c) Bow-tie tree

Fig 1.2 Examples of water tree types

b. Thermal oxidative degradation

XLPE and ethylene propylene rubber (EPR) are used as insulating materials in CV cables. These are polymeric and rubber materials respectively. These materials become degraded due to heat, light, as well as mechanical and electrical conditions [4] [5]. Oxidative degradation due to heat (thermal oxidative degradation) occurs depending on the structure of an insulating material and the environment. However, the degradation caused by heat is presumed to be a long-term effect because antioxidants are generally added to the insulating materials as a countermeasure [6].

The study on thermal oxidative degradation of CV cables has been reported for a 66-kV tape-lapped joint (TJ) using an EPR tape [7]. This study demonstrated that the TJ breaks down during electric charging tests at 105° C using model and actual TJs. However, there are no reports on insulation breakdowns in used TJs. There is also no report on the thermal oxidative degradation of XLPE.

c. Others

In recent years, there have been reports on insulation breakdowns due to the deposits and the depletion of silicone oil on pre-mold insulation [1]. In addition, the degradation process has also been reported [1].

(2) OF Cables

a. Switching surge and overlap of oil gap

In joint boxes, the tightening due to semi stops and the thermal behavior of cables cause an overlap of the oil gap [1]. As a result, the insulation performance of the joint boxes promotes degradation. Partial discharge can occur because of the penetration of switching surges. Moreover, carbonization due to the partial discharge is increased via repetition, as a result of which insulation breakdown occurs. Many studies of this process have been reported [8-16].

b. Others

In recent years, aged joint boxes have been disassembled and investigated [1] [17-19]. The formation of black parts on insulating paper have been confirmed. However, the cause of the black parts has not been elucidated.

In the case of used cables, there has been no report on the degradation of insulating oil due to water entry and heat. In addition, there have not been many reports on the degradation of insulating paper and insulating oil in OF cables, unlike on that in transformers. Moreover, the insulating oil used in OF cables is mainly synthetic oil, whereas the insulating oil used in transformers is mainly mineral oil. Therefore, there is little knowledge of degradation of aged synthetic oil.

1.1.4 Status of diagnostic techniques for detecting long-term and natural degradation

(1) CV cables

a. Water tree degradation

The direct hazardousness of water trees was mainly evaluated in terms of water tree length using optical observation. The degradation diagnoses practically used for CV cables of capacity 66 kV or more are loss current measurement and residual charge measurement [1]. The loss current measurement uses the relationship between the generated density and the water tree length (N–L distribution) and the harmonic current obtained through test data [1] [20]. The residual charge measurement uses the relationship between the AC breakdown voltage and the residual charge accumulated in a long water tree [1] [21].

For reference, the degradation diagnoses at less than 66 kV mainly involve insulation resistance and DC leakage current measurements [22]. However, the diagnosis of water trees that do not penetrate an insulating material is not effective. For cables carrying 66 kV or more, these methods are not used because the water trees are mainly nonpenetrating.

In the available degradation diagnostic methods, factors other than the length of water trees were not fully considered. In other words, it is possible that diagnostic accuracy is affected adversely because of the complicated generation/growth process of water trees.

b. Thermal oxidative degradation

Degradation diagnosis has not been put to practical use; however, a method for estimating the lifetime of TJs has been proposed [23]. The lifetime diagnosis is a quantitative method based on the oxygen induction time (OIT), which correlates with the amount of antioxidant in the EPR. In addition, the OIT is measured via thermal analysis with differential scanning calorimetry (DSC). This method has been established through heating test data at 140 °C or more. However, it is reported that it is necessary to confirm the heating test data at 110 °C, which is the maximum service temperature of a CV cable, or lower.

(2) OF cables

a. Insulation oil analysis

The abnormality of OF cables is diagnosed through insulation oil analysis. First, the insulating oil collected from joint boxes and valves is analyzed [1]. The degradations of the diagnosis target are thermal degradation, electrical degradation, and degradation due to the penetration of moisture. The main diagnostic items are the amount of gas in the oil generated during these degradations. This diagnosis has been put to practical use since the 1990s. However, achieving a high accuracy is difficult. In fact, in the report of the disassembly investigation of used joint boxes, only a part of the diagnostic results coincided with the disassembly result [1]. Moreover, detecting the abnormality by

analyzing the dissolved gas in oil is difficult because gas diffusion to the outside of the insulating paper is very gentle [24]. Therefore, reviews of judgment values and statistical methods (support vector machine, decision tree) were proposed [1]. However, the chemical process associated with each degradation type is not taken into consideration in these methods. The diagnosis through insulation oil analysis has been widely put to practical use; however, there are many problems to be resolved.

b. Degradation determination of joint box disassembly

The distinction of degradation situation in four ranks was proposed [1]. The four ranks are classified into ranks of A, B, C, and D due to the situation of carbonization and discoloration on insulating paper. However, the chemical degradation process of the carbonization and discoloration is not taken into consideration because only visual checking is performed.

1.2 Purposes of this study

In CV and OF cables of capacity 66 kV or more, long-term degradation and natural degradation due to aging are points of concern. In the CV cable, the degradation caused in the used cables was due to water trees. This degradation caused many dielectric breakdown accidents, and many studies on this degradation type have been reported. However, the degradation process because of water trees has not been sufficiently elucidated due to complicated factors. In fact, long-term and natural degradation other than that due to water trees has hardly been studied because there is hardly any insulation breakdown accident. The degradation diagnosis of CV cables that has been put to practical use is the diagnosis of degradation due to water trees. The degradation diagnosis of OF cables is the abnormality diagnosis performed by analyzing insulation oil. However, the water-tree degradation diagnosis does not fully consider factors other than the length of water trees, and diagnosis by insulation oil analysis does not consider chemical degradation. As a result, diagnostic accuracy was sometimes worse. Therefore, the degradation of each insulating material of CV and OF cables was considered to be not discussed from a chemical point of view. Moreover, it was considered that diagnostic accuracy could be improved by developing a degradation diagnosis method based on a chemical point of view. In addition, the discussion from a chemical point of view is possible via using chemical analysis methods.

The insulating materials of the cables are all organic compounds: XLPE is a polymer; EPR is a rubber material; insulation oil is obtained by refining petroleum; and insulating paper is made from pulp material. In other words, these insulating materials degrade long-term and naturally because the organic compounds cause various chemical reactions due to heat, oxygen, materials, and other factors.

The purpose of this study is to elucidate the long-term and natural degradation of the insulating materials from the chemical point of view, and to establish new degradation diagnostic methods.

Relevant topics of study on the CV cables are thermal oxidative degradation considered in part [7], and water tree degradation on factors other than length. The subject of study on the OF cables is the black parts on the insulating paper that were discovered through the disassembly of joint boxes. [1] [17-19].

1.3 Contents of thesis

In this paper, the degradation process of insulating materials for underground power transmission cables is clarified from the chemical point of view. Moreover, degradation diagnostic methods are developed based on the clarified degradation process.

These details of the study as well as the development of degradation diagnostic methods are presented in five chapters.

Chapter 1 Introduction

In this chapter, the background and purpose of this study are described.

The background subsection describes the present conditions and problems associated with the degradation of the cables and the degradation diagnostic methods available.

The purpose of the study is to elucidate the degradation process from the chemical point of view, and to establish new degradation diagnostic methods.

Chapter 2 Detecting thermal oxidative degradation of insulating materials for CV cables

Thermal oxidative degradation of XLPE and EPR, which are insulating materials for CV cables, is the focus of this chapter. The degradation process was clarified in terms of the increase and decrease tendencies on carbonyl group and antioxidant in the materials. Degradation diagnostic methods were developed to determine the lifetime of cables based on the increase and decrease tendencies. In addition, the degradation tendency of used cables was confirmed by the developed degradation diagnostic methods.

Chapter 3 Detecting water tree degradation of insulating materials for CV cables

Water tree degradation that is a main cause of long-term and natural degradation of insulating materials for CV cables is the focus of this chapter. Solvents (ions) in the water tree that are one of the degradation causes are the focus points. First, a qualitative method to analyze the ions in water trees was developed because polyatomic ions could not be analyzed using conventional methods. The ion species and the degradation tendencies in the water trees formed in used cables were confirmed using this method. Based on the

results, simulated samples of water trees containing each ion were prepared.

The differences in degradation due to the ion species were clarified through the growth rate of the water tree and the AC breakdown voltage by using the simulated samples. The degradation diagnostic methods were developed to evaluate the harmfulness of the water trees based on the results obtained.

Chapter 4 Detecting Electric charging degradation of insulating materials for OF cables

Black parts on insulating paper confirmed in used OF cables is the focus of this chapter. First, the black parts were confirmed to be deposits of organocopper compounds through qualitative analysis. Moreover, these compounds were confirmed to be the cause of insulation breakdown. In other words, these compounds are deposited on insulating paper through a still unknown degradation process. Therefore, the degradation process was clarified through simulation tests of the process and analysis of the black parts in used cables. The methods for diagnosing degradation by performing insulation oil analysis were developed based on this result. In addition, the degradation tendency of used cables was confirmed by the developed degradation diagnostic methods.

Chapter 5 Conclusion

In this chapter, the main results of this study are summarized and are presented future directions of research.

REFERENCES

[1] Electric Technology Research Association, “Maintenance methods for underground transmission cable systems,” Electr. Technol. Res, Vol. 70, No. 1, 2014.

[2] IEEJ Technical report, “Insulation degradation diagnosis form of particularly high pressure CV cable and trend of insulation diagnosis technology,” IEE Japan, No. 668, 1998.

[3] IEEJ Technical report, “Basic course of treeing degradation in polymer Insulation materials,” IEE Japan, No. 674, 1998.

[4] S. Schnabel (1982), “Polymer Degradation –Principles and Practical Applications-,” In: J Soma, Japan, Shokabo, pp. 1-8, 1993.

[5] The Society of Rubber Science and Technology, Japan, “Rubber Industry Handbook,” No. 4 Edition, pp. 118-121, 1994.

[6] Z. Oosawa, “Prolong of Lifetime and Environmental Measures for Polymeric Materials,” Japan, OMC, pp. 15-45, 2000.

[7] M. Nakade, and T. Matsui, “Oxidative Degradation Characteristics of a Tape Lapped Cable Joint,” T.IEE Japan, Vol. 121-B, No. 11, pp. 1524-1531, 2001.

[8] M. Inoue, T. Doi, T. Nishikawa, T. Kiguchi, K. Suzuki, and K. Akita, “Estimation of Deterioration Characteristic for OF cables,” Annual Conference of Power and Energy Society, IEE Japan, No. 256, 2010.

[9] M. Inoue, T. Shiro, T. Iida, T. Tsutsumi, K. Akita, and Y. Sakaguchi, “Study of partial discharge deterioration characteristic for oil gap of OF cable”, Annual Conference of Power and Energy Society, IEE Japan, No.45, 2012.

[10] Y. Iwashita, T. Kurihara, T. Takahashi, and T. Okamoto, “Partial discharge characteristics of oil impregnated insulation system with an oil gap,” Annual Conference of Power and Energy Society, IEE Japan, No. 304, 2013.

[11] T. Kurihara, Y. Iwasita, T. Takahashi, and T. Okamoto, “Voltage Application Method to Obtain Time Transition of Partial Discharge Characteristics of Oil Gap in Oil Impregnated Insulation System,” National convention, IEE Japan, No. 7-134, 2014.

[12] Y. Iwasita, T. Kurihara, T. Takahashi, and T. Okamoto, “Time Transition of Partial Discharge Characteristics of an Oil Gap Defect in Oil Impregnated Insulation System,” National convention, IEE Japan, No. 7-135, 2014.

[13] Y. Makino, T. Kurihara, T. Takahashi, and T. Okamoto, “A Study on Lead Time from Generation of Continuous Partial Discharge to Breakdown of OF Cable Model Insulation System with an Oil Gap,” Annual Conference of Power and Energy Society, IEE Japan, No. 327, 2015.

[14] Y. Iwashita, M. Kozako, M. Hikita, Y. Makino, T. Kurihara, T. Takahashi, and T. Okamoto, “Influence of Repetitive Impulse Voltage Superimposed on AC Voltage on

Fundamental Partial Discharge Characteristics in Oil Impregnated Paper Insulation System," Annual Conference of Power and Energy Society, IEE Japan, No. 311, 2016.
[15] Y. Makino, T. Kurihara, T. Takahashi, and T. Okamoto, "Continuity of Partial Discharge at Oil Impregnated Paper Insulation System with Bubbles in Oil gap Defect," Annual Conference of Power and Energy Society, IEE Japan, No. 312, 2016.
[16] Y. Makino, T. Kurihara, T. Takahashi, and T. Okamoto, "Observation Result of an Oil Gap in Oil Impregnated Paper Insulation System under Lightning Impulse Voltage Superimposed on AC Voltage," National convention, IEE Japan, No. 7-149, 2016.
[17] S. Nsukawa, H. Amanai, and K. Fukuda, "Investigation of the oldest 154 kV Oil-filled cable in japan," National convention, IEE Japan, No. 7-197, 2009.
[18] Y. Tanimura, T. Doi, and M. Nishiuchi, "Investigation of Aged Oil-filled Cable," Annual Conference of Power and Energy Society, IEE Japan, No. 255, 2010.
[19] Y. tanimura, T. shiro, T. Iida, Y. aihara, Y. Morishita, and T. Nagano, "Investigation of Aged Oil-filled Cable Joint," Annual Conference of Power and Energy Society, IEE Japan, No. 422, 2012.
[20] Y. Yagi, K. Adachi, H. Tanaka, T. Tsujimoto, and M. Nakade, "Practical On-site Diagnosis of Water-treed XLPE Cables Based on Harmonics in AC Loss Current," IEEJ Society of Wire and Cable, EWC 03-04, 2003.
[21] I. Ootaka, M. Aoki, H. Togashi, T. Tsujimoto, and M. Nakade, "Direct-detect Type Residual Charge Method with Short-term Voltage Up-down for Water Tree Deterioration Diagnosis in XLPE Cable," T.IEE Japan, Vol. 126-B, No. 4, pp. 452-459, 2006.
[22] T. Hayami, "Insulation Diagnosis of Electrical Equipment," Ohmsha, Ltd., 2001.
[23] A. Tanaka, M. Nakade, and T. Matsui, "LifeTime Estimation of a Tape Lapped Joint for a XLPE Cable," T.IEE Japan, Vol. 121-B, No. 11, pp. 1532-1537, 2001.
[24] M. Inoue, T. Shiro, T. Iida, T. Tsutsumi, K. Akita, and Y. Sakaguchi, "Study of Partial Discharge Deterioration Characteristic for Oil Gap of OF Cable," T.IEE Japan, Vol. 133-B, No. 8, 2013.

Chapter 2 Detecting thermal oxidative degradation of insulating materials for CV cables

2.1 Introduction

In this chapter, the thermal oxidative degradation characteristics of XLPE and EPR, which is the insulation materials in a CV cable, are investigated and degradation diagnostic methods are developed. In previous similar studies, the thermal oxidative degradation characteristics of EPR were investigated in samples heated at 140 °C or more [1]. The degradation characteristics were confirmed through volume resistivity, tensile elongation, OIT, and the amount of carbonyl groups that are oxidative products by Fourier-transform infrared spectroscopy (FTIR). As a result, a lifetime diagnosis method by using OIT was proposed.

XLPE degrades due to heat and oxygen because it is a polymeric material containing the same antioxidant as EPR; nevertheless, there are no studies on the degradation characteristics and reports on insulation breakdowns in used TJs. It is necessary to elucidate the degradation characteristics of XLPE, because dielectric breakdown accidents may occur due to the aging of CV cables in the future. In addition, the degradation is presumed to be very gentle because of the effect of the antioxidant. In the present paper, the degradation characteristics of XLPE are studied by using the same method as that used for EPR [1]. Moreover, the lifetime diagnosis method of XLPE is also developed based on the result.

In previous similar studies, it was reported that the thermal oxidative degradation characteristics of EPR need to be confirmed by heating at 140 °C or lower. In other words, heating tests are performed near the operating temperature of the CV cable. In the present study, the thermal oxidative degradation characteristics of EPR are explored through a heating test conducted at 110 °C, which is the maximum operating temperature of CV cables, or less. However, an alternative method for the OIT-based evaluation method is necessary, because the accuracy and usability of the OIT-based method was unsatisfactory. Therefore, the alternative method is discussed and a lifetime diagnosis method using the alternative method is also developed.

2.2 Thermal oxidative degradation of XPLE

2.2.1 Examination of thermal oxidative degradation characteristics

(1) Samples and Methods

a. Samples

The XLPE insulation of a new CV cable was cut to a rotary-cut sheet with a width of approximately 25 mm and a thickness of approximately 0.5 mm in a lathe. In addition, an XLPE sheet having a length of 10 cm was cut off from near the center of the rotary-cut sheet. The CV cable manufactured by one company (Company A) was arbitrarily selected. Fig 2.1 shows the rotary-cut sheet and the XLPE sheets fitted in a sample holder. The XLPE sheets were heated for 24 h at 90 °C in a vacuum oven, and the residuals of cross-linking were removed.

b. Heating methods

The XLPE sheets were heated at 140 °C, 160 °C, and 180 °C. Fig 2.2 shows the heating situation. The sheets fitted in the sample holder were placed in a gear-type aging oven and heated at the prescribed temperature. The sheets were taken out to divide a few times until reach to the life. The heating was performed in atmospheric-pressure air. The gear-type aging oven used was a No102-SHF-77 (Yasuda Seiki Seisakusho Limited, Japan).

(a) Rotary-cut sheet (b) XLPE sheet fitted in sample holder

Fig 2.1 XLPE sheet

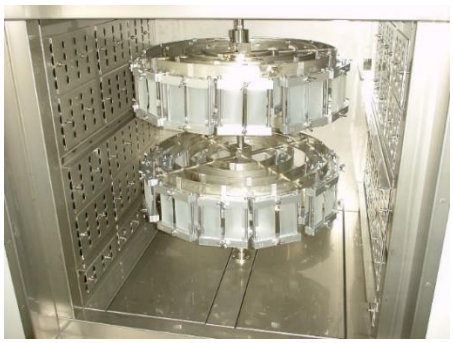

Fig 2.2 Heated situation in gear-type aging oven

c. Confirmation methods of degradation characteristics

The thermal oxidative degradation characteristics of the heated samples were compared and examined through volume resistivity measurement and FTIR.

The volume resistivity measurement confirmed the degradation characteristics due to the decrease trend. Fig 2.3 shows the electrode shape. The leakage current from the edge was removed with the guard electrode. The XLPE sheet was sandwiched between the electrodes. The charging voltage was 500 V AC, the charging time was 35 s, and the measurement start was 25 s after the end of charging. The measured value was the average value measured 10 times at 5-s intervals. The measuring device used was a digital ultra-high resistance/micro-ammeter R8340A (Advantest Corporation, Japan).

The quantity of carbonyl groups in XLPE was measured using FTIR and was quantitatively evaluated in terms of the absorbance ratio of the carbonyl groups. In fact, plastics such as XLPE cause oxidative degradation due to heat [2]. The oxidative degradation of plastics is considered to proceed in a chain reaction through the mechanisms expressed in (1-7) as follows.

$R\cdot, RO_2\cdot$ *Radical generation* (1)

$R\cdot + O_2 \rightarrow RO_2\cdot$ (2)

$RO2\cdot + RH \rightarrow ROOH + R\cdot$ (3)

$2R\cdot \rightarrow$ (4)

$R\cdot + RO2\cdot \rightarrow$ } *Inert products* (5)

$2RO2\cdot \rightarrow$ (6)

$ROOH \rightarrow RO\cdot + HO\cdot$ (7)

(RH: Polyolefin)

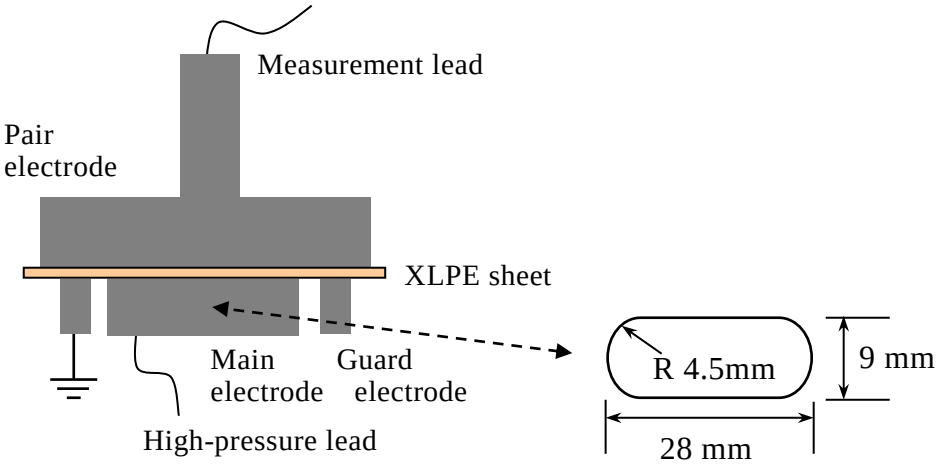

Fig 2.3 Electrode shape

Carbonyl groups such as ROOH are formed in XLPE due to oxygen binding. As a result, the thermal oxidative degradation characteristics can be examined from the increase tendency of the carbonyl groups. FTIR is employed to measure the infrared (IR) absorption spectrum correlated with molecular vibration via irradiating IR light in samples [3]. The IR spectrum correlated with the molecular vibration of the carbonyl groups appears in the vicinity of 1600 to 1950 cm^{-1} [4]. The Beer–Lambert law (8) holds for the IR spectrum [3].

$$A = log\ (I_0/I) = \varepsilon bc \quad (8)$$

A: Absorbance, I_0: Intensity of incident light, I: Intensity of transmitted light

B: Thickness, c: Concentration, ε: Absorptivity

The strength of absorbance is proportional to the concentration and the thickness of a sample. In other words, the absorbance of carbonyl groups is a quantitative value of the concentration. However, samples with an uneven thickness are not able to be quantified by absorbance, because the absorbance also varies because of the thickness of the sample. The thickness error of the XLPE sheet was less than ±1 mm. Therefore, an unchangeable absorbance (standard spectrum) is selected even after thermal oxidative degradation. The ratio of the absorbance (absorbance ratio) between the carbonyl groups and the standard spectrum is the quantitative value. As a result, in the quantitative analysis in terms of the absorbance ratio, the effect of thickness is removed.

The XLPE sheets were measured by using the transmission method with FTIR. Any three points of the XLPE sheet were measured. Therefore, the measurement value was the average value of the absorbance ratios at the three points. The absorbance positions of carbonyl groups and a standard spectrum were selected using the measurement result of the heated sample at 140 °C. The FTIR used was a NEXU670 (Thermo Fisher Scientific K.K., USA). The measurement conditions were a scan number of 32 times and a resolution of 4 cm^{-1}.

(2) Results

a. Change over time of volume resistivity

Fig 2.4 shows the change over time of volume resistivity at the heated temperature of 140 °C and 160 °C. Fig 2.5 shows the change over time at the heated temperature of 180 °C. The volume resistivity at all the heating temperatures was constant for a while duration after the start of heating, but sharply decreased after a certain time.

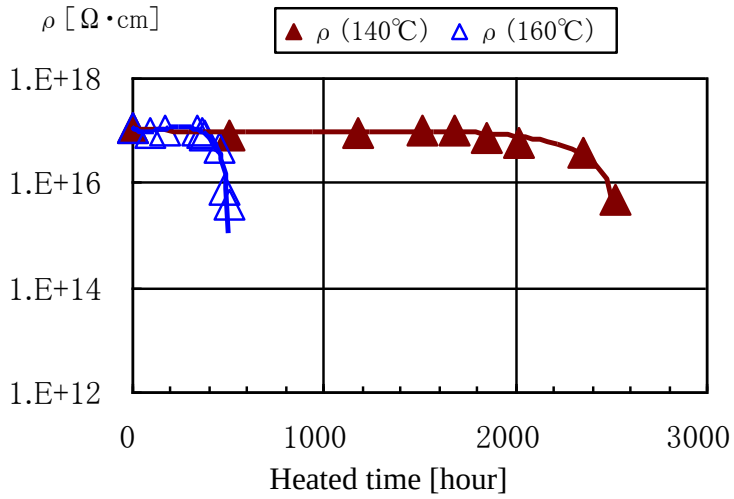

Fig 2.4 Change over time of volume resistivity (at heated temperatures of 140 °C and 160 °C)

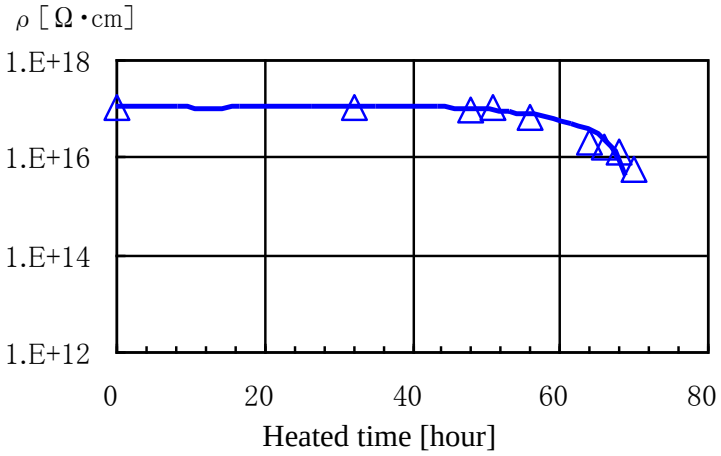

Fig 2.5 Change over time of volume resistivity (at the heated temperature of 180 °C)

b. The absorbance positions of carbonyl groups and standard spectrum

Fig 2.6 shows the IR spectra from 1550 to 2000 cm^{-1} at the heated temperature of 140 °C. The absorption band of carbonyl groups from 1600 to 1800 cm^{-1} increased with heated time. However, the absorption peak at 1897 cm^{-1} did not change.

Fig 2.7 shows the change over time of the absorbance at 1897 cm^{-1} and volume resistivity at the heated temperatures of 140 °C and 160 °C. Fig 2.8 shows the change over time of the absorbance at 1897 cm^{-1} and volume resistivity at the heated temperature of 180 °C. The absorbance at 1897 cm^{-1} was unchanged even when the volume resistivity sharply decreased regardless of the heated temperature. This absorption is one of the absorption bands of polyethylene and is attributed to the vibration of the methylene group [5]. Thus, the standard spectrum was set to an absorption peak at 1897 cm^{-1}. However, the standard spectrum is not limited to this absorption peak if it is unchanged. In addition, the influence of the background was removed by drawing a baseline. Each absorbance was the height from the baseline.

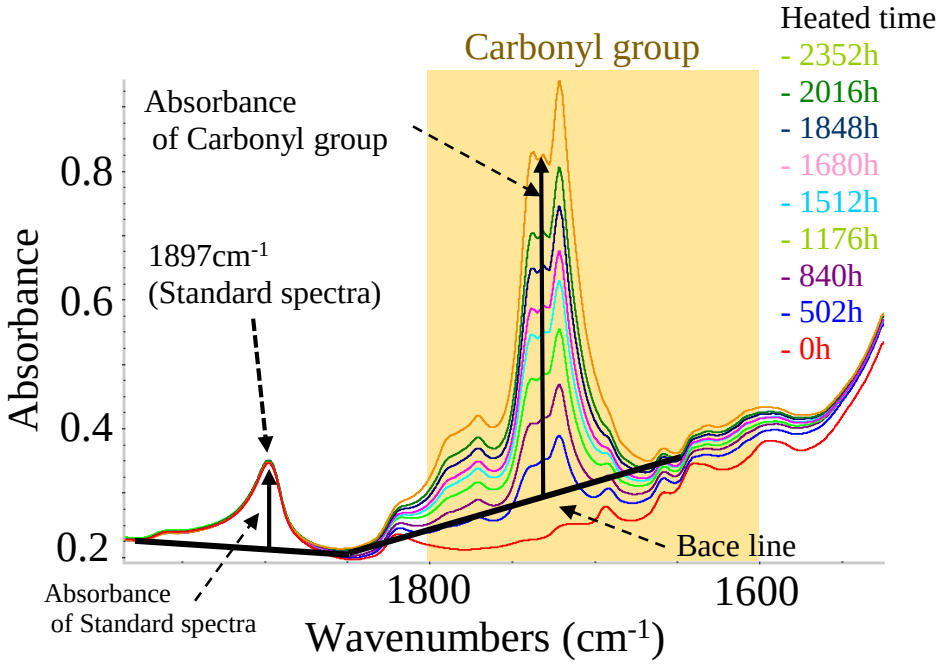

Fig 2.6 Infrared absorption spectra of XLPE (at the heated temperature of 140 °C)

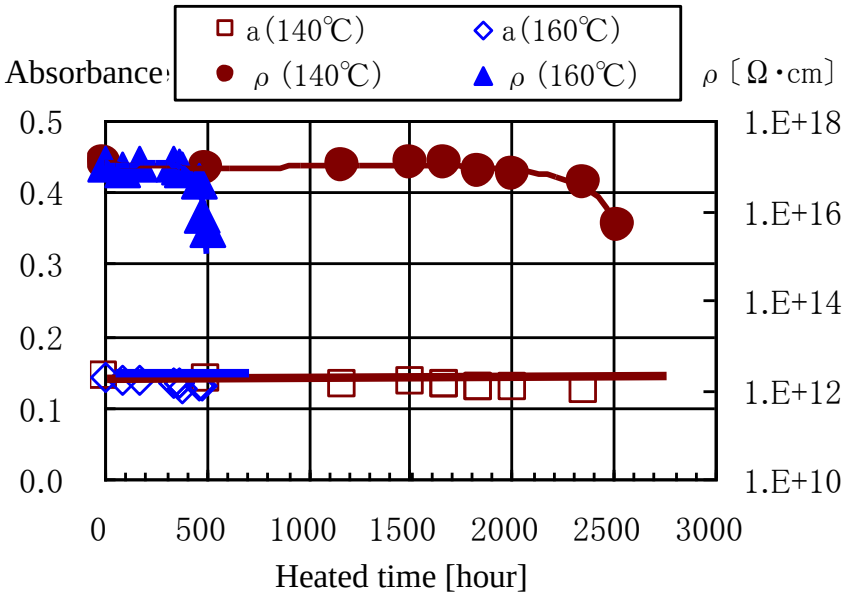

Fig 2.7 Change over time of absorbance at 1897 cm^{-1} (at the heated temperatures of 140 °C and 160 °C)

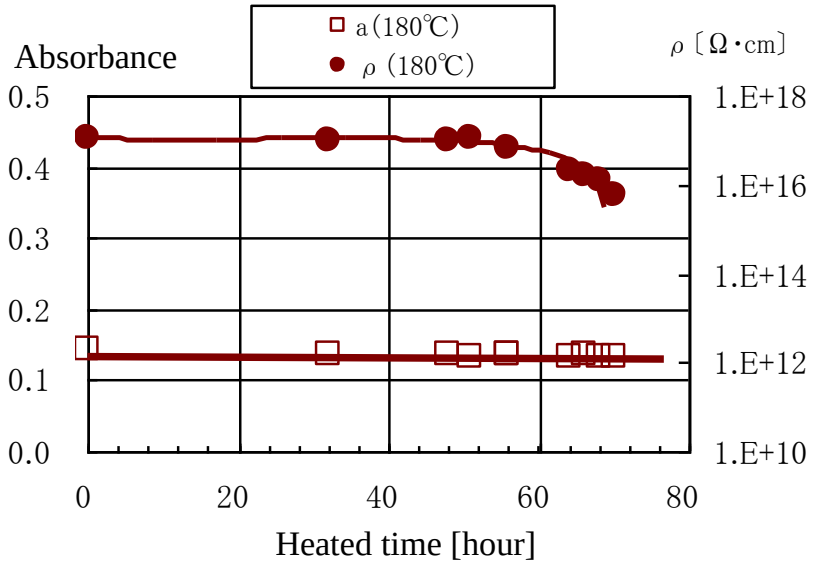

Fig 2.8 Change over time of absorbance at 1897 cm^{-1} (at the heated temperature of 180 °C)

c. Increase trend of carbonyl groups

Fig 2.9 shows the change over time of the absorbance ratio at 1712, 1732, and 1769 cm^{-1} and volume resistivity at the heated temperature of 140 °C. The absorption peaks of carbonyl groups are at 1712, 1732, and 1769 cm^{-1}. The initial value of the absorbance ratio was almost zero for all three absorption peaks. The increase trend after the start of heating was linear. After that, the absorbance ratios increased sharply after a certain time, whereas the volume resistivity began to decrease at the same time. The absorption peak of the maximum increase was 1732 cm^{-1}.

Fig 2.10 shows the change over time of the absorbance ratio at 1732 cm^{-1} and volume resistivity at the heated temperatures of 140 °C and 160 °C. In addition, Fig 2.11 shows the change over time at the heated temperature of 180 °C. The trends in the absorbance ratio and volume resistivity values were the same for the three temperatures. Moreover, the absorbance ratio at the end of the linear trend was the same 2.2 at the three temperatures.

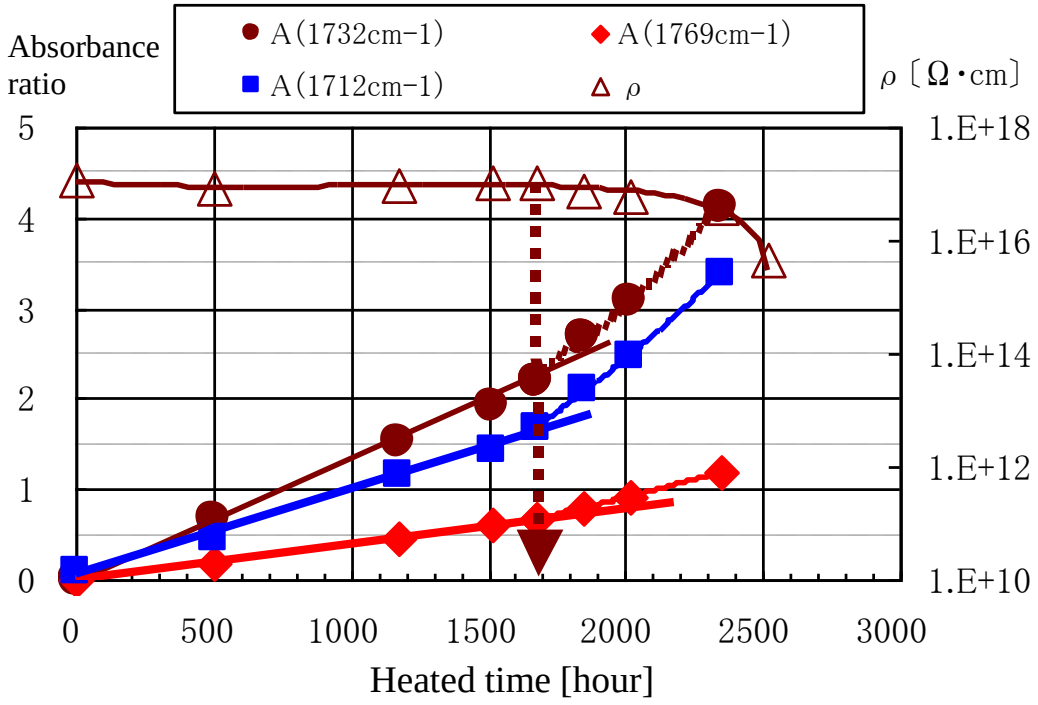

Fig 2.9 Change over time of absorbance ratio at 1712, 1732, and 1769 cm^{-1} (at the heated temperature of 140 °C)

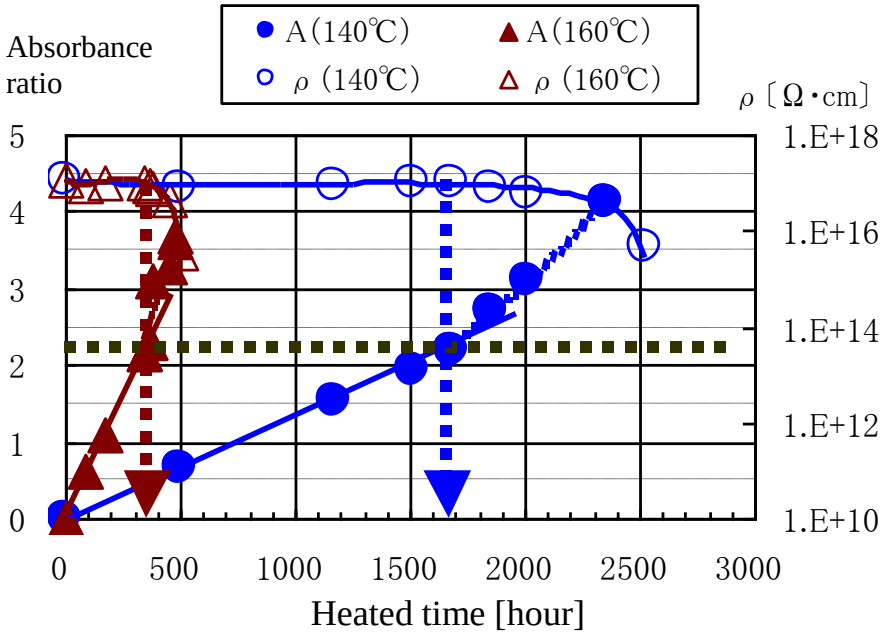

Fig 2.10 Change over time of absorbance ratio at 1732 cm^{-1} (at the heated temperature of 140 °C)

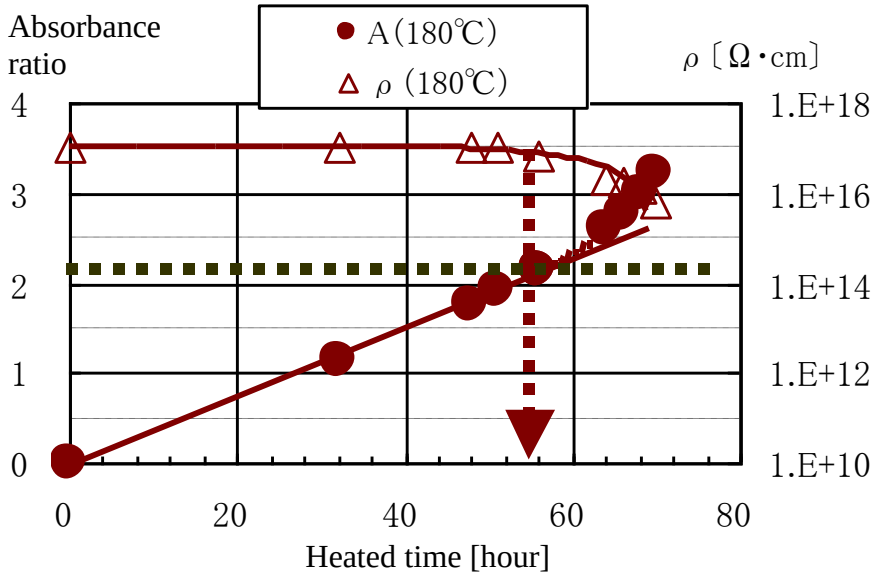

Fig 2.11 Change over time of the absorbance ratio at 1732 cm^{-1} (at the heated temperature of 180 °C)

(3) Discussion

The increase and decrease trend of carbonyl groups and volume resistivity were the same regardless of heated temperature. Therefore, the thermal oxidative degradation characteristics of XLPE until the lifetime are a volume resistivity that does not change, and linearly increasing carbonyl groups. The time at which the volume resistivity begins to decrease coincides with the time at which the dielectric loss tangent value begins to decrease, and the time is the electrical lifetime of XLPE [6]. In addition, the quantity of carbonyl groups linearly increases until the lifetime. It is possible that the linear increase trend is due to the influence of antioxidants. The antioxidants are additives for polyolefin such as XLPE. The antioxidants supplement radicals generated by heat and suppress oxidative degradation [2]. As a result, it is possible that the carbonyl groups in XLPE linearly increased due to the suppression. Moreover, it is possible that a lifetime diagnosis method can be developed due to this linear increase.

2.2.2 Development of lifetime diagnostic methods

(1) Research methods

Thermal oxidative degradation characteristics that can be used for the diagnostic method were extracted from the elucidated characteristic data. In addition, the characteristics data of CV cables made by another company (Company B) were also investigated. The methods were the same as the methods used for CV cables made by Company A, as described in 2.1.1. However, the heated temperature was only 140 °C. The absorption peak of the carbonyl group was a peak of 1732 cm^{-1} with a large change.

(2) Research results

The characteristics data that can be used for the life diagnosis method are as follows.

- The lifetime is the point at which the volume resistivity begins to decrease.
- The increase in carbonyl group is linear.
- The initial value of carbonyl group is extremely near zero, and the lifetime value is 2.2.
- The lifetime value does not change with heated temperature.

Fig 2.12 shows the change over time of the absorbance ratio at 1732 cm^{-1} and volume resistivity at the heated temperature of 140 °C with the XLPE made by Company B. The lifetime value of the carbonyl group was 0.8. Other degradation characteristics were the same as the characteristics of Company A.

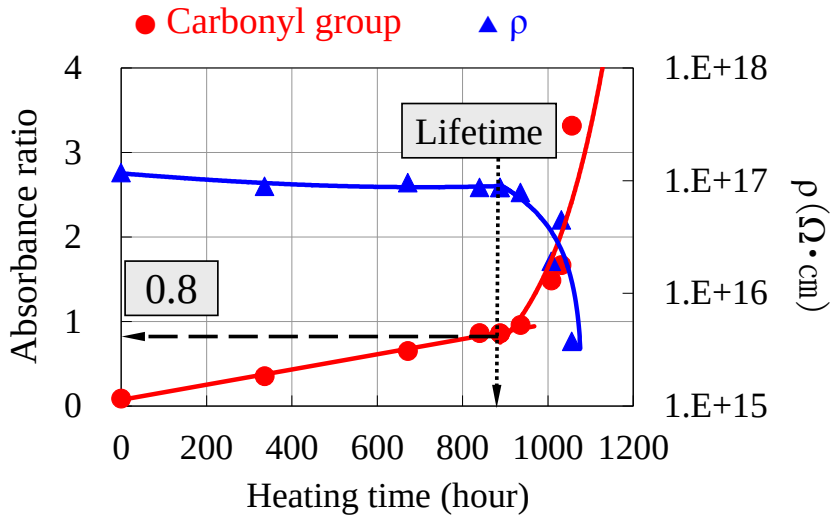

Fig 2.12 Change over time of absorbance ratio at 1732 cm^{-1} with XLPE made by Company B (heated temperature = 140 °C)

(3) Development of lifetime diagnostic methods

The thermal oxidative degradation characteristics of XLPE do not change regardless of manufacturer or operating temperature. As a result, the lifetime diagnosis method can be established through the linear increase in the absorbance ratio of carbonyl group. Therefore, a new lifetime diagnosis method was developed for CV cables based on the results of this study.

Fig 2.13 shows the summary of the lifetime diagnostic methods. The new value of the carbonyl groups is zero, or a new measurement value. The absorbance ratio [A_m] of the carbonyl group, the age [A] at the time of measurement, and the new value are connected by a straight line. The lifetime [X] of the cable is the number of years to reach the absorbance ratio [A_L] at the lifetime on linear extension. The remaining life [X_{RL}] is obtained by subtracting the age [A] from the lifetime [X]. However, the lifetime value [V_L] of the carbonyl group is different for different manufacturers. It is possible that the difference in the amount of antioxidant mixed by each manufacturer creates a difference in lifetime value. Therefore, it is necessary to obtain the lifetime value from each manufacturer in advance. The methods are to conduct a heating test for each cable specification in advance. The effective absorption peak of standard spectrum is 1897 cm^{-1}, and the peak of carbonyl group is 1732 cm^{-1}. In addition, the effective absorption can also select other peaks that meet the conditions. The condition for standard spectrum is invariable absorption even if thermal oxidative degradation occurs. The condition for carbonyl group is absorption having a linear increase.

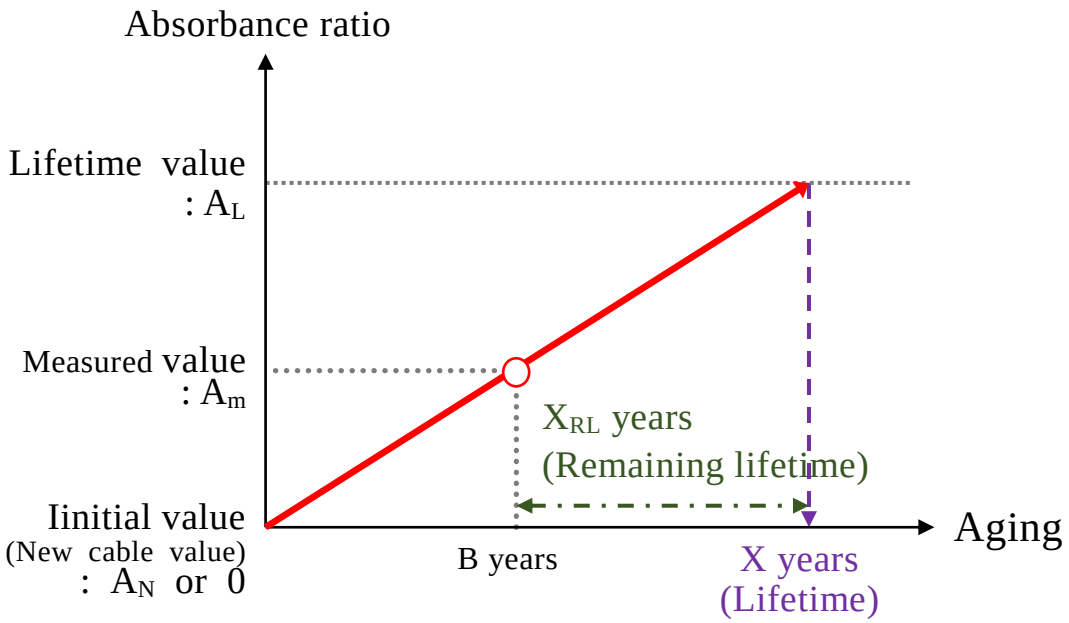

Fig 2.13 Summary of lifetime diagnostic methods

2.2.3 Deterioration status of used cables

(1) Methods

The target samples were 140 lines of used 66-kV CV cables. The thermal oxidation degradation status of used cables was confirmed through the absorbance ratio of carbonyl group using FTIR. The method is the same as the XLPE sheet preparation method and FTIR measurement method shown in 2.1.1. The lifetime was diagnosed by the developed lifetime diagnosis method.

(2) Results

Fig 2.14 shows the relationship between the aging and the absorbance ratio of the used CV cables made by Company A. In addition, the graph added an approximation straight line, a lifetime value of the CV cables made by Company A, and estimated time to reach the lifetime value. The estimated time to reach the lifetime value is the time to reach the lifetime due to extending the approximate line.

Fig 2.15 shows the enlarged view of the graph in Fig 2.14 for a CV cables less than 30 years old. The absorbance ratio was found to increase with age. However, the degree of degradation was low overall. The lifetime was 250 years. Moreover, the lifetimes of all 140 lines that include used cables made by other companies were all greater than 100 years.

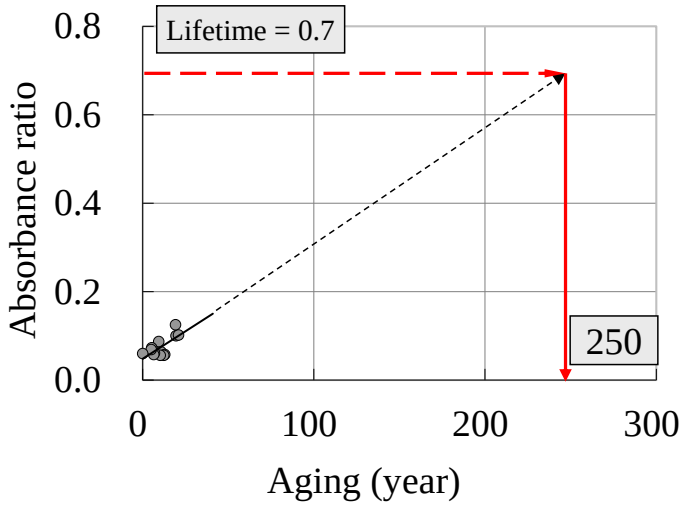

Fig 2.14 Relationship between the aging and the absorbance ratio (for CV cables made by Company A)

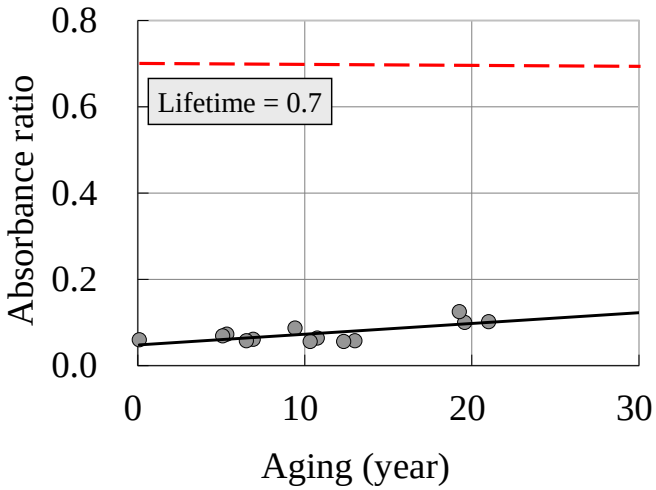

Fig 2.15 Enlarged view of graph in Fig 2.14 for CV cables less than 30 years old

(3) Discussion

The used cables suffered low thermal oxidative degradation. As a result, the dielectric breakdown of 66-kV CV cables is not realistic in the current usage status because the results of lifetime diagnosis was 100 years or more. However, polymer materials such as XLPE have the characteristic that the lifetime is halved by temperature rise of approximately 10 °C. Therefore, it is possible that the lifetime of a cable when used at higher temperatures than that at present will be realistic usable years. The results indicate that thermal oxidative degradation cannot be ignored in the future owing to the usage changes.

2.2.4 Investigation of an insulation breakdown cable

(1) Samples

Fig 2.16 shows the status of cable laying. The outline of the investigation of the cable is as follows.

- The structure of the cable
  6 kV CVT (150 mm^2), E-T cable, nonwater barrier, 1989 (aged 22 years).
- Load situation
  Long-term high load (day and night continuous operation), 500–600 A (load current value for normal operation)

(2) Methods

a. Measurement samples

The XLPE insulation was cut into round slices with approximately 0.5 mm thickness. Herein, rotary cutting was impossible because of the thin XLPE insulation.

b. External Observation

The entire cable and the slice sample were observed by visual observation and by using a microscope. The microscope used was a VHX2000 (Keyence Corporation, Japan).

c. Investigation of contaminations and water trees

Contaminations and water trees in the slice were confirmed with a metallurgical microscope. The metallurgical microscope used was an ECLIPSE ME600D (Nikon Corporation, Japan).

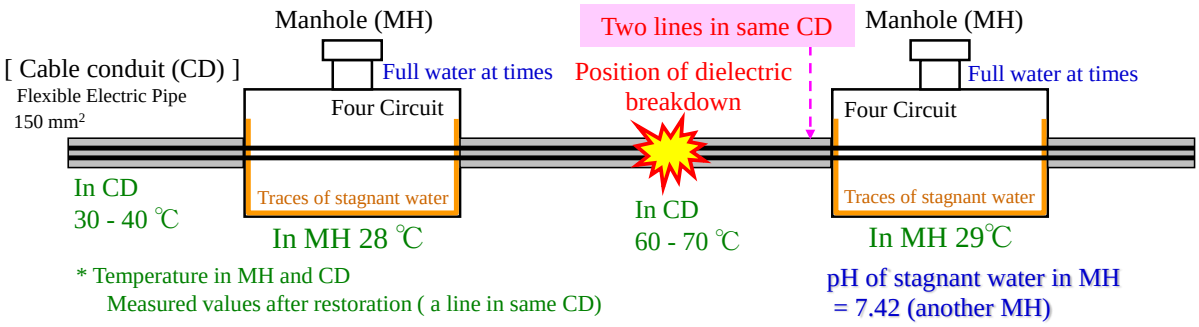

Fig 2.16 Cable laying scenario

d. Thermal history measurement

The thermal history of the XLPE insulation was measured using DSC. The sample of approximately 10 mg was cut out from the slice of XLPE. The measurement places were the XLPE insulation in the dielectric breakdown area and the sound area. The measurement points were the inner semiconductive layer side and the outer semiconductive layer side. The differential scanning calorimeter used was a Thermo Plus 2 DSC 8230 (Rigaku Corporation, Japan). The measurement conditions were a measurement atmosphere of 30 mL/min of nitrogen, a measurement temperature of 25–140 °C, and a heated speed of 10 °C/min.

e. Investigation of thermal oxidative degradation

The absorbance of carbonyl group was measured near the center of the slice by using the transmission method of FTIR, at any three points of the slice. The measured value was the average value of absorbance ratios at the three points. The place of measurement was the near breakdown point in the breakdown phase, near breakdown point in the sound phase, and the sound part of the sound phase. The lifetime was diagnosed by the developed lifetime diagnosis method. The absorbance ratio of carbonyl group at the lifetime was 0.7. The FTIR spectrometer used was a NEXU670 (Thermo Fisher Scientific K.K., USA). The measurement conditions were a scan number of 32 times and a resolution of 4 cm^{-1}.

f. Investigation of thermal oxidative degradation by layer

The differences in degradation tendency were compared through the distribution tendencies of the absorbance ratio of carbonyl group. The distribution tendencies were measured by line mapping of microscopic FTIR. The line mapping was measured every 50 μm from the inner layer to the outer layer. The measurement conditions were a scan number of 64 times and a resolution of 8 cm^{-1}. The microscopic FTIR spectrometer used was a Nicolet Continumμm (Thermo Fisher Scientific K.K., USA).

(3) Results

a. External Observation

Fig 2.17 and Fig 2.18 show the aspects of the breakdown phase and the sound phase. The polyvinyl chloride (PVC) sheaths of the breakdown phase and the part of sound phase were hardened, cracked, and easily peeled off. In addition, green rust was considerably generated in the copper shielding tapes. However, the hole was not open on the copper shielding tapes.

Fig 2.19 shows the aspects of an XLPE slice. The near breakdown point in the breakdown phase and the sound phase was discolored to yellow and/or orange. Moreover, the discoloration on the conductor side in the breakdown phase was particularly dark.

(a) Appearance of the cables (b) Aspect of the breakdown point

Fig 2.17 Aspect of the breakdown phase

(a) (b)

Fig 2.18 Aspect of the sound phase

(a) Near breakdown point in the breakdown phase

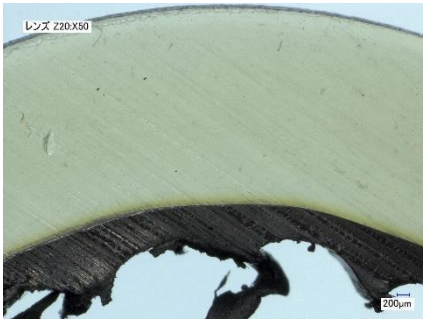

(b) Near breakdown point in the sound phase (c) Sound part of the sound phase

Fig 2.19 Aspect of the XLPE

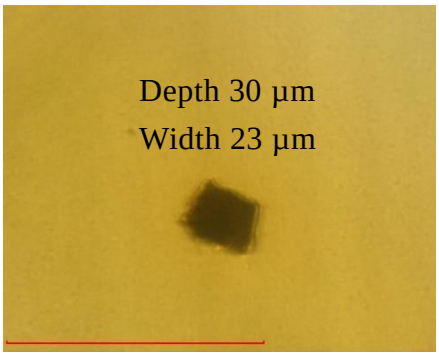

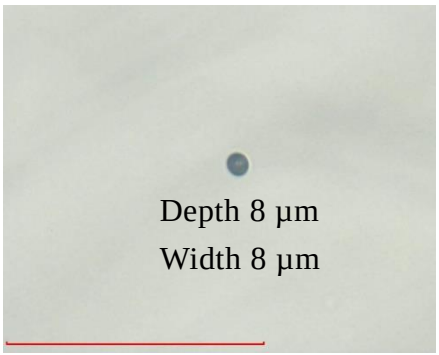

(a) Foreign substance (b) Void

Fig 2.20 Maximum foreign substance and void

b. Investigation of contamination and water trees

There were no water trees. Fig 2.20 shows the maximum foreign substance and void. They were sized with no problem in insulation performance.

c. Thermal history measurement

Table 2.1 shows the measurement results. The thermal history of near breakdown points

was more than the melting point of XLPE (approximately 107 °C), and that of the sound parts was less than the melting point, which was a high temperature.

d. Investigation of thermal oxidative degradation

Table 2.2 shows the absorbance ratio of carbonyl group and the lifetime diagnosis (remaining lifetime). The near breakdown points in the breakdown phase and the sound phase had reached the lifetime. The remaining lifetime of the sound part in the sound phase was 45 years.

Table 2.1 Result of the thermal history

Measurement points	Near breakdown point	Sound part in the breakdown phase
Interior semiconductive layer side	108 °C	90 °C
External semiconductive layer side	113 °C	89 °C

Table 2.2 Measurement results of thermal oxidative degradation

Measurement points		Absorbance ratio of Carbonyl group	Remaining lifetime
Breakdown phase	Near breakdown part	2.51	Expiration of the lifetime
Sound phase	Near breakdown part	0.87	Expiration of the lifetime
	Sound part	0.27	45 years

e. Investigation of thermal oxidative degradation by layer

Fig 2.21 shows the result of line mapping. The inner layer from the middle layer near the breakdown point of the breakdown phase and the innermost layer near the breakdown point of the sound phase were complete oxidative. The sound phase was not completely oxidized; however, the innermost layer had reached the lifetime. Thermal oxidative degradation of other parts had also progressed. In addition, the complete oxidative degradation is the state in which rapid oxidation reactions such as main chain decomposition in XLPE occurred after the lifetime.

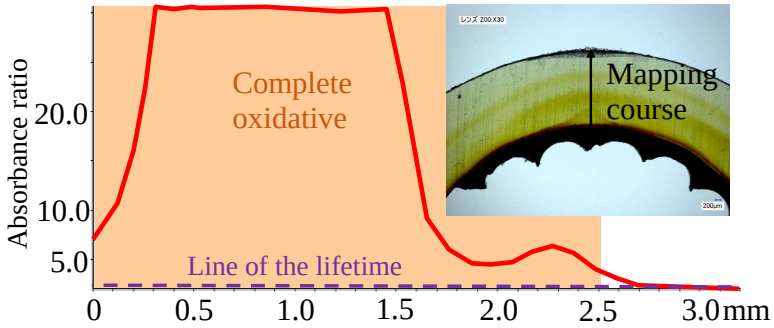

(a) Near breakdown point of breakdown phase

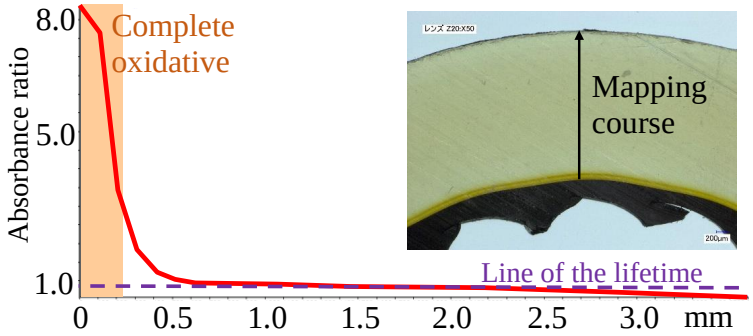

(b) Near breakdown point of sound phase

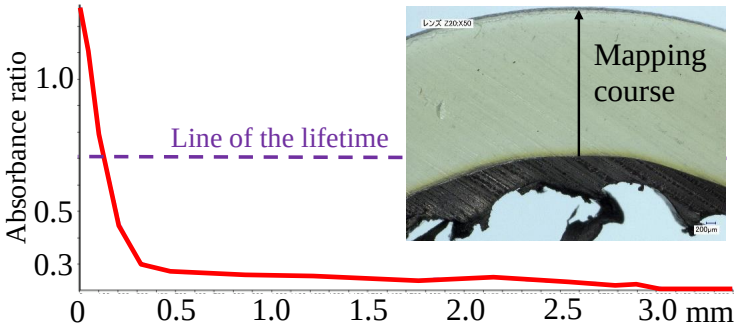

(c) Sound part of the sound phase

Fig 2.21 Distribution of the absorbance ratio of carbonyl group

(4) Discussion

a. Factors of dielectric breakdown

The cause of dielectric breakdown was concluded to be thermal oxidative degradation of the XLPE insulation. Moreover, it was assumed that the direct cause is separating or cracking between the XLPE insulation and the semiconductive layer due to the lifetime of the XLPE. In addition, the cause of discoloration of the XLPE is thermal oxidative degradation.

The tendency of thermal oxidative degradation of the XLPE insulation progressed considerably, and the near breakdown point reached the lifetime. Fig 2.22 shows the aspect between the XLPE insulation and the semiconductive layer near the breakdown point. Part of the gap between the XLPE insulation and the semiconductive layer was separating or cracking. The cause of the phenomenon was concluded to be the thermal expansion and contraction of the cable during use; however, it is possible that the cause was also sample preparation. The phenomenon could be reproduced by a small load.

Thus, it is assumed that the points became weak points in insulation performance. However, it is also possible that the cause of breakdown was the insulation performance degradation of the XLPE insulation due to the complete oxidation of XLPE.

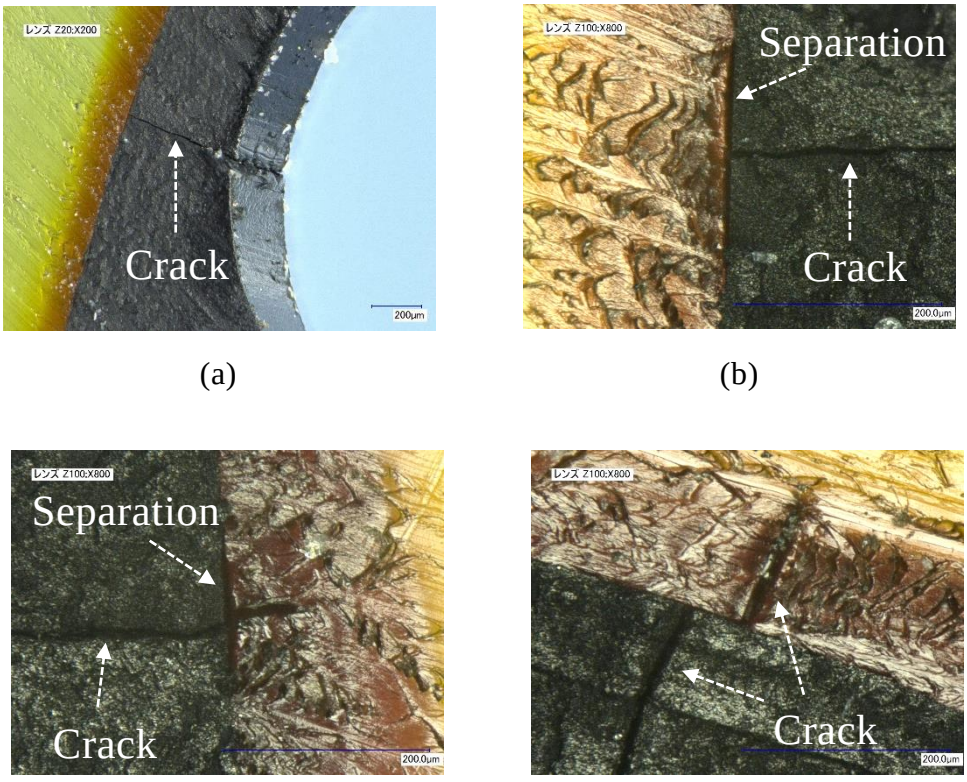

(a) (b)

(c) (d)

Fig 2.22 Crack and separation between XLPE insulation and semiconductive layer

b. Factors of thermal oxidative degradation

The cause of thermal oxidative degradation was concluded to be long-term use at a temperature higher than the melting point of XLPE due to a high load. The temperature condition of the XLPE insulation can be concluded through the temperature inside the conduit, thermal history, and load situation. The thermal oxidative degradation near the inner layer of the XLPE insulation progressed considerably. In other words, the heat of the conductor greatly affected the degradation. The results also indicate that the sheath cracks were due to the thermal oxidative degradation of the sheath. In addition, the degradation speed of XLPE increased because the invasion of oxygen into the XLPE was promoted from the cracks. As a result, the vicinity of the breakdown point was the most easily degraded place.

c. Thermal oxidative degradation of CV cable

The possibility of a dielectric breakdown of the 66-kV CV cables was low in the current usage scenario from the lifetime diagnosis result. However, this investigation revealed that thermal oxidative deterioration was one of the causes of the dielectric breakdown of CV cables. In fact, the lifetime diagnosis method was effective for the diagnosis of thermal oxidative degradation through this investigation. On the other hand, the results indicated that CV cables did not breakdown for more than 20 years even when used long-term at a temperature greater than the melting point.

2.3 Thermal oxidative degradation of EPR

2.3.1 Examination of thermal oxidative degradation characteristics

(1) Samples and Methods

a. Samples

The new EPR tape was cut every 10 cm. Fig 2.23 shows the EPR tapes fitted in a sample holder. In addition, the tapes were not tensioned.

b. Heating methods

The EPR tapes were heated at 75 °C, 90 °C, 105 °C, 140 °C, 160 °C, and 180 °C. The EPR tapes of the two companies (Company A and Company B) actually used were samples. The heated methods and the devices were the same as that used for the examination of the XLPE sheets.

c. Confirmation methods of degradation characteristics

The confirmation methods were the same as the high-temperature heated test at 140 °C or more [1].

d. Volume resistivity measurement

The measured methods and the devices were the same as for the examination of the XLPE sheets.

Fig 2.23 EPR tapes fitted in sample holder

e. OIT measurement

The OIT was measured using DSC. Fig 2.24 shows the measurement conditions. Nearly 10 mg of the sample was cut out from the center of an EPR tape. The sample was placed flat on the bottom of an aluminum pan. The aluminum pan was not closed. The reference material was an aluminum plate of approximately 10 mg. The differential scanning calorimeter used was a Thermo Plus 2 DSC 8230 (Rigaku Corporation, Japan).

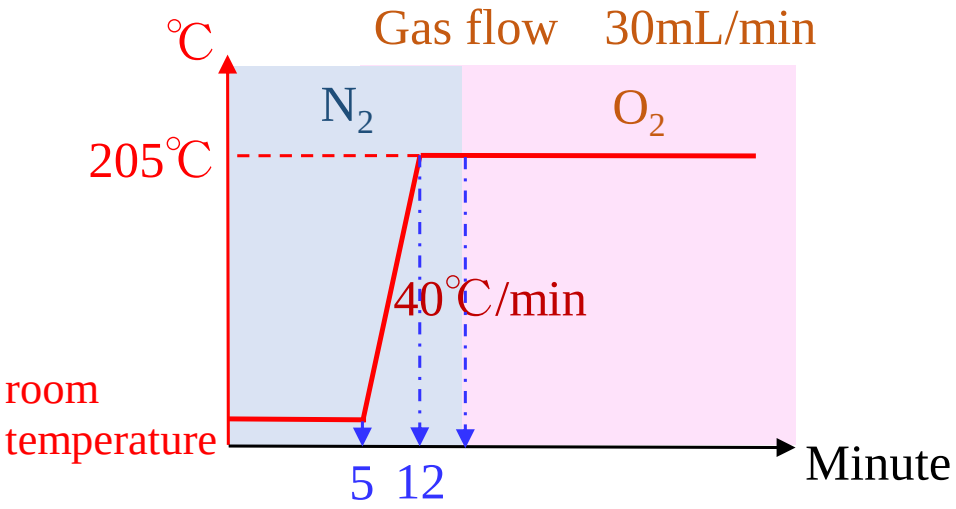

Fig 2.24 Measurement conditions of DSC

(2) Results

Fig 2.25 and Fig 2.26 show the change over time of the OIT and the volume resistivity for samples from Company A and Company B. The OIT decreased linearly with time in all of the test conditions, and the volume resistivity began to decrease at 2–3 min of OIT.

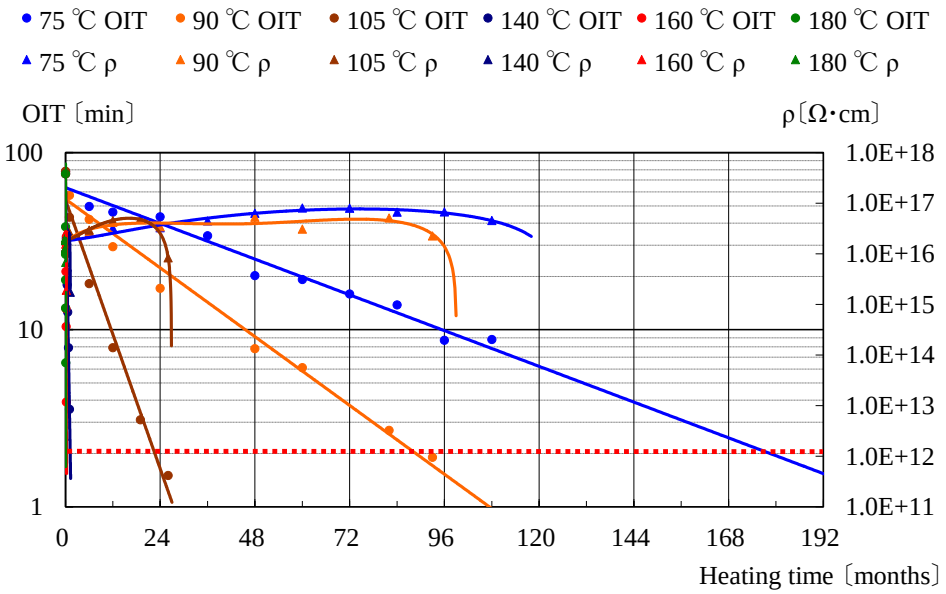

(a) Heating temperature at 75 °C, 90 °C, 105 °C, 140 °C, 160 °C, and 180°C

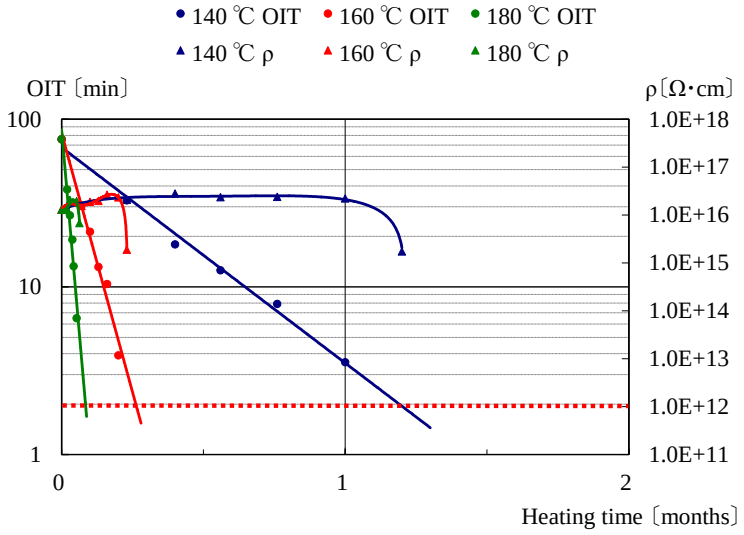

(b) Heating temperatures = 140 °C, 160 °C, and 180°C

Fig 2.25 Change over time of volume resistivity and OIT (Company A)

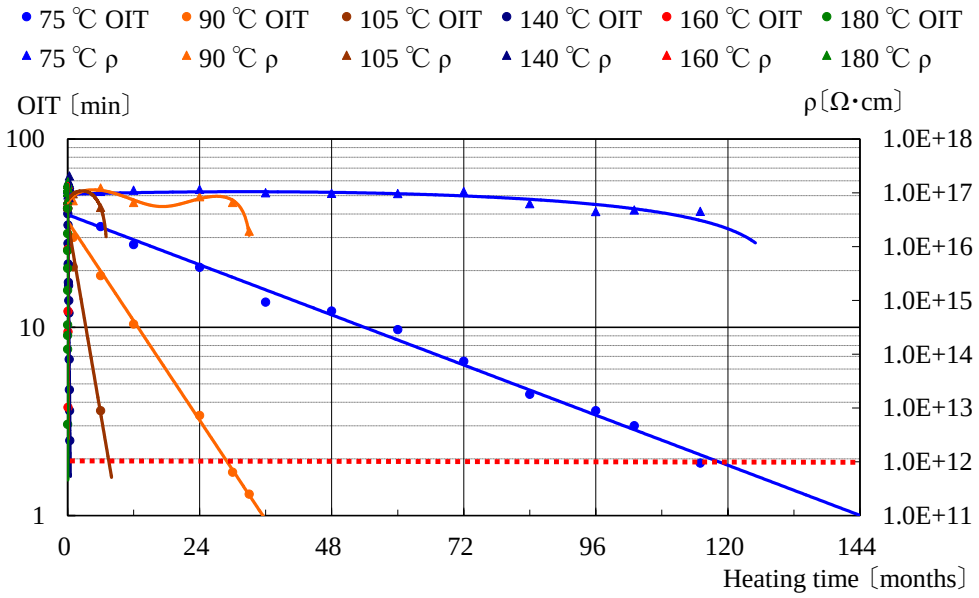

(a) Heating temperatures = 75 °C, 90 °C, 105 °C, 140 °C, 160 °C, and 180°C

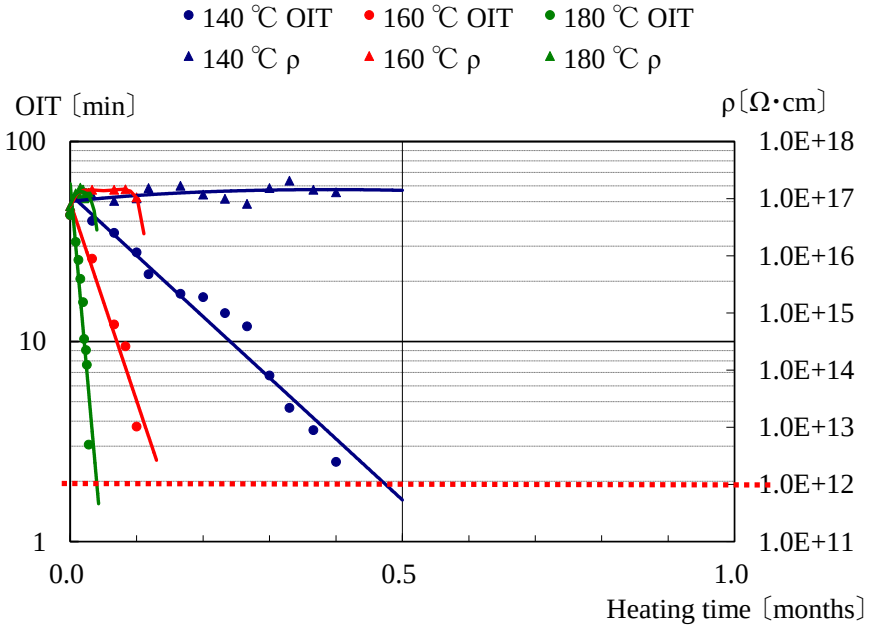

(b) Heating temperatures = 140 °C, 160 °C, and 180°C

Fig 2.26 Change over time of volume resistivity and OIT (Company B)

(3) Discussion

The tendency of thermal oxidative degradation is the same regardless of the heating temperature and the manufacturer. Fig 2.27 shows the Arrhenius plot when the OIT at the lifetime is 2 min. The Arrhenius plot was plotted linearly from 75 ° C to 180 ° C. In fact, the EPR with a long life was from Company A. The lifetime change rate from 50 °C to 90 °C was the same 0.014 for the samples from both companies. Therefore, the inclination of the straight line of the Arrhenius plot is common to EPR regardless of the manufacturer, whereas the lifetime is different for samples from different manufacturers. It is possible that the difference in lifetime is the difference in the amount of antioxidant compounded at the time of manufacture. The OIT at the lifetime was confirmed to be approximately 2–3 minutes when the volume resistivity decreased. In conclusion, the effectiveness of the proposed lifetime diagnosis by the OIT method [1] was verified through confirming measurement data at 105 °C or less.

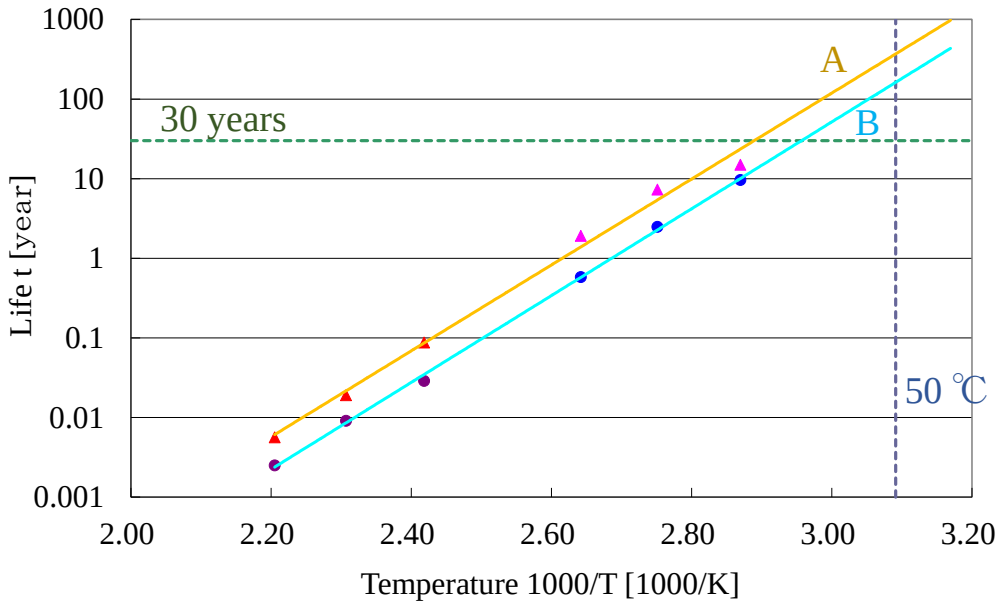

Fig 2.27 Arrhenius plot of EPR

2.3.2 Degradation status of used cables

(1) Confirmation methods

The degradation tendency of used 66-kV cables were confirmed through the lifetime diagnosis using the OIT of the removed TJs. The used TJs were Company A Line 20 and Company B Line 18. The removed TJs were removed from the lead pipe and the waterproof compound. The samples were cut out in a block shape from the vicinity of the conductor at the side of the sleeve as it is the easiest degradation position [1] [7]. Moreover, the block of approximately 1 mm square area was cut out from the sample. The OIT measurement method and the devices were the same as that mentioned in 2.3.1.

(2) Results

Fig 2.28 shows the relationship between aging and OIT. Both the OITs tended to be shorter with age. The lifetime was 60 to 100 years on the average, and was 20 to 25 years on the shortest.

(3) Discussion

The EPRs of TJs were definitely degraded by thermal oxidation. Some TJs had realistic lifetimes unlike the XLPEs. In addition, the change in lifetime when the temperature of TJs changed from 50 °C to 90 °C sharply decreases to an average of approximately 1–1.5 years due to the rate of change shown in Fig 2.27. In other words, dielectric breakdown becomes realistic due to the usage environment.

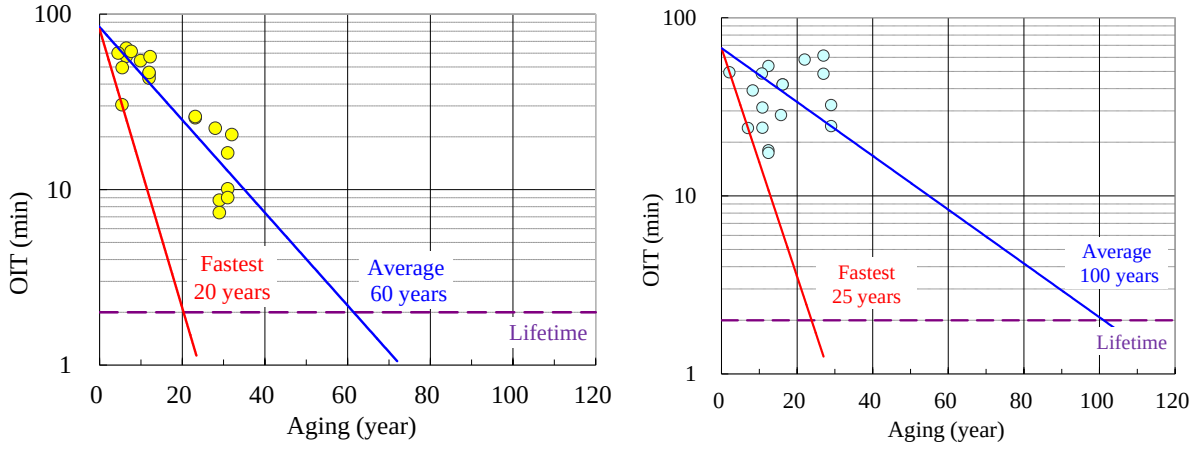

(a) Company A (b) Company B

Fig 2.28 Relationship between aging and OIT of used cables

2.3.3 Development of lifetime diagnostic methods

(1) Problems associated with OIT

OIT measurement of EPR had problems concerning measurement accuracy and usability.

The first problem was that the measurement error was large for most samples. Fig 2.29 shows the example of the OIT charts measured three times for the same sample. The difference between the maximum and minimum was 30 min, and the measurement error was very large. As a result, the actual measured value was the median measured 5–10 times owing to this problem.

The second problem was the difficult analysis of the OIT chart. Fig 2.30 shows the OIT charts showing an example of this problem. The OIT value was the intersection of the baseline and the tangent line of the point where the slope of the exothermic peak was large. However, the exothermic peaks were multiple cases or unknown. As a result, the method to draw the tangent line was different for each measurer owing to this problem, and the measurement error increased.

The third problem was the long measurement time. One measurement time was from 30 min to more than 120 min. As a result, the measurement time of one sample was one day or more in some cases because of the measurement performed 5–10 times with one sample.

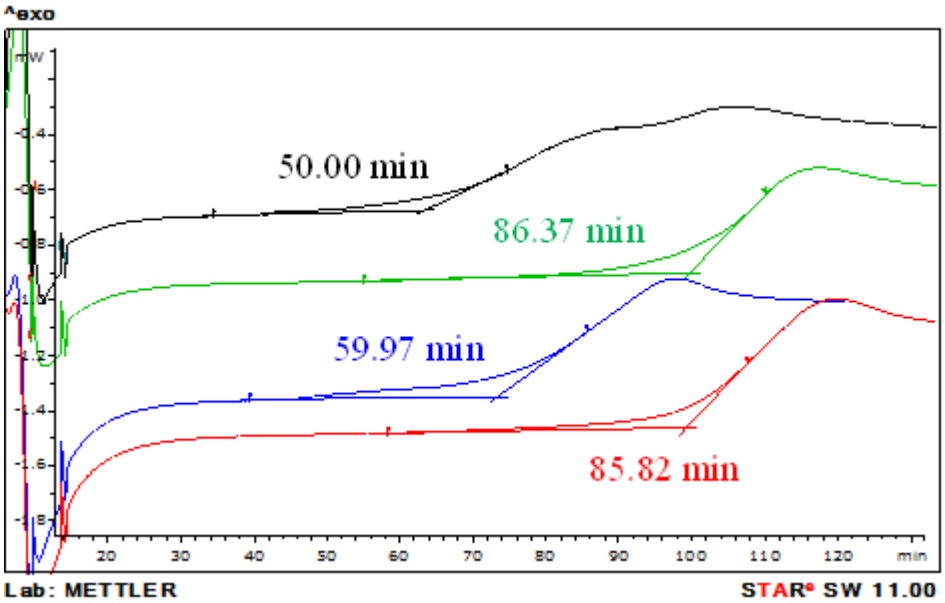

Fig 2.29 OIT charts of the same sample

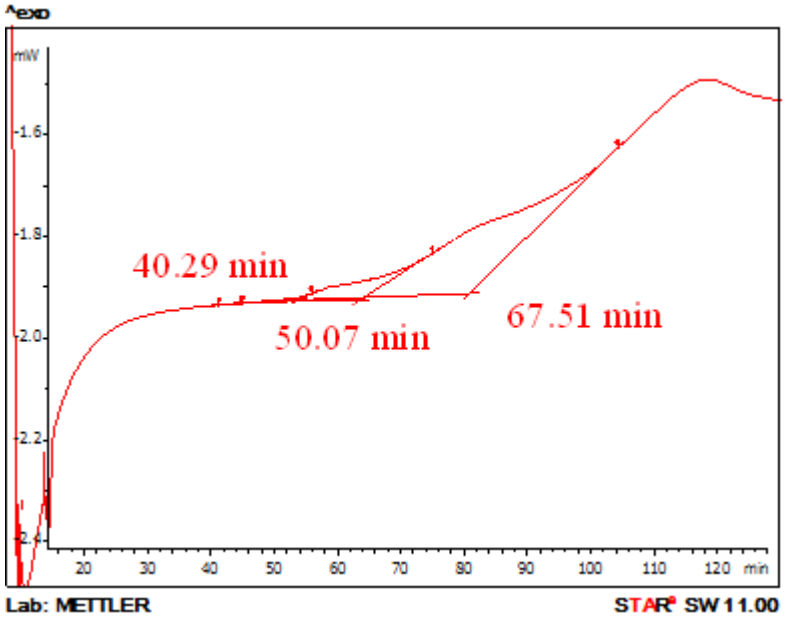

(a) Multiple cases of an exothermic peak

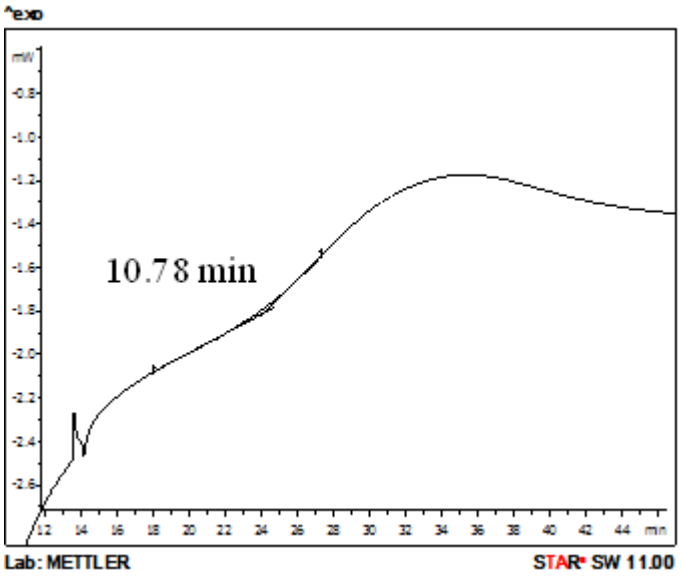

(b) Case where an exothermic peak was unknown

Fig 2.30 OIT charts that were difficult to analyze

In conclusion, the development of measurement methods with high accuracy and short measurement time was thought to be necessary. The point of view is the initial oxidation temperature (IOT). The IOT method measures the temperature at which oxidation starts while raising the temperature at a constant speed. The IOT is effective as an oxidative degradation index of vulcanized rubber, plastics, and so on. The oxidative degradation index of the IOT and OIT is different because of temperature and time. However, the principle as an oxidative degradation index is the same. In addition, the IOT is high-

accuracy and short-measurement time as compared to the OIT because the large exothermic peak can be obtained with a small amount of a sample [8] [9] [10]. In other words, the IOT can be the alternative method to solve this problem associated with the OIT. Therefore, it was confirmed that the thermal oxidation degradation characteristics of EPR could be measured using the IOT.

(2) Research methods

The new EPR tapes manufactured by the two companies (Company A and Company B) actually used were samples. In addition, the EPR tapes of Company A were two specifications.

The EPR tapes were heated. The heating method and the devices were the same as for the examination of the thermal oxidative degradation characteristics of the EPR tape. Table 2.3 shows each heated time. The research method was a comparison of thermal oxidative degradation characteristics by measuring the IOT and the OIT of each sample.

Table 2.3 Heated samples

Manufacturer	Heated temperature	Heated time (h) for samples
Company A (Specification 1)	105 °C	24, 144 ,240, 288, 456, 624
	90 °C	24, 144, 288, 576, 1152, 1440, 1968, 2232
Company A (Specification 2)	180 °C	0.5, 2, 4, 6, 8, 24
	160 °C	27, 48, 72, 96, 104
Company B	90 °C	24, 144, 288, 576, 720, 792

(3) Measurement methods

a. OIT Measurement

The measurement method was the same as for the EPR tape in 2.3.1. The differential scanning calorimeter used was a DSC1 (Mettler Toledo International Inc., Switzerland).

b. IOT Measurement

The IOT was measured by using DSC. The samples and the sample containers were the same as that used in the OIT method. Fig 2.31 shows the measurement conditions. The differential scanning calorimeter used was a DSC1 (Mettler Toledo International Inc., Switzerland).

(4) Research results

a. Measurement time

The measurement time was approximately 30 min even for the new EPR tapes under the measurement conditions. As a result, the measurement time of the IOT was clearly shorter than that of the OIT, and the superiority of the IOT was confirmed.

b. Exothermic peak

Fig 2.32 shows the IOT charts when changing the sample weight. The heavier the weight was, the sharper and higher the peak chart was and the more lowered the baseline was.

Figure 2.33 shows the IOT and OIT charts with the sample weight of approximately 1 mg. The calorific value of the exothermic peak is 2.48 mW for the IOT and 0.48 mW for the OIT. The IOT chart was clearly sharp and had a high peak.

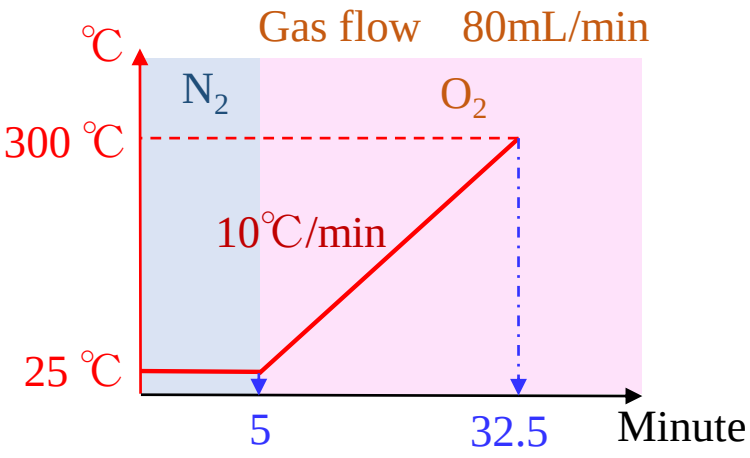

Fig 2.31 Measurement conditions of IOT method

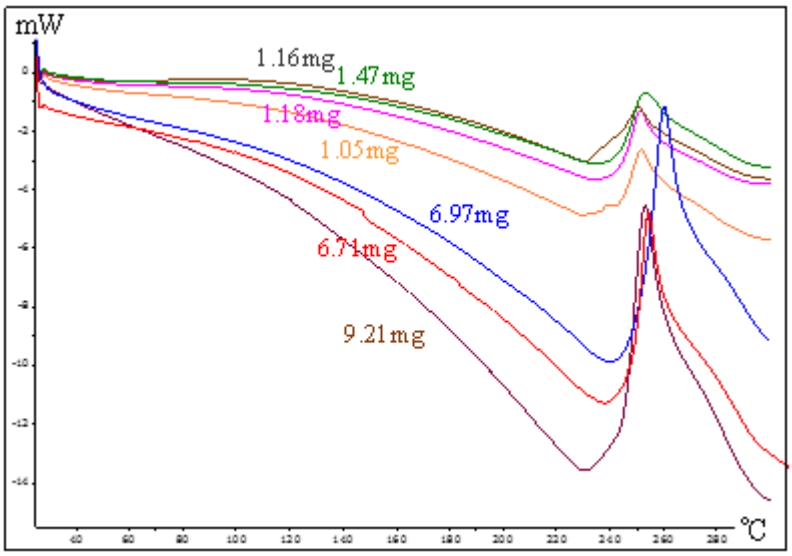

Fig 2.32 IOT charts by sample weight

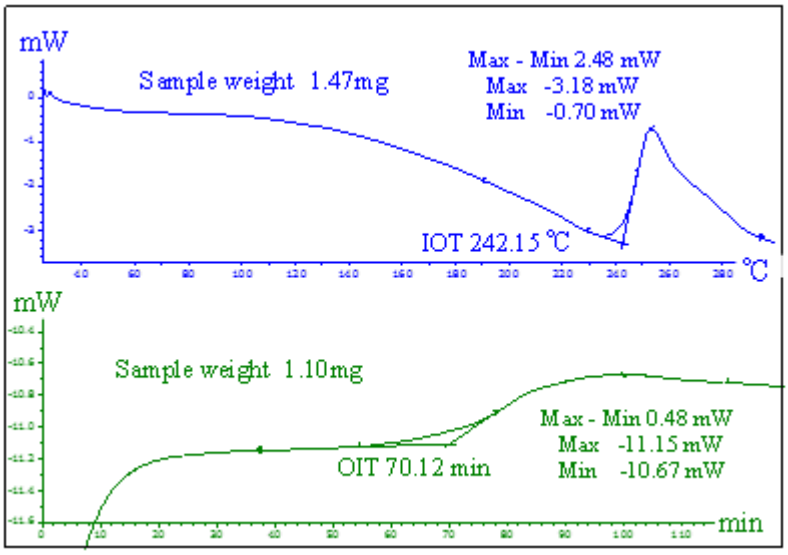

Fig 2.33 IOT and OIT charts with the same sample weight

c. Measurement accuracy

Table 2.4 shows the results of the OIT and the IOT measurements for the new EPR tapes. The number of measurements was 6 or 10. The totals for the average (Ave.), the standard deviation (σ), and the relative standard deviation (RSD) are listed.

The RSD of the all samples was the OIT of 10.10% and the IOT of 0.91%. Therefore, the RSD of the OIT was ten times that of the IOT, and each sample showed the same trend.

Table 2.4. Measurement result of the new EPR

	A Specification 1 Lot. 1		A Specification 1 Lot. 2		A Specification 1 Lot. 3		A Specification 1 Total of 3 lots		A Specification 2		B	
	IOT	OIT	IOT	OIT	IOT	OIT	IOT	OIT	IOT	OIT	IOT	OIT
1	243.58	51.42	243.22	65.63	236.41	88.15			246.36	103.35	241.70	40.50
2	245.67	85.87	244.54	78.56	245.31	82.90			248.22	98.96	243.39	42.60
3	239.75	61.86	241.86	70.59	244.01	86.09			248.80	91.19	243.47	48.20
4	237.36	85.29	243.47	69.98	244.49	97.45			248.99	88.79	242.95	36.80
5	239.65	74.43	242.80	73.79	243.89	91.51			249.21	97.24	243.03	45.10
6	236.80	75.97	237.71	66.31	242.25	93.52			247.09	87.28	242.50	31.90
7												40.30
8												41.00
9												47.80
10												47.10
Ave.	240.47	72.47	242.27	70.81	242.73	89.94	241.82	77.74	248.11	94.47	242.84	42.13
σ	3.49	13.53	2.40	4.83	3.25	5.28	3.07	12.17	1.15	6.35	0.71	5.20
RSD	1.45 %	18.67%	0.99 %	6.82 %	1.34 %	5.87 %	1.27 %	15.66%	0.46 %	6.72 %	0.29 %	12.34%

d. Thermal oxidative degradation characteristics

The IOT and the OIT of all the heated samples were measured three times each, and the average of the three times was the measured value. Fig 2.34 shows the relationship between the measured value and heating time. The IOT was linearly decreasing regardless of the heating temperature, manufacturer, and specifications, similar to the case of the OIT. However, the vertical axis of the OIT was logarithmic, and the IOT was an integer. The IOT at the lifetime was judged 200–210 °C, because the IOT at the time of OIT 2-3 shown in Fig 2.34 (C) was about 200 to 210 ° C. The OIT at the lifetime was confirmed due to Fig 2.25 and Fig 2.26.

Fig 2.35 shows the relationship between heating time and all measurement data that is not average, for the samples with Specification 1 (Company A). In addition, the linear approximation was drawn by all plots, and the correlation coefficient (R) was shown on the graph. The correlation coefficient of the IOT was 0.95 or more, and the OIT was 0.69 and 0.83.

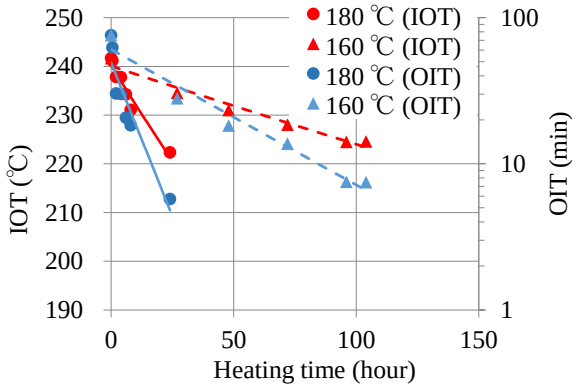

(a) Specification 1 of Company A

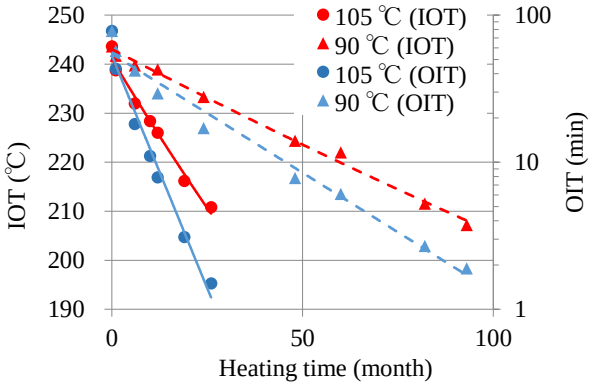

(b) Specification 2 of Company A

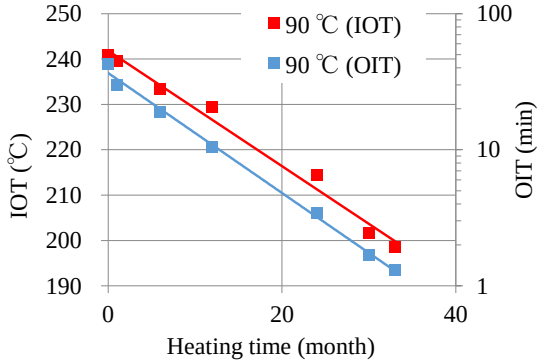

(c) Company B

Fig 2.34 Thermal oxidative degradation characteristics of IOT and OIT

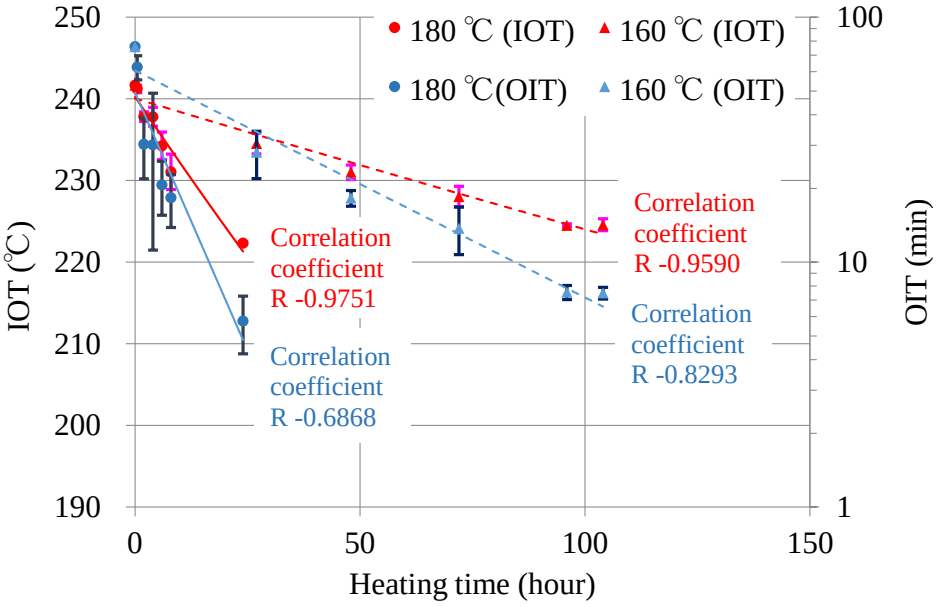

Fig 2.35 Thermal oxidative degradation characteristics of IOT and OIT with all measurement data for Specification 1 (Company A)

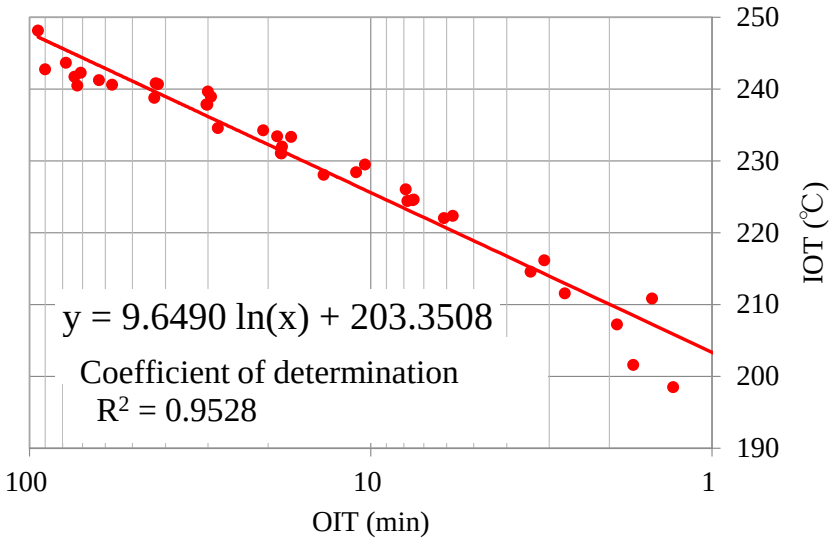

Fig 2.36 Relationship between IOT and OIT with all measurement data

e. Correlation between OIT and IOT

Fig 2.36 shows the relationship between the OIT and the IOT with all measurement data. The relationship was linear via logarithmic approximation.

(5) Development of lifetime diagnostic methods

a. Advantage of IOT method

The IOT method is superior to the OIT method as an evaluation method of thermal oxidative degradation of EPR. The advantages are the short measurement time and the high accuracy of measurement. The advantage of the measurement time was confirmed through the measurement conditions. The advantage of measurement accuracy was confirmed from the RSD of one tenth of the OIT. Moreover, three measurements per sample were sufficient from the RSD, whereas the OIT was necessary 5–10 times because the RSD was the ten times than the IOT. Therefore, the total measurement time of one sample was shortened because of the decrease in the number of measurements per sample. The measurement accuracy of the IOT was excellent also in analysis. The methods to draw the tangent line were not different for each measurer, because the IOT chart was clearly sharp and had a high peak compared with the OIT chart.

The IOT method has the problem that the heavier the weight was, the more lowered the baseline was. It is possible that the factor was a change in the contact area between the sample container and the sample because of the change in the sample shape due to temperature rise. However, the exothermic peak with the sample of approximately 1 mg was a peak of a size that was easy to analyze, and the fall of the baseline was suppressed. As a result, the valid sample weight was determined to be approximately 1 mg.

b. Lifetime diagnostic methods by IOT

The lifetime diagnostic methods by using the IOT can be established by the same principle as with the OIT and is highly accurate compared with the OIT. The change of the IOT due to the thermal oxidative degradation of EPR is the same linear decrease as with the OIT. In addition, the correlation coefficient of the straight line was 0.95 or more, and the linearity was clearly stronger than with the OIT.

As a result, a more useful lifetime diagnosis method by using the IOT than the conventional method by using the OIT was developed. Fig 2.37 shows the summary of the lifetime diagnosis method, and the basic principle is the same as the OIT method. However, the difference compared with the OIT method is the vertical axis of integers, and the lifetime value is 200–210 °C.

The IOT can interconvert with the OIT. The interconversion exploits the linearity of logarithmic approximation between the OIT and the IOT. The formula in Fig 2.36 is the conversion formula. The interconversion can be carried out by assigning to each of the formula. Therefore, the past OIT can be compared with the latest IOT by conversion. However, the problem is that the accuracy of the converted value also decreases owing to the low accuracy of the OIT.

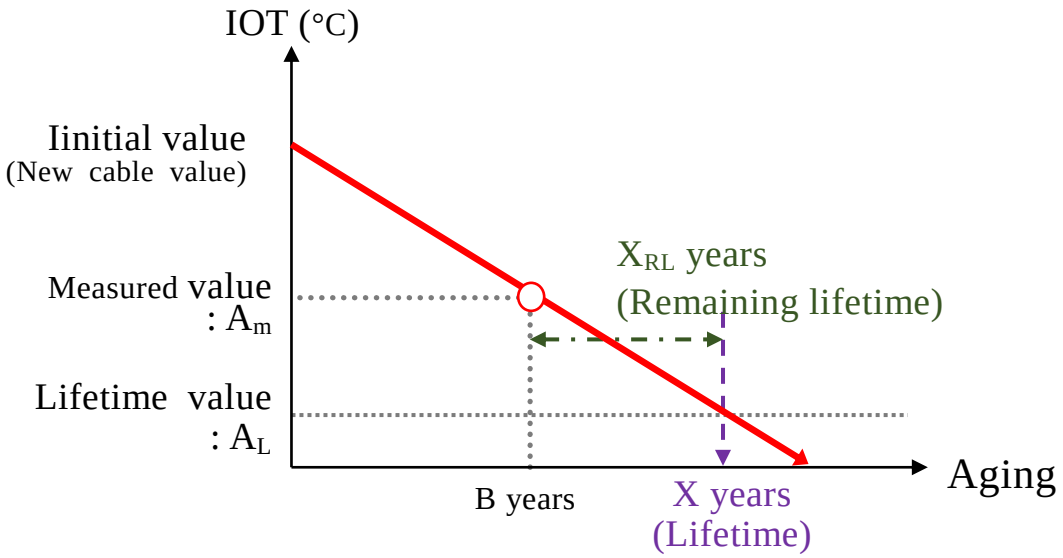

Fig 2.37 Summary of lifetime diagnostic methods

2.4 Conclusion

In this report, the thermal oxidative degradation characteristics of XLPE and EPR of CV cable insulation material are elucidated, and degradation diagnostic methods are developed based on these characteristics. The XLPE focuses on the carbonyl group, which is an oxidation product resulting from degradation. The thermal oxidative degradation characteristics of XLPE until the lifetime are a volume resistivity that does not change, and linearly increasing carbonyl groups. In addition, the characteristics are not influenced by temperature or manufacturer. A lifetime diagnosis method based on the linear increase was developed.

The thermal oxidative degradation characteristics of EPR until the lifetime are a volume resistivity that does not change and linearly decreasing OIT and IOT. The characteristics are not influenced by temperature or manufacturer. The already proposed lifetime diagnosis method based on the OIT had problems associated with accuracy and usability. Therefore, a lifetime diagnosis method by using the IOT that is based on the same principle as the OIT was developed.

Moreover, the degradation tendency of the used cables was investigated by these diagnostic methods. The possibility of a dielectric breakdown in the XLPE of 66-kV CV cables is low in the current usage scenario because the results of lifetimes obtained by the diagnosis of cables were 100 years or more. However, dielectric breakdown due to thermal oxidation degradation occurs with a 6-kV CV cable. The EPRs of the 66-kV cables confirmed the lifetime of 20 years at the shortest.

In conclusion, in the present study, thermal oxidative degradation was confirmed to be one of the breakdown factors of CV cables. In addition, it is expected that the developed lifetime diagnosis method becomes widely adopted in the future.

REFERENCES

[1] A. Tanaka, M. Nakade, and T. Matsui, “Lifetime Estimation of a Tape Lapped Joint for a XLPE Cable,” T.IEE Japan, Vol. 121-B, No. 11, pp. 1532-1537, 2001.

[2] Z. Oosawa, “Prolong of Lifetime and Environmental Measures for Polymeric Materials,” Japan, OMC, pp. 16-24, 2000.

[3] The Japan Society for Analytical Chemistry, “Polymer analysis handbook,” Japan, Kinokuniya, pp. 127-135, 1995.

[4] K. Nishikida, and R. Iwamoto, “Material analysis with infrared light,” Japan, Kodansha, pp. 53, 1986.

[5] Krimm, “Fortschr Hochpolym-Fortschr,” Bd. 2, pp. 51, 1960.

[6] M. Nakade, M. Hatanaka, K. Kunii, H. Tomogane, and S. Sugimoto, “Life Estimation of XLPE Cables in consideration of Oxidative Degradation,” T.IEE Japan, Vol. 122-B, No. 1, pp. 90-95, 2002.

[7] M. Nakade, and T. Matsui, “Oxidative Degradation Characteristics of a Tape Lapped Cable Joint,” T.IEE Japan, Vol. 121-B, No. 11, pp. 1524-1531, 2001.

[8] K. Nakayama, T. Watanabe, Y. Ohtake, and M. Furukawa, “Accuracy and Degradation Detection by the Dynamic Method and the Isothermal Method Using Differential Scanning Calorimetry,” Japan, Nippon Gomu Kyokaishi, Vol. 81, No. 11, pp. 447-453, 2008.

[9] K. Nakayama, T. Watanabe, Y. Ohtake, and M. Furukawa, “Degradation Detection of Vulcanized Rubbers and Plastics Using Initial Oxidation Temperature,” Japan, Nippon Gomu Kyokaishi, Vol. 81, No. 11, pp. 467-472, 2008.

[10] M. Inamine, Y. Mizutani, H. Shinkai, and A. Matsuda, “Applicability of Thermoanalysis methods to Evaluation for Thermal Degradation of EP-Rubber O-rings in Substation Equipments,” Japan, Transactions of JSME Ibaraki Lecture, No. 906, 2010.

Chapter 3 Detecting water tree degradation of insulating materials for CV cables

3.1 Introduction

In this chapter, the water tree degradation characteristics of CV cable insulation are investigated, and the degradation diagnostic methods are developed. Moreover, ions in water trees that become one of the degradation factors are the points of focus of this chapter. The ions affect the generation and development of water trees [1-3]. In fact, the hazardousness assessment of dielectric breakdown of the ion species has been indirectly estimated through accident records, the development trend of water trees, conductivity, and so on [2-5]. In addition, the direct hazard of water trees has been evaluated by the length of water trees [1]. Thus, the direct hazard assessment method via the viewpoint of ions was thought to be necessary.

The conventional investigation of water trees was optical observation of the sliced insulation (XLPE). Ions in the water trees were estimated by using elemental analysis performed with scanning electron microscopy with energy dispersive X-ray spectroscopy (SEM-EDX). However, most of the water trees were buried in the sliced XLPE. As a result, the analysis methods by SEM-EDX required time and skill to put out the measuring point, and polyatomic ions were difficult to qualify by using SEM-EDX. The relationship between ions and the development of water trees could not be fully clarified using SEM-EDX. Therefore, the elucidation of this relationship required new analytical methods using which polyatomic ions can be analyzed.

First, in this study, the measurement methods that can be used to analyze polyatomic ions are developed. Moreover, the relationship between ions and the development of water trees is discussed using the developed methods. The points of view are the development speed of water trees in each ion species, tree shapes, and AC breakdown voltage value. The results indicate the relationship between ion species and water tree insulation performance. In fact, the hazardousness of water trees can be determined based on the results. Thus, the hazardousness assessment methods for water trees via discriminating ion species is developed.

3.2 Development of ion analysis methods in water trees

3.2.1 Development methods

(1) Simulated water trees

a. Samples

XLPE block samples were cut out from CV cables and processed. Fig 2.1 shows the block sample shape. An electrolyte aqueous solution was filled into the water needle with a centrifugal separator. The centrifugal separator used was a CR3i (Thermo Fisher Scientific K.K., USA).

b. Methods

Fig 3.2 shows the electric charging test method. The water trees were generated and developed via electric charging for 150 days at 1 kHz, 2 kV. The temperature of tap water was set to 60 °C, which was the simulated assumed temperature of XLPE in used cables. Table 3.1 shows the electrolytes used.

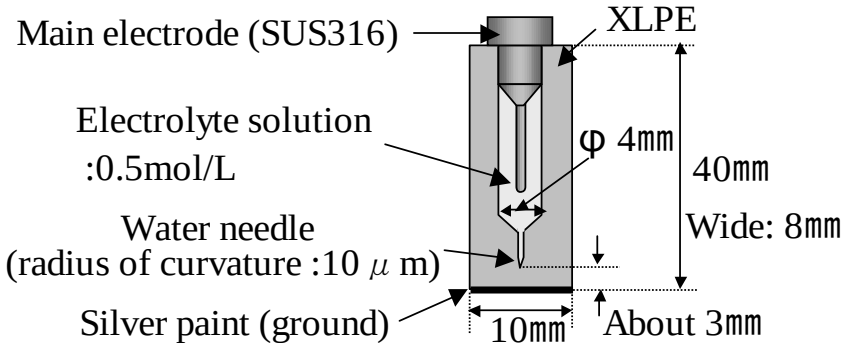

Fig 3.1 Block sample of XLPE

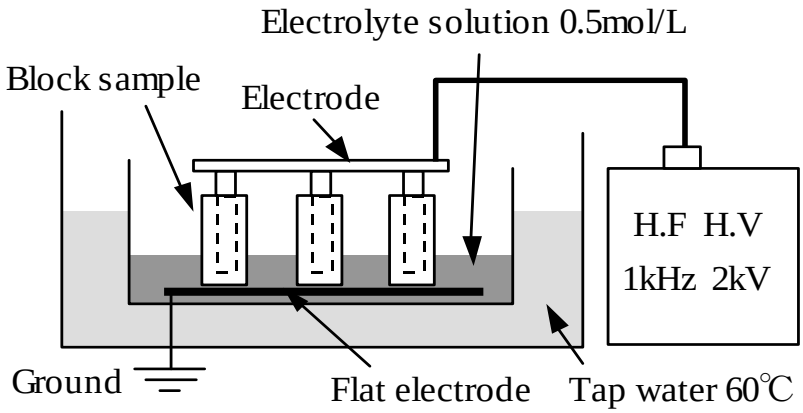

Fig 3.2 Electric charging test method

Table 3.1 Electrolytes and ions in aqueous solution

Electrolyte	Cation	Anion
$FeSO_4$	Fe^{2+}	SO_4^{2-}
$Fe_2(SO_4)_3$	Fe^{3+}	SO_4^{2-}
$MgSO_4$	Mg^{2+}	SO_4^{2-}
CH_3COONa	Na^+	CH_3COO^-
$Mg(CH_3COO)_2$	Mg^{2+}	CH_3COO^-
$(CH_3COO)_2Ca$	Ca^{2+}	CH_3COO^-
$FeCl_2$	Fe^{2+}	Cl^-
$MgCl_2$	Mg^{2+}	Cl^-
$CaCl_2$	Ca^{2+}	Cl^-

(2) Analysis methods

The measurement point was any selected point of the water tree part. The measurement was a transmission method using a microscopic FTIR. The samples were sliced to approximately 0.5 mm including water trees. The measurement conditions were an MCT-A* detector, a scan number of 32 or 64 times, a resolution of 8 cm^{-1}, and an aperture size of 50 or 100 μm. In addition, some samples were measured for area mapping. The measurement area was an arbitrary area including the water tree. The measurement unit of the mapping was 100 μm × 100 μm. The mapping conditions were an MCT-A* detector, a scan number of 4 times, and a resolution of 8 cm^{-1}. The microscopic FTIR was performed using a Nicolet Continuμm IR microscope (Thermo Fisher Scientific K.K., USA).

(3) Research methods

a. Moisture removal in water trees

The absorption peaks of water appear largely in the vicinity of 3400 cm^{-1} and 1640 cm^{-1} due to the water in a water tree [6]. As a result, it is possible that the peak of ions disappears due to the absorption of water. Moreover, the absorption spectrum of monoatomic ions cannot be measured. Therefore, the water was removed via a vacuum drying treatment at 70 °C, and the ions remained in the water tree as an electrolyte. As a result, it was confirmed that the electrolyte remaining in the water tree could be measured using FTIR.

b. Removal of XLPE absorption

The spectrum of the water tree part measured after the moisture removal contains the absorption peaks of the electrolyte and XLPE. The absorption peak of organic salt is around 1580 cm^{-1} and the absorption peak of inorganic salt is around 1140 cm^{-1}, but the specific qualitative analysis methods have not been shown [1]. In other words, the spectrum of the

electrolyte is the difference spectrum between this spectrum and the spectrum of XLPE. In addition, the spectrum of XLPE was the spectrum of the healthy part. However, it is possible that the absorption peaks of XLPE become disturbance peaks of the electrolyte because of large absorption peaks. Therefore, the difference spectrum between the water tree part and the healthy part measured after the moisture removal was confirmed to be shown the spectrum of the electrolyte.

c. Effect of boiling

For investigating a water tree, it is first dyed by boiling, because the water tree is almost colorless. As a result, it is possible that the situation of electrolyte in water trees changes due to the boiling. In that case, the measurement using FTIR after the boiling becomes impossible. Therefore, the changes in the electrolytic solution before and after the boiling were confirmed. The presence or absence of the changes was compared between the difference spectrum and the distribution of the electrolyte before and after the boiling. The area mapping of electrolyte peak was measured using FTIR. The sample was a blue water tree of a used cable, and the XLPE that included the water tree was sliced to approximately 0.5 mm. The water tree in the slice was confirmed using a metallurgical microscope. The metallurgical microscope used was an EPLIPSE ME600D (Nikon Corporation, Japan). The slice was stained by boiling it in methylene blue solution at 95 °C for 20 min.

3.2.2 Development results

(1) Moisture removal in water trees

Fig 3.3 shows an example of the spectra of a water tree in sodium acetate before and after moisture removal.

The peaks other than for XLPE before moisture removal were for water and acetate ion. However, the peaks other than for XLPE after the moisture removal was only the peak for the electrolyte. The other electrolytes listed in Table 3.1 also showed the same results.

(2) Removal of XLPE absorption

Fig 3.4 shows the difference spectrum of calcium acetate and the spectrum of calcium acetate powder. The two spectra are the same. In addition, the difference spectrum in the vicinity of 2900 cm^{-1} and 1400 cm^{-1} were no peak data because the peaks were saturated. The other electrolytes listed in Table 3.1 also showed the same results.

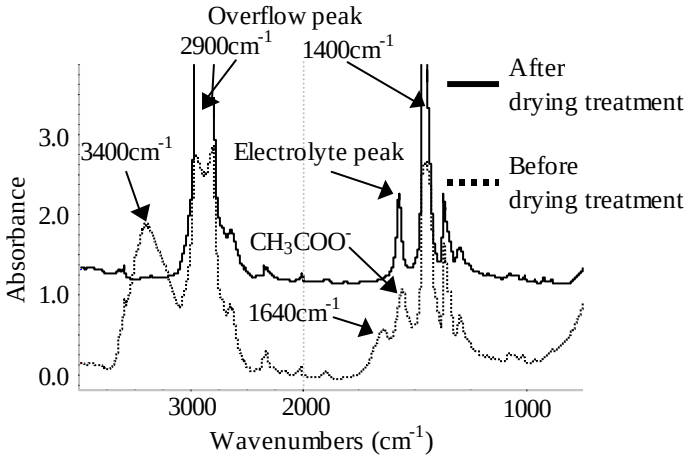

Fig 3.3 Spectra of water tree part before and after drying treatment

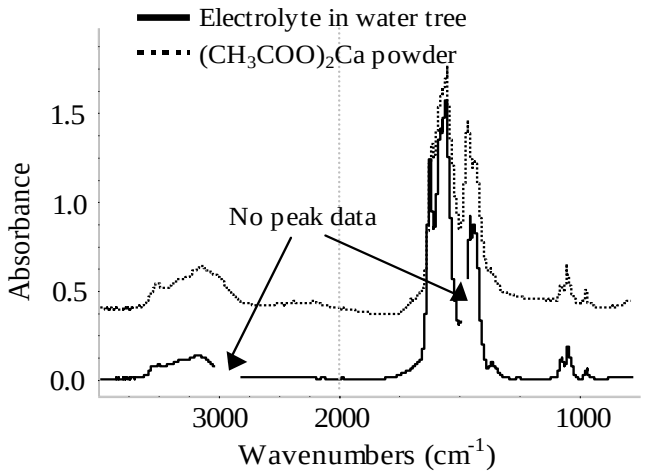

Fig 3.4 Comparison between difference spectrum and calcium acetate

(3) The effect of boiling

Fig 3.5 shows the difference spectra after boiling. For comparison, the difference spectrum of a block sample using magnesium acetate that was not boiled was added. The two difference spectra are the same.

Fig 3.6 shows the distribution of the largest magnesium acetate peak at 1590 cm^{-1} before and after boiling. Its distribution did not change.

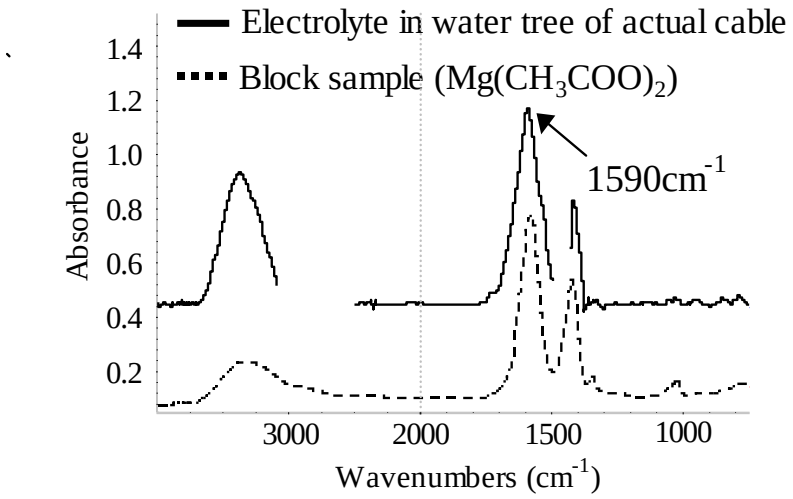

Fig 3.5 Comparison of difference spectra after and no boiling

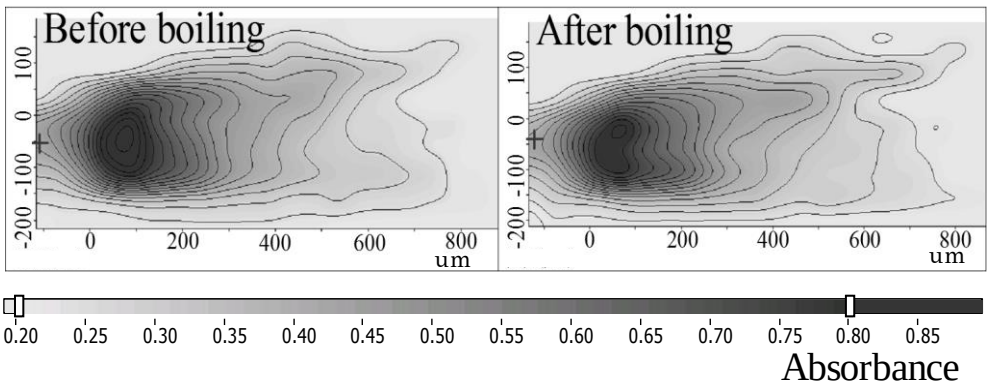

Fig 3.6 Absorbance distribution of 1590 cm^{-1} before and after boiling

3.2.3 Discussion

The electrolyte peaks in water trees after moisture removal could be measured. Therefore, the effect of moisture could be removed by moisture removal. The difference spectrum was a sufficient spectrum to identify calcium acetate. As a result, the ions in the water tree could be identified as calcium and acetate ions because the electrolyte is calcium acetate. Moreover, the electrolyte does not change by boiling. In other words, the qualitative analysis of the electrolyte in water trees is possible via the difference spectrum after moisture removal. Thus, polyatomic ions such as acetate ions in the water tree can be identified through the identified electrolyte.

3.3 Relationship between development speed and ions

3.3.1 Research methods

(1) Samples

The block samples that simulated water trees as described in 3.2.1 were diverted to the samples.

(2) Confirmation methods of development speed

The development speed was confirmed by the length of a water tree after 150 days of charging. The length of the water tree was measured with a microscope from the tip of a water needle to the tip of the water tree. The microscope used was a VHX2000 (Keyence Corporation, Japan).

3.3.2 Results

Table 3.2 shows the length of each water tree after charging. The tendency of cations was long for the sodium ion (Na^+) and magnesium ion (Mg^{2+}) and was short for the ferrous ion (Fe^{2+}) and the calcium ion (Ca^{2+}). The tendency of anions was short for the chloride ion (Cl^-) and was the same for the sulfate ion (SO_4^{2-}) and acetate ion (CH_3COO^-).

3.3.3 Discussion

The relationship between ions and development speed is strongly influenced by cations [2] [3] [5]. The experimental results almost matched the past reports.

Hazardous ions are sodium and magnesium ions owing to their development speed. The results indicate that the hazardousness assessment based on development speed can be performed by identifying ions.

Table 3.2 Progress length of water trees

Electrolyte	Cation	Anion	Length (μm)
$FeSO_4$	Fe^{2+}	SO_4^{2-}	379.5
$Fe_2(SO_4)_3$	Fe^{3+}	SO_4^{2-}	599.7
$MgSO_4$	Mg^{2+}	SO_4^{2-}	1622.1
CH_3COONa	Na^+	CH_3COO^-	2298.7
$Mg(CH_3COO)_2$	Mg^{2+}	CH_3COO^-	1905.9
$(CH_3COO)_2Ca$	Ca^{2+}	CH_3COO^-	772.6
$FeCl_2$	Fe^{2+}	Cl^-	58.4
$MgCl_2$	Mg^{2+}	Cl^-	391.8
$CaCl_2$	Ca^{2+}	Cl^-	177.8

3.4 Degradation characteristics of used cables

3.4.1 Confirmation methods

(1) Samples

The samples were 40 water trees in 17 lines of the 66-kV CV cables. The samples were sliced XLPE at arbitrary parts in the cable to approximately 0.5 mm. The slice samples were stained by boiling in methylene blue solution at 95 °C for 20 min.

(2) Confirmation of water trees

The water trees in the slices were confirmed by using a metallurgical microscope. The metallurgical microscope used was an ECLIPSE ME600D (Nikon Corporation, Japan).

(3) Qualitative analysis of ions in water trees

The electrolytes and ions were identified by the developed analysis methods. The measurement method and equipment used were the same as that described in 3.2.1.

(4) Elemental analysis of foreign matters at generating point of water trees and water trees

The foreign matters at generating point of water trees and water trees were observed and elemental analysis was carried out using SEM-EDX after qualitative analysis of the ions.

A slice containing foreign matter was gradually cut from the slice surface using a cryo-ultra microtome, and the slice was cut until the foreign matter appeared on the slice surface. The cutting temperature was set to −130 °C lower than the glass transition temperature of XLPE. The cryo- ultra microtome used was an EM UC6 and FC6 (Leica Microsystems GmbH, Germany).

3.4.2 Results

Table 3.3 shows the results of ion analysis and elemental analysis in water trees. There are some important points.

- If more than one electrolyte is detected in a water tree, the number of "Number of times of detection" in Table 3.3 is counted with each electrolyte.
- The composition elements of the foreign matters at generating point of water trees are classified into the major elements in the composition (main element) and the elements detected in a small amount or a part (small amount of element).
- The elements detected only in a part of the foreign matters are given in parentheses.
- The tree are classified on the basis of the following shapes: tree shape (T), needle shape (N), or marimo shape (M). Water trees are classified under these categories

regardless of whether a tree is a vented tree (VT) or a bow-tie tree (BTT). Fig 3.7 shows an example of the shapes of water trees.

Most of the anions were sulfate ion (SO_4^{2-}) and acetate ion (CH_3COO^-). Many of the cations were sodium ion (Na^+), magnesium ion (Mg^{2+}), and calcium ion (Ca^{2+}). The anions of ferrous ion (Fe^{2+}), ferric ion (Fe^{3+}), cuprous ion (Cu^{2+}), and zinc ion (Zn^{2+}) were limited to sulfate ion (SO_4^{2-}). The electrolyte that was detected comparatively many times was magnesium acetate. The most common shape was the marimo. The electrolytes in the tree-shaped water trees were iron sulfate and copper sulfate, and that in the needle-shaped water trees were parts of magnesium acetate, calcium acetate, and magnesium sulfate. The main elements of the foreign matter in ferrous ion (Fe^{2+}), ferric ion (Fe^{3+}), cuprous ion (Cu^{2+}), and zinc ion (Zn^{2+}) were iron (Fe), copper (Cu) and zinc (Zn) that were the same as each ion. However, the elements of the foreign matter in sodium ion (Na^+), magnesium ion (Mg^{2+}), and calcium ion (Ca^{2+}) were not a main element but a small amount of elements.

Table 3.3 Ion analysis and elemental analysis in water trees of used cables

Electrolyte	**Cation**	**Anion**	Shape and Number of times of detection (Shape:Number)		length (μm)	Elements of foreign matters at generating point of water trees			
						Main element		Small amount of element	
			BTT	VT		**Related to the ion**	Unrelated to the ion	**Related to the ion**	Unrelated to the ion
$FeSO_4$	**Fe^{2+}**	**SO_4^{2-}**	T:2	T:5	20–600	**Fe**		**S**	(Si, Cu)
$Fe_2(SO_4)_3$	**Fe^{3+}**	**SO_4^{2-}**	T:1	T:1	400–1400	**Fe**		**S**	
Na_2SO_4	**Na^+**	**SO_4^{2-}**	M:7		300–1000	**(Na)**	(Cavity)	**(Na), S**	(Fe, Cl, and others)
$MgSO_4$	**Mg^{2+}**	**SO_4^{2-}**	M:1	N:1	400–1200		Si	**Mg, S**	(Cu and others)
$CaSO_4$	**Ca^{2+}**	**SO_4^{2-}**	T:1		900		Cavity	**Ca, S**	
$CuSO_4$	**Cu^{2+}**	**SO_4^{2-}**	T:3 M:1		700–2100	**Cu, (S)**		**(S)**	(Fe, Sn, and others)
$ZnSO_4$	**Zn^{2+}**	**SO_4^{2-}**	M:1	M:1	1100–2200	**Zn, S**			
CH_3COONa	**Na^+**	**CH_3COO^-**	M:3		300–500	**(Na)**		**(Na)**	(Mg, Cl, Fe)
$Mg(CH_3COO)_2$	**Mg^{2+}**	**CH_3COO^-**	M:5	N:2 M:4	400–3900		Si	**Mg**	(Ca, Fe, and others)
$(CH_3COO)_2Ca$	**Ca^{2+}**	**CH_3COO^-**	M:5	N:1 M:1	400–3800	**(Ca)**	Si	**(Ca)**	(Mg, Fe, and others)
$Mg_3(PO_4)_2$	**Mg^{2+}**	**PO_4^{3-}**		M:1	400–600	**P**	Si	**Mg**	Ca, Fe

(a) Tree [T]

(b) Needle [N]

(C) Marimo [M]

Fig 3.7 Shapes of water trees

3.4.3 Discussion

The water trees of the tree and needle shapes are highly hazardous, because electric field analysis reveals that dielectric breakdown can occur due to the water trees of these shapes under operating voltage [4]. Therefore, highly hazardous electrolytes are iron sulfate, copper sulfate, magnesium acetate, and calcium acetate. The results indicate that the water trees containing these electrolytes can be considered to be highly hazardous.

The types of ions in the water trees are determined through the construction elements of the foreign matters at generating point of water trees. Moreover, ions and foreign matters were related to the ionization tendency. The ionization tendency of sodium, magnesium, and calcium is strong, and the ionization tendency of iron, copper, and zinc is weak. In fact, in the case of water trees containing sodium ion, magnesium ion, and calcium ion, the elements in the foreign matters were small. In addition, in the case of water trees containing iron ion, copper ion, and zinc ion, the elements in the foreign matters were a main element. Therefore, the strength of ionization tendency and the content in foreign matter were inversely proportional. The results indicate that ion species can be estimated via the elemental analysis of foreign matters and the hazard can be assessed.

Herein, the relationship between the water tree length and the electrolyte was unknown, because the age of use and environment also affect its length.

3.5 Relationship between ion and insulation performance

3.5.1 Confirmation methods

(1) Samples

The block samples that simulated water trees in 3.2.1 were diverted for this confirmation. However, the electrolytes of the block samples were only magnesium acetate and iron sulfate (II). Magnesium acetate is the most detected electrolyte in used cables. Iron sulfate (II) is one of highly hazardous electrolytes in water trees. The remaining insulation thickness of the block samples in magnesium acetate were 2750, 2500, 2000, 1500, 1000, 500, 0 μm, and in iron sulfate (II) were 2750, 2500, 2000 μm. Herein, the remaining insulation thickness was the distance between the water tree tip and the ground surface on the block sample. The distance of the block sample was measured with a microscope. The microscope used was a VHX2000 (Keyence Corporation, Japan). Iron sulfate (II) was abandoned to produce less than 2000 μm because the development speed of the water tree was slow.

(2) Confirmation of water tree shape

The water tree shape in the block samples and used cables were confirmed to be the same. The shape was observed with a microscope. The microscope used was a VHX2000 (Keyence Corporation, Japan).

(3) Confirmation of electrolyte spectrum

The electrolyte spectra of the block samples and used cables were confirmed to be the same. The electrolyte spectra were confirmed using the developed ion analysis method, and the block samples of iron sulfate (III) as described in 3.2.1 were added. Herein, the matching of magnesium acetate was already confirmed at the time of effect confirmation of boiling shown in 3.2.2 (3). The measurement conditions were an MCT-A* detector, a scan number of 64 times, a resolution of 8 cm^{-1}, and an aperture size of 100 μm. The microscopic FTIR used was Nicolet Continuμm (Thermo Fisher Scientific K.K., USA).

(4) AC breakdown voltage test

Fig 3.8 shows the AC breakdown voltage test methods. The temperature of the silicone oil was 60 °C, which is the same temperature as the voltage impression test of the block samples shown in Fig 3.2.

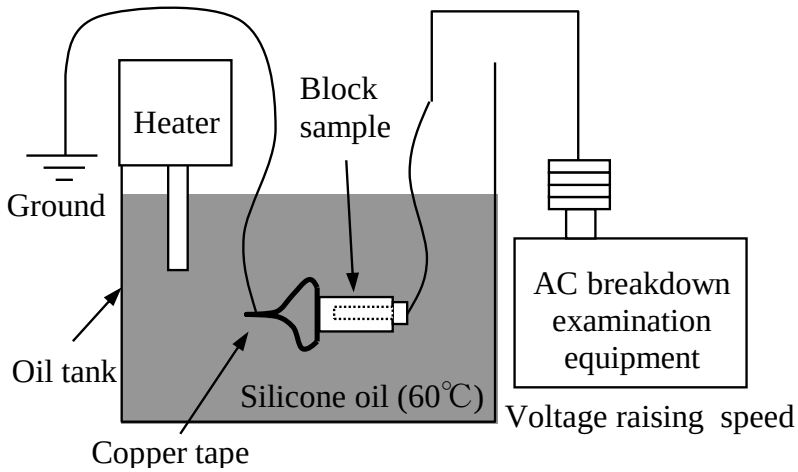

Fig 3.8 AC breakdown test methods

(5) Investigation of breakdown aspects

The block samples were sliced to a thickness of approximately 0.5 mm after the AC breakdown test. The breakdown aspects were observed in the slices by using a microscope. The microscope used was a VHX2000 (Keyence Corporation, Japan). The investigation samples were magnesium acetate with a remaining insulation thickness of 1500 and 0 μm, and iron sulfate (II) with a remaining insulation thickness of 1500 μm. The magnesium acetate of 0 μm was bridging water trees.

The distribution of electrolyte was confirmed by line mapping by using microscopic FTIR. The measurement samples were magnesium acetate and iron sulfate (II) with a remaining insulation thickness of 1500 μm. The line mapping area was from the water tree tip to the ground surface on the block sample. The measurement unit of the mapping was 50 μm. The mapping conditions were an MCT-A* detector, a scan number of 32 times, and a resolution of 8 cm^{-1}. Moreover, magnesium acetate of insulation thickness 0 μm was confirmed by area mapping near the water needle. The measurement unit of the mapping was 100 μm × 100 μm. The mapping conditions were an MCT-A* detector, a scan number of 4 times, and a resolution of 8 cm^{-1}. Microscopic FTIR used was a Nicolet Continuμm (Thermo Fisher Scientific K.K., USA).

(6) Relationship between remaining insulation thickness and AC breakdown voltage value

The remaining insulation thickness was measured again for the slices with a microscope and was compared with the breakdown voltage value.

3.5.2 Results

(1) Confirmation of water tree shape

Fig 3.9 shows the aspect of the water trees. The shape of the iron sulfate (II) was tree. The shape of the magnesium acetate was needle or marimo; confirming the shape was difficult in this case.

(2) Confirmation of electrolyte spectrum

Fig 3.10 shows the spectra of iron sulfate (II) and iron sulfate (III) detected in the block sample. The spectra of iron sulfate (II) detected in a used cable, iron sulfate (II) reagent, and iron sulfate (III) reagent were also added. The spectra were arranged so as not to overlap to facilitate the comparison of spectra. The peaks around 1100 cm^{-1} of the block samples were slightly divided into three unlike in the case of used cable.

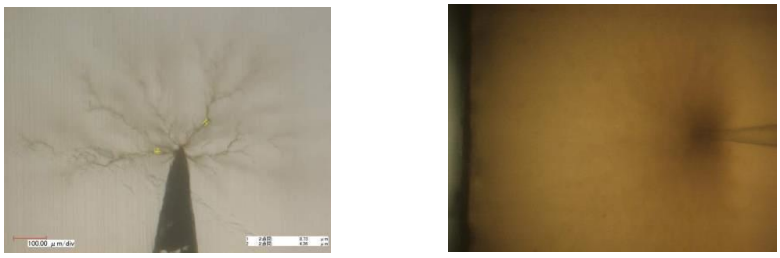

(a) Iron sulfate (II) (b) Magnesium acetate

Fig 3.9 Water tree in block sample

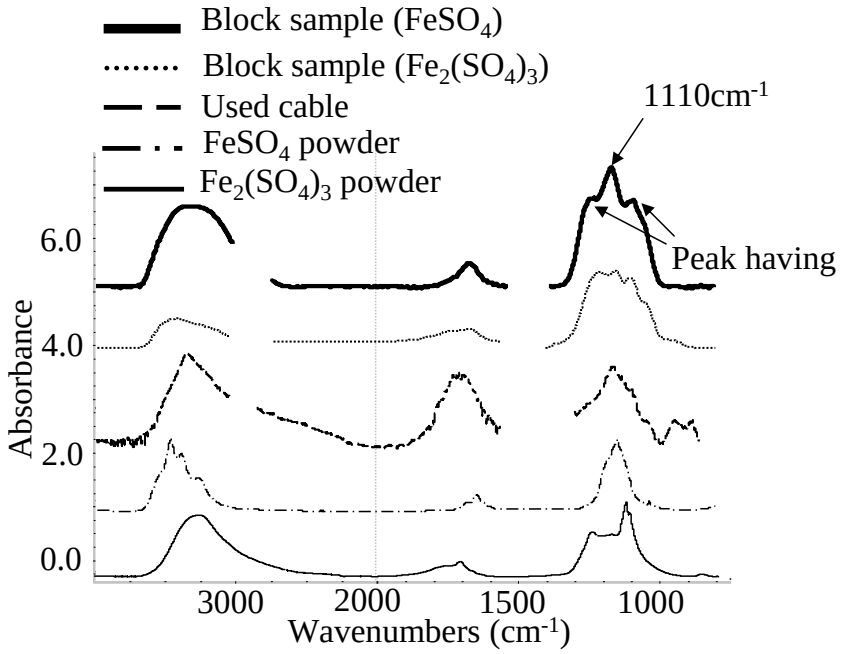

Fig 3.10 Comparison of spectra of $FeSO_4$ and $Fe_2(SO_4)_3$

(3) Investigation of breakdown aspects

a. The block samples of iron sulfate of a remaining thickness of 2000 μm and magnesium acetate of a remaining thickness of 1500 μm

Fig 3.11 shows the breakdown aspect of the iron sulfate (II). The origin of breakdown was unknown because the water tree was small. However, electric trees were generated near the tip of the water tree.

Fig 3.12 shows the breakdown aspects of the magnesium acetate. The aspects were observed before and after boiling. The origin of breakdown was near the middle of the water tree due to the aspects of the breakdown hole and electric trees.

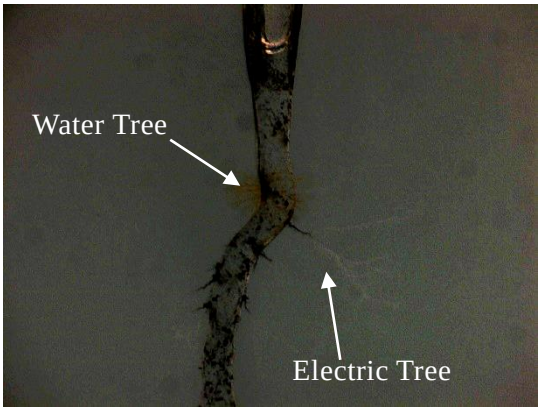

Fig 3.11 Breakdown aspect (Iron sulfate (II))

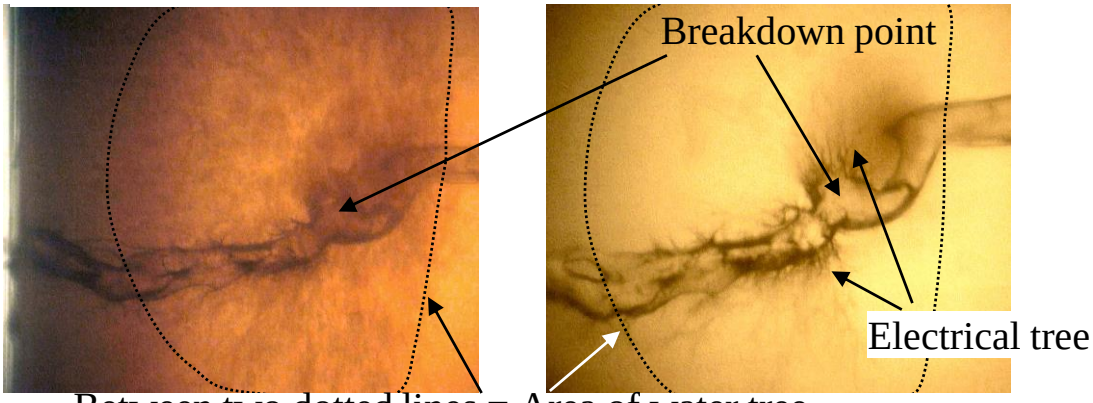

(a) After boiling (b) Before boiling

Fig 3.12 Breakdown aspect (Magnesium acetate)

Fig 3.13 shows the results of line mapping. The distribution of the electrolytes was the distribution of absorbance at 1110 cm^{-1} for the iron sulfate (II) and 1590 cm^{-1} for the magnesium acetate. The iron sulfate (II) sample was distributed considerably from the tip of the water needle to the tip of the water tree. However, the magnesium acetate sample was hardly distributed near the tip of the water tree of 1,000 to 1,500 μm from the tip of the water needle. The tendency of other samples was the same.

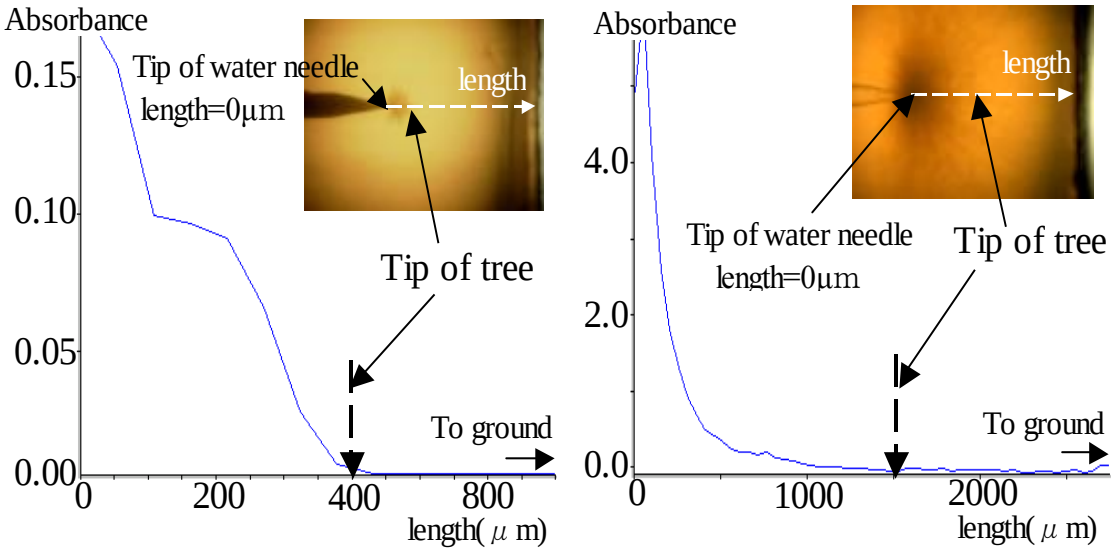

(a) $FeSO_4$ (b) $Mg(CH_3COO)_2$

Fig 3.13 Distribution of electrolyte (between water needle and ground)

b. The block samples of bridging water tree (remaining insulation thickness of 0 μm)

Fig 3.14 shows the aspect before the AC breakdown test of the water tree in magnesium acetate and the distribution of the electrolyte near the tree origin. The water tree was bridging on the side of the block sample.

Fig 3.15 shows the aspect near the tree origin after the AC breakdown test. There was no electrolyte near the tip of the tree, whereas the peak intensity of the electrolyte near the tree origin was 3 to 4 times stronger than the nonbridging tree samples. Moreover, electric trees were generated in the whole area near the tree origin. In addition, the same electric trees were confirmed to be already generated when charging was stopped before the dielectric breakdown (the charging voltage is 14 kV).

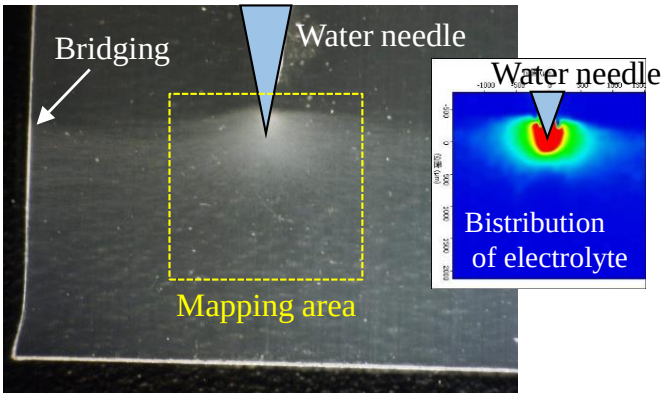

Fig 3.14 Aspect before AC breakdown test of water tree in magnesium acetate and electrolyte distribution near tree origin.

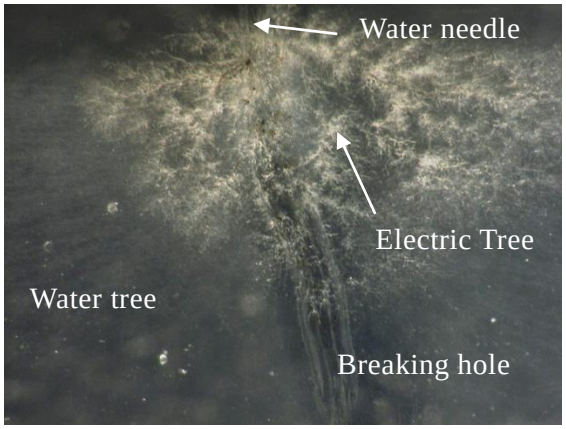

Fig 3.15 Aspect near tree origin after AC breakdown test

(4) Relationship between remaining insulation thickness and AC breakdown voltage value

Fig 3.16 shows the relationship between the AC breakdown voltage and the remaining insulation thickness. The electrolyte with the low breakdown voltage at the same remaining insulation thickness was iron sulfate (II). As the remaining insulation thickness reduced, the breakdown voltage values decreased in both electrolytes. In addition, the breakdown voltage values of bridging water trees in magnesium acetate were approximately 15–20 kV.

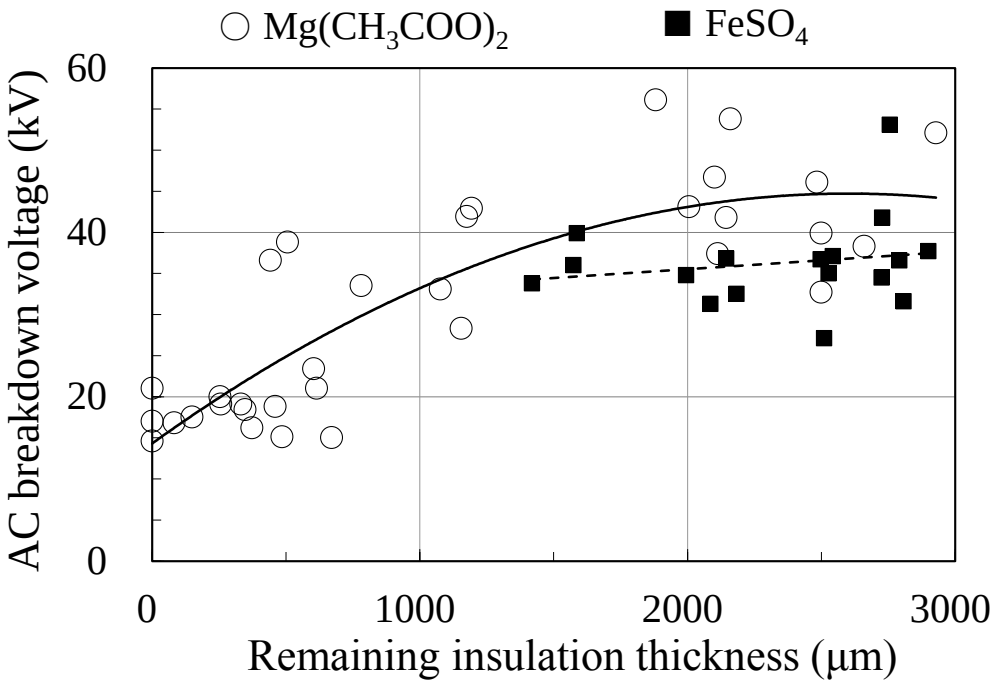

Fig 3.16 Relationship between AC breakdown voltage and remaining insulation thickness

3.5.3 Discussion

(1) Block samples and used cables

The water trees formed in the block samples of magnesium acetate have the same characteristics as that in used cables, because the shapes of the water trees and the electrolyte spectra were the same.

The water trees in the block samples of iron sulfate (II) were assessed to be having almost the same characteristics as the water trees in the used cables. The shapes of the water trees were the same as that in the used cables. The electrolytes of the used cables were iron sulfate (II), whereas the peak shapes of the electrolyte spectra of the block samples were different near 1110 cm^{-1}. In addition, the peak shapes had three peak tops, and were similar to the shape obtained by adding the iron sulfate (II) spectrum and the iron sulfate (III) spectrum. Iron sulfate (II) slowly becomes basic iron sulfate (III) due to oxidation [7]. Therefore, the part of Fe^{2+} in the water tree changed to Fe^{3+} due to this oxidation under charging. Moreover, Fe^{2+}, Fe^{3+}, and SO_4^{2-} become electrolytes due to the drying treatment at the time of measurement, and the iron sulfate (II) and the iron sulfate (III) were mixed. As a result, the electrolyte spectrum was formed by adding the iron sulfate (II) and the iron sulfate (III). In other words, it can be concluded that iron sulfate (II) was present in the block sample, because the two electrolytes were mixed in the water tree.

(2) Relationship between electrolyte distribution and dielectric breakdown

a. Water trees that had remaining insulation thickness

In previous similar studies, electric trees were generated due to the electric field concentration at the tip of a water tree, and dielectric breakdown occurred [2]. However, the destruction origin was not necessarily the tip of the water tree; the edge of the distribution area of the electrolyte was the origin. The iron sulfate (II) was distributed to the tip of the water trees, and the electric trees were generated from the tip of the water trees. The destruction origin of the magnesium acetate was not at the tip of the water trees but was near the middle of the water trees that was the edge of the distribution of the electrolyte. In other words, the edge of the distribution of electrolytes becomes the destruction origin.

The difference between the destruction origins of the two electrolytes is the influence of the tree shapes. The water trees of iron sulfate (II) had thick passes due to the shape of tree. As a result, the ions are able to reach the tip of the trees through the thick passes. However, ions in the magnesium acetate trees cannot easily reach the tip, because there is no thick pass. Therefore, when the length of the trees with different shapes is the same, the harmfulness of the tree-like water tree is higher, because the ions reach the tip of trees.

b. Bridging water tree (Magnesium acetate)

The breakdown of the bridging water trees occurs due to the electric tree formed at low voltages near the water tree origin, because the insulation performance of the whole area near the tree origin drastically deteriorates. However, the breakdown voltage value is 15 kV or more and the insulation performance is maintained, because there is no ion near the water tree tip. In fact, the remaining insulation thickness is sufficient because the edge of the ion distribution is near the water tree origin. However, the amount of ions in the distribution area increases with time and the insulation performance of the whole area deteriorates. As a result, electric trees are generated in this area at a voltage of 15 kV or less, and the electric trees become the dielectric breakdown origin. In conclusion, it is possible that their characteristics are one of the causes why dielectric breakdown does not occur in low-voltage cables with the bridging water trees.

(3) Relationship between remaining insulation thickness and AC breakdown voltage value

At first, the remaining insulation thickness was the distance from the tip of the water tree to the ground area. After that, the remaining insulation thickness changed to the distance from the breakdown point to the surface of the block sample in the breakdown direction.

Fig 3.17 shows an example of the breakdown aspects of magnesium acetate samples. The edge of the distribution of electrolyte was the breakdown point, and the breakdown position and direction were various. The results indicated that the initial idea of the remaining insulation thickness is wrong, because the breakdown point is the weakest part of the water tree.

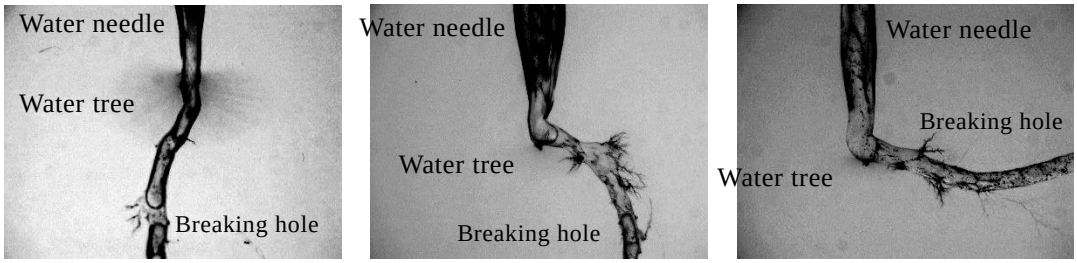

(a) (b) (c)

Fig 3.17 Examples of breakdown aspects

Fig 3.18 shows the relationship between the AC breakdown voltage value and the modified remaining insulation thickness for the water trees in magnesium acetate. In addition, the bridging water tree data were excluded due to another breakdown process. The relationship due to the modified data showed a linear increase.

Fig 3.19 shows the value of iron sulfate (II) and the precursor interruption value added to Fig 3.18 via the modified remaining insulation thickness. The approximate straight line was extended to the remaining insulation thickness of 3 mm or more. The precursor interruption value was the data on the used cable for confirming magnesium acetate. The water tree was a vented tree with an insulation thickness of 11 mm and a tree length of 1200 μm.

Iron sulfate (II) is electrically harmful than the magnesium acetate, because the breakdown voltage is lower than that for magnesium acetate. The relationship between the AC breakdown voltage value and the remaining insulation thickness is linear regardless of electrolyte types. The data of block samples correspond with the data of the used cable, because the precursor interruption value of the used cable is on the straight line. Therefore, the harmfulness of water trees can be assessed electrically via electrolyte types and the remaining insulation thickness. However, further study including other causes is necessary because the tree length and the curvature radius of the tip of a tree are not taken into consideration in this work. Besides, the number of data of the preliminary interruption value is not sufficient.

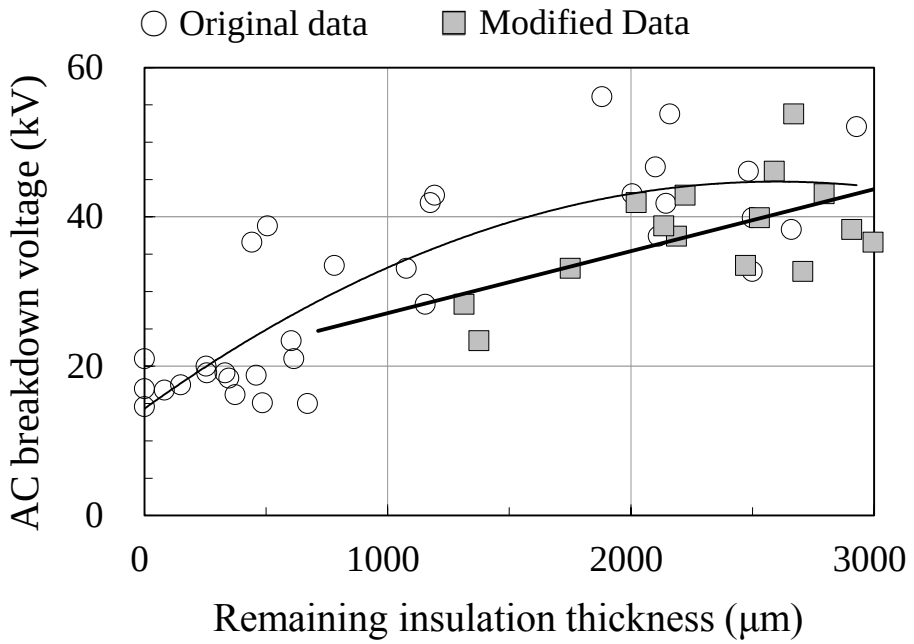

Fig 3.18 Relationship between AC breakdown voltage value and modified remaining insulation thickness for the water trees of magnesium acetate

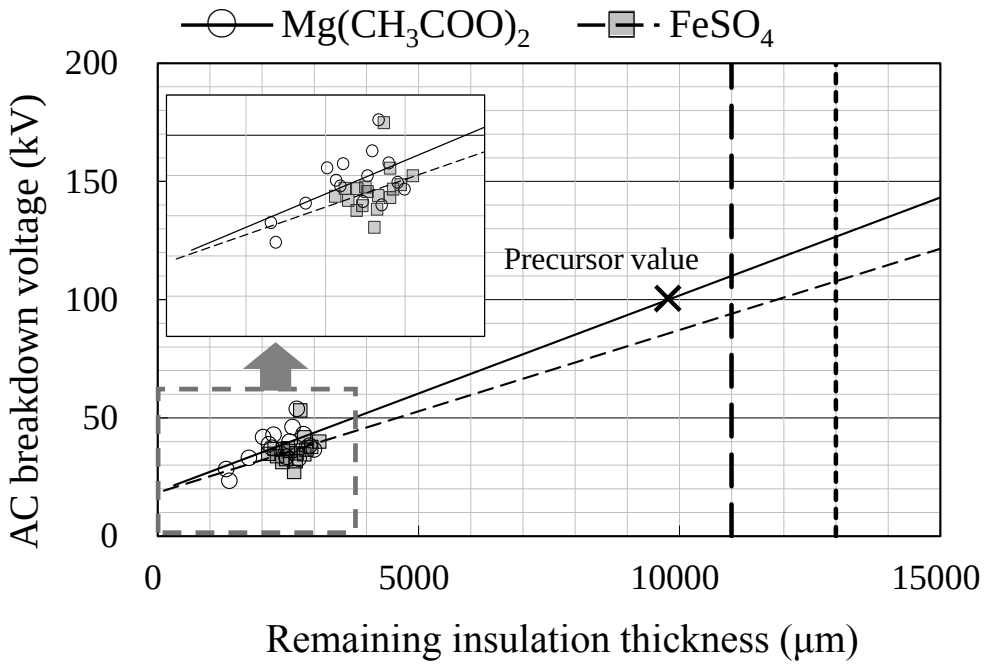

Fig 3.19 Remaining insulation thickness is a guess result of 3 mm or more

3.6 Establishment of hazardousness assessment method of water trees with ions

The hazardousness of water trees was mainly evaluated in terms of water tree length [2]. However, the ion types in water trees affect the development speed, shape, and insulation performance. Moreover, the destruction origin is not necessarily the tip of water trees but the edge of the distribution area of the ions. In other words, the hazardousness assessment in terms of water tree length alone is not appropriate. The hazardousness assessment methods confirm the types and distribution areas of electrolytes, and the hazardousness is evaluated by the electrical characteristics and the development speed for different electrolyte types. The measurement data in this paper are important as the hazardousness assessment standard. Harmful ions are magnesium acetate and iron sulfate (II) in terms of electrolytes according to the measurement data. In addition, iron sulfate (III) and copper sulfate (II) are also harmful because of the tree shape. However, further studies are needed that consider the tree length as well as the curvature radius of the tip of a tree.

3.7 Conclusion

Qualitative analysis methods of ions in water trees was developed to facilitate qualitative analysis of monatomic ions and polyatomic ions. It was confirmed that the types of electrolytes and ions are closely related with the foreign matters at generating point of water trees by using the methods. In addition, the ions in water trees were elucidated to affect the development speed, shape, breakdown origin, and insulation performance. In conclusion, it was demonstrated that the methods for assessing the hazardousness of water trees need to be evaluated by considering the types and distribution area of electrolytes, electrical characteristics, and development speed.

The developed methods will be useful for water tree analysis in the future, because the water trees are one of the major causes of degradation of CV cables.

REFERENCES

[1] S. Mutou, and Y. Maruyama, “Study on Chemical Characteristics of Water Tree,” 1994 National Convention Record, IEE Japan, No. 399, 1994.

[2] Technical report of IEE Japan, “Basic process of treeing degradation in polymer insulating materials,” IEE Japan, No. 674, 1998.

[3] Y. Sekii, D. Inoue, M. Okashita, H. Ima, and A. Someya, “Generation and Development of Water Tree - Impact of Polymer High Order Structure and Chemical Process - ,” Joint Study Group on Discharge and Dielectric/Insulating Material, IEE Japan, ED-0064 DEI-00-69, 2000.

[4] M. Nakade, and D. Inoue, “A Study of Characteristics of Water Tree Growth by Electric Field Analysis,” T.IEE Japan, Vol. 123, No. 6, pp. 772-777, 2003.

[5] H. Ohno, A. Toya, M. Nishimoto, F. Aida, and Y. Fujiwara, “Influence of impurity ions on water tree progress,” 1994 National convention Record, IEE Japan, No. 398, 1994.

[6] N. Kondo, and H. Miyata, “Evaluation of water in water tree by μ-FTIR,” 2001 Annual Conference of Fundamentals and Materials Society, T.IEE Japan, No. 14-8, 2001.

[7] Wako Pure Chemical Industries, Ltd, “Iron (II) Sulfate Heptahydrate,” SDS No. JW090108.

Chapter 4 Detecting electric charging degradation of insulating materials for OF cables

4.1 Introduction

In this chapter, the black parts on the insulating paper that were confirmed in used OF cables are investigated, and the degradation diagnostic methods are developed. It has been considered that OF cables do not deteriorate under the operating voltage unless pressure becomes negative. In fact, breakdown accidents because of long-term and natural degradation have hardly occurred in OF cables. However, dielectric breakdown accidents of OF cables that carry 275 kV and 154 kV have occurred in cables installed by the Tokyo Electric Power Co (TEPCO). In addition, in recent years, aged joint boxes have been disassembled and investigated [1-4]. These investigations have confirmed the presence of many black parts on the insulating paper. In Japan, the black part on the insulating paper is considered to be carbonized based on the evaluation criterion [1]. The cause of carbonization was estimated to be due to partial discharge; however, the cause of the discharge was not clarified. After that, copper sulfide was discovered on the black part by TEPCO. As a result, the cause of the accidents was considered to be electric charging degradation due to copper sulfide, and the degradation process was devised.

It is therefore necessary to study the process and origin of this copper sulfide deposition on insulating paper in OF cables for the purpose of accident prevention. The problem of copper sulfide deposition on insulating paper in OF transformers is well recognized [5] and is caused by the highly corrosive sulfur content in mineral oils. In recent years, sulfur contents have been decreasing following the introduction of improved refining techniques [5]. However, the addition of the anti-oxidant dibenzyl disulfide (DBDS) to the oils opens a new avenue for producing corrosive sulfur, and many transformer failures have occurred as a result. Therefore, many recent studies have focused on the hazardousness of DBDS [3-9]. However, since insulating oil in Japan does not use DBDS [12] and the deposition of copper sulfide was confirmed in OF cables using nonsulfurous BAB, copper sulfide is deposited in OF cables through a still unknown process. Moreover, the relationship between copper sulfide and the black part has not been not clarified.

In the present paper, the elucidation of the still unknown degradation process is discussed based on physical property investigations and the demonstration of the degradation process. In fact, degradation diagnoses by insulation oil analysis actually used did not capture the signs of dielectric breakdown due to this electric charging degradation. However, the analysis is easy to use, because the insulating oil can be taken regularly from the connector

of joint box. Therefore, in the present study, a degradation diagnosis method by performing insulation oil analysis was developed, targeting this electric charging degradation.

4.2 Qualitative analysis of the black parts on the insulating paper

4.2.1 Introduction

Copper sulfide was discovered on the black part; however, the relationship between the copper sulfide and the black part was not clarified. Therefore, the black part on the insulating paper of the used cable was analyzed anew.

4.2.2 Analysis methods

(1) Samples

The analyzed samples were insulating papers with black parts after disassembly investigation. The samples were aged joint boxes for 275-kV, 154-kV, and 66-kV cables, and were an accident box and a healthy box. Each sample was cut to a length of 10 cm. However, the insulating paper after disassembly contained insulating oil, which had to be removed prior to analysis. Therefore, the samples were naturally dried after immersion in acetone for approximately 10 min. In addition, the nonsolubility of the black parts in acetone was confirmed by optical observation. The number of samples was 22 in 11 lines.

Fig 4.1 shows an example of the analysis point. The black parts were the same as the aspect of the black part that were determined to be carbonizations in the past [1].

(2) Methods

The qualitative analysis is performed using SEM-EDX, FTIR, and Raman spectroscopy. Elemental analysis was performed with EDX after observation at ×200 magnifications with SEM. The scanning electron microscope used was a S3400N (Hitachi High-Technologies Corporation, Japan). The samples were nonevaporated. The observed images were backscattered electron (BSE) images at a low-vacuum mode of 30 Pa. The EDX used was an Edax Detecting Unit CD-S/S3400N (Ametek Ink., USA). The accelerating voltage was 15 kV.

With Raman spectroscopy, for places of weak fluorescence within the distribution of copper and sulfur, point analysis was performed. Fig 4.2 shows the standard spectra of copper(I) sulfide (Cu2S) and copper(II) sulfide (CuS) used to determine copper(I) sulfide and copper(II) sulfide. Copper sulfide was specified by the standard spectrum. The Raman spectroscope used was a Nicolet Almega XR (Thermo Fisher Scientific K.K., USA). The measurement conditions were a laser wavelength of 532 nm and a laser output of 1%. Furthermore, the lens was operated at a distance of ×100 magnifications, the exposure time was 30 s or more, and the scan number was 5 times or more.

The black deposit sample was collected with a metal needle, placed on a diamond window, and measured by the transmission method with FTIR. In addition, the absorbance difference spectra of the black deposit sample and the insulating paper were obtained. The FTIR used was a Nicolet Continuμm (Thermo Fisher Scientific K.K., USA). The measurement conditions were an MCT-A* detector, a scan number of 68 times, and a resolution of 8 cm^{-1}.

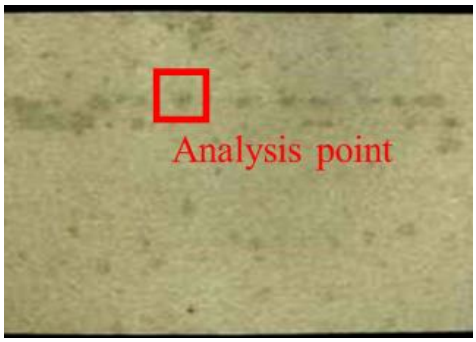

Fig 4.1 An example of the analysis point of a black part

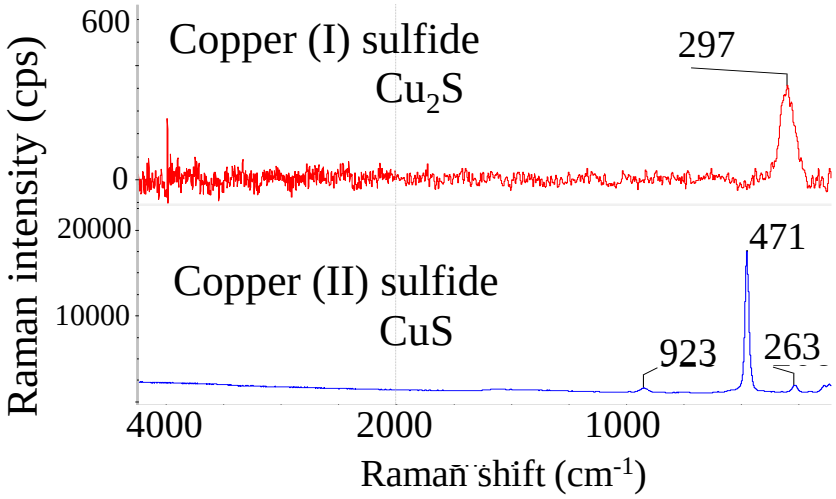

Fig 4.2 Standard Raman spectra of copper sulfide

4.2.3 Analysis results

The analysis result shows an example, because the results of the 22 samples in 11 lines were similar. Fig 4.3 shows EDX analysis results. Copper and sulfur were detected.

Fig 4.4 shows Raman analysis results. The Raman spectrum shows the 468 cm^{-1} band of copper(II) sulfide, and the 288 cm^{-1} band of copper(I) sulfide.

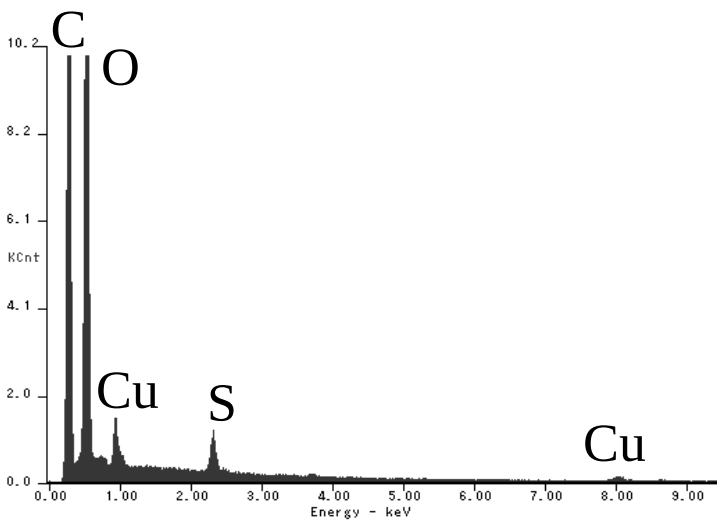

Fig 4.3 Elemental analysis result of the black part on insulating paper

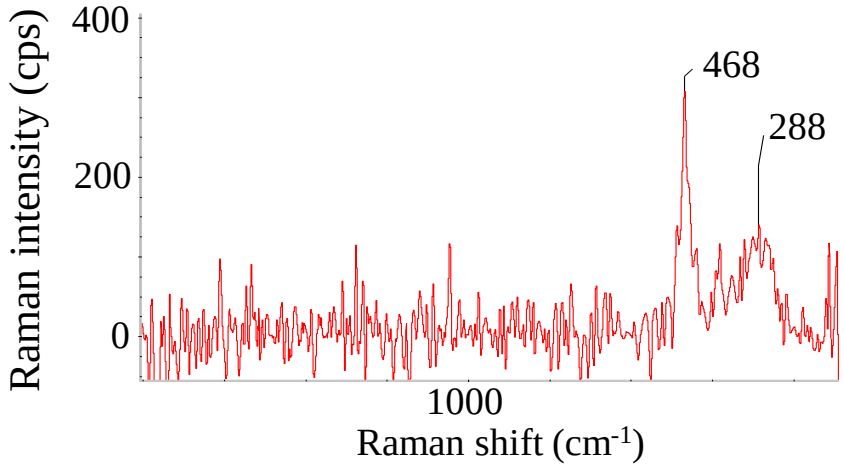

Fig 4.4 Raman analysis result of the black part at the insulating paper

Fig 4.5 shows FTIR analysis results. The marked areas indicate the IR absorption peaks corresponding to the three types of molecular structures. The peaks near 2,900 cm^{-1} and 1,400 cm^{-1} (Peak 1 in Fig 4.5) correspond to hydrocarbons, those near 3,300 cm^{-1}, 1,700 cm^{-1}, and 1,300 cm^{-1} (Peak 2 in Fig 4.5) correspond to oxidation products, and the ones near 1,100 cm^{-1} (Peak 3 in Fig 4.5) correspond to sulfur oxidation products. In addition, the 22 samples were similar in all parts.

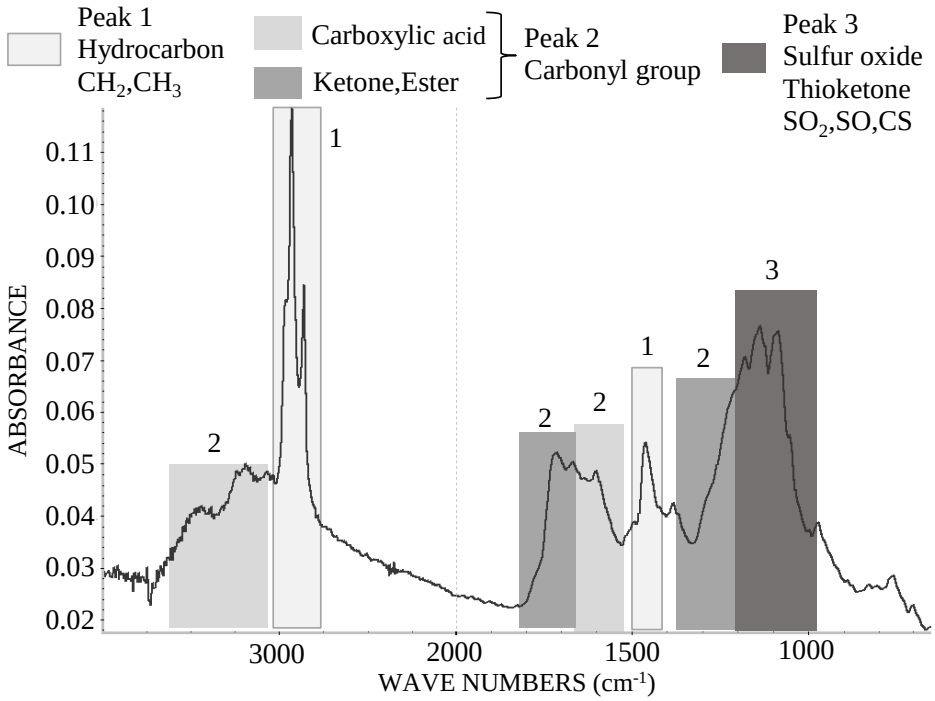

Fig 4.5 Qualitative analysis result

4.2.4 Discussion

The black parts were copper sulfide (Cu_2S, CuS) and a material (oxidation sludge) in which insulating oil was oxidized and solidified by oxygen or sulfur. In addition, this oxidized sludge was a copper compound based on Fig.4.3 and Fig.4.5. Therefore, many black parts were not carbonization due to discharge but were deposited oxidation sludge and/or copper sulfide. As a result, the copper sulfide was presumed to cause dielectric breakdown due to its conductivity. The oxidation sludge was presumed via the IR peaks of FTIR. The 22 samples were not carbonization in all parts. The insulation oil of the breakdown cables was synthetic oil; however, the black parts of the 66-kV cables containing mineral oil also were a similar trend. In other words, these black parts are generated regardless of the oil type. Fig 4.6 shows the construction of a middle joint box and the main area of deposition of copper compounds. The area is located at the central part of the insulation, such as the rising part of the reinforcing layer and/or on the cable core near the rising part.

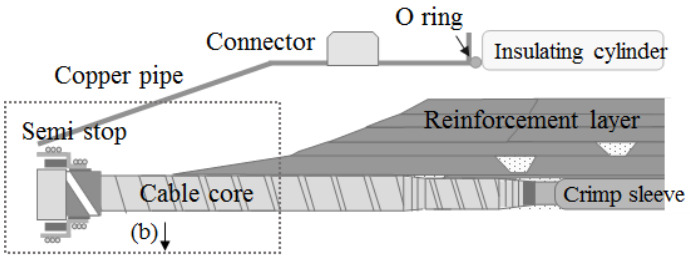

(a) Schematic of joint box

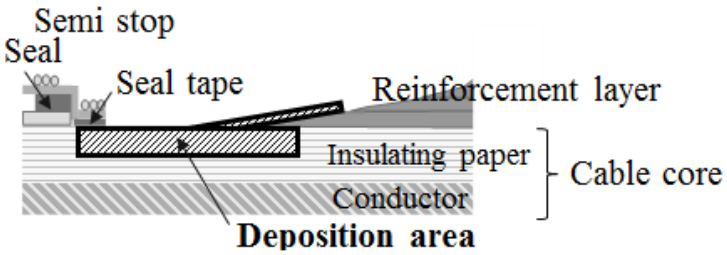

(b) Main area of deposition of copper compounds

Fig 4.6 Schematic diagram of middle joint box

4.3 Elucidation of electric charging degradation process

4.3.1 Introduction

An electrical charging degradation process has been devised; however, it has not been demonstrated. Therefore, this degradation process was demonstrated through the simulation of the process.

4.3.2 Electrical charging degradation process

Copper sulfide was confirmed in the black part by disassembly investigation, and the cause of the dielectric breakdown was presumed to be electrical charging degradation due to copper sulfide. Therefore, the degradation process was devised by TEPCO [13]. Thereafter, this process was revised, because oxidation sludge was confirmed. Fig 4.7 shows the mechanism after revision. Herein, the figure shows the location of the gap composed of the conductor and insulating paper in a cable. Table 4.1 shows the process of each step of the process.

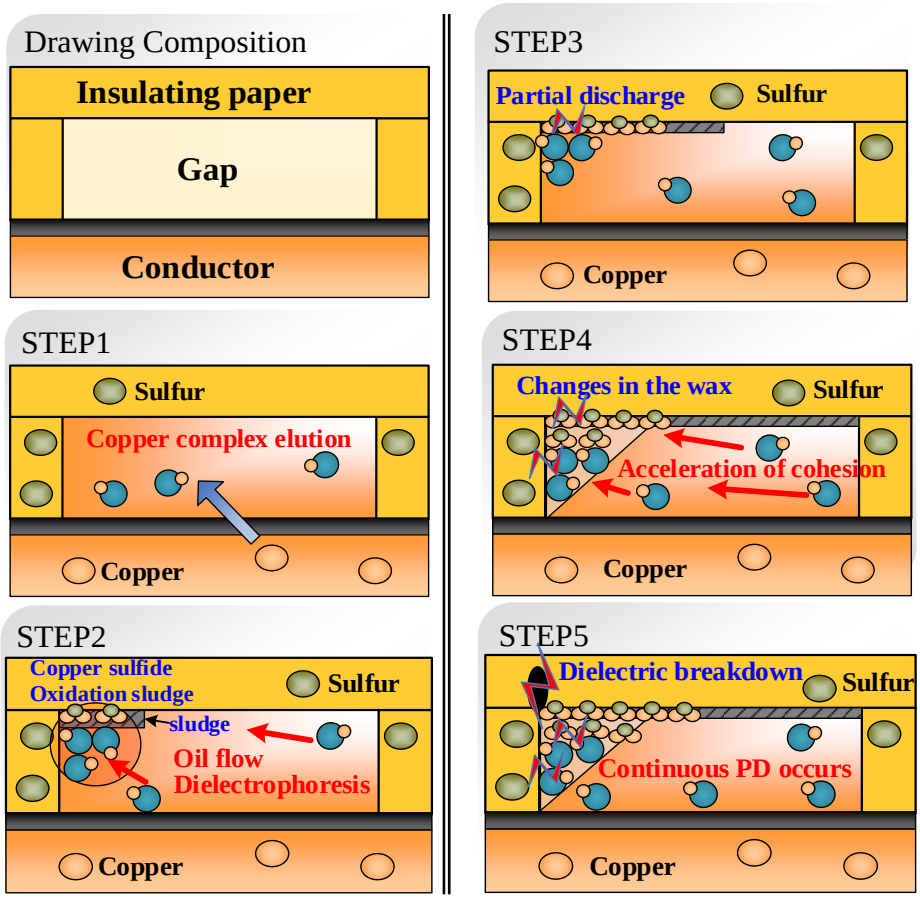

Fig 4.7 Steps of the electric charging degradation process

Table 4.1 Process of the electric charging degradation process

Step 1	Elution of the copper compound such as copper complex from the conductor.
Step 2	Aggregation of copper compound by physical methods (oil flow) or dielectrophoresis. (Generation of oxidation sludge and copper sulfide by reaction with sulfur, etc. and the release of gas by their generation. Oxidation sludge and copper sulfide are both black materials.)
Step 3	Sporadically partial discharge (PD) occurs.
Step 4	Wax is generated, and aggregation of copper compound is accelerated.
Step 5	Occurrence of continuous PD leading to dielectric breakdown.

The key for this process is the dielectrophoretic force shown in STEP 2. Fig 4.8 shows the electric-field gradient analysis model of a terminal joint box for a 275-kV cable in which a dielectric breakdown had occurred. The breakdown point was presumed to be within the same area as in the deposition area shown in Fig 4.6 due to the state of the breakdown hole. Moreover, in the terminations of the other phase in the same line, oxidation sludge and copper sulfide were frequently detected in the black regions shown in Fig 4.8. The dielectrophoretic force is calculated by using equation (1).

$$F=2\pi r^3 \varepsilon_1 \varepsilon_0 \frac{\varepsilon_2 - \varepsilon_1}{\varepsilon_2 + 2\varepsilon_1} \, grad\, E^2 \quad \cdots\cdots\cdots (1)$$

F: Dielectrophoretic force ε_1: Relative permittivity of an oil
E: Electric-field r: Radius of a particle (copper compound)
ε_2: Relative permittivity of a particle

Fig 4.9 shows the result of calculations using $gradE^2$ around the black region. The calculation software used was JMAG-Studio (JSOL Corporation, Japan). In positions e–f, the material of a high dielectric constant is confined through the resistance between dielectrophoretic forces owing to the maximization of positive or negative values of $gradE^2$. This region is also characterized by the presence of overlapping gaps because it is close to the semi stop part on the cable core, wherein disturbances are most likely to occur because of the tightening of insulating papers.

In addition, insulation oil is flowed through temperature change owing to factors such as load variations. When the oil was flowed outward from the conductor owing to a rise in the temperature of the conductor, copper compounds were arrested by dielectrophoretic forces, oxygen, and sulfur, and were consequently precipitated. After that, the reverse flow occurred due to decreases in the conductor temperature, and copper compounds were precipitated similarly in this circumstance. Copper compounds further deposited due to the heat cycle over decades, particularly, in the direction of the electric field in overlapping

gaps. Therefore, partial discharges were generated, and dielectric breakdown presumably occurred. The estimated breakdown point of copper compounds was consistent with the calculated deposition point.

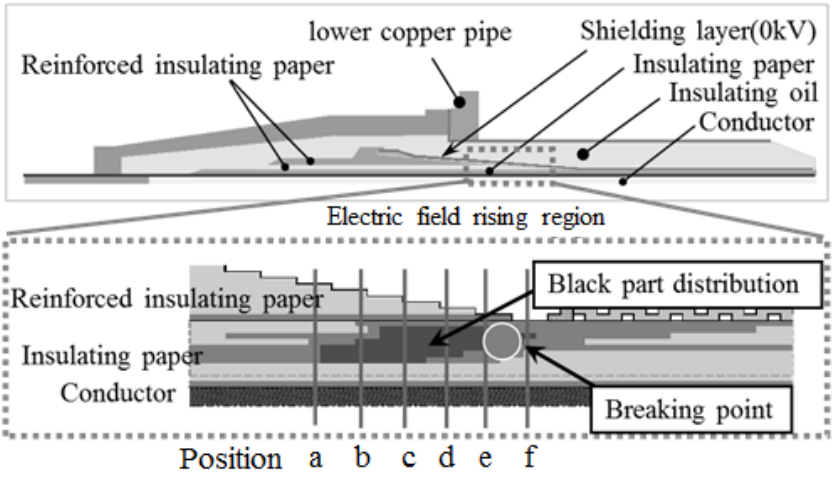

Fig 4.8 Electric-field gradient analysis model

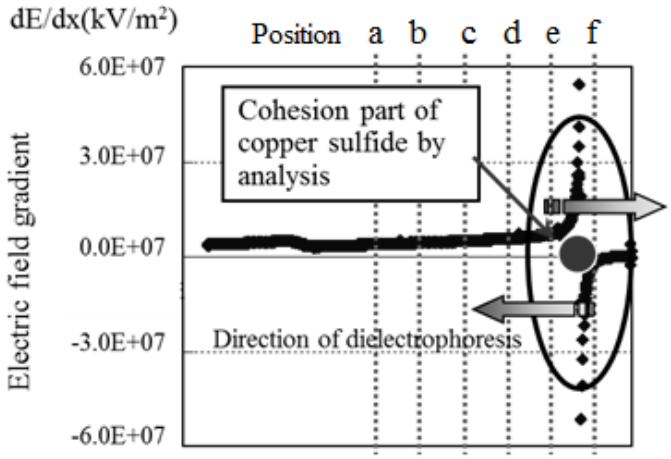

Fig 4.9 Electric-field gradient analysis result

4.3.3 Quantity of dissolved copper and sulfur in the used cable

(1) Introduction

The start of this degradation is the dissolution of copper shown in Fig 4.7. Therefore, the quantity of dissolved copper in the insulating oil of the used cables was analyzed because the dissolution of copper is demonstrated through the result. In addition, the quantity of sulfur in the oil was analyzed.

(2) Samples

Selected samples were insulating oil collected from 1352 terminal and middle joint boxes of used cables. Approximately 0.8–1.0 g of the insulating oil was an analysis sample. The analysis sample was diluted 10-fold with xylene. The xylene used was of Wako Special Grade (Wako Pure Chemical Industries Corporation, Product code 244-00081, Japan).

(3) Methods

The quantity of elements in the sample was quantitatively analyzed with inductively coupled plasma atomic emission spectrometer (ICP-AES). The target elements were copper (Cu) and sulfur (S). The measured value was the average value measured three times. The unit of the quantity (concentration) was “mg/kg (wt).” The quantitative analysis method was a calibration curve method, and four samples with different concentrations were prepared for calibration samples. In addition, the samples were prepared by dilution with standard sample, xylene, and base oil. The ICP-AES used was an iCAP6500 (Thermo Fisher Scientific K.K., USA). The standard sample used of copper was CONOSTAN Standard S-21 900 mg/kg (wt) (SCP SCIENCE Corporate, Canada). The standard sample used of sulfur was a Reference Material of Sulfur in Residual Fuel Oil, Sulfur Content 0.2 mass% level (Tokyo Chemical Industry Co, Japan). The xylene used was of Wako Special Grade (Wako Pure Chemical Industries Corporation, Product code 244-00081, Japan). The base oil used was CONOSTAN METALLO-ORGANIC STANDARDS 75 Base Oil (SCP SCIENCE Corporate, Canada).

(4) Results

Fig 4.10 shows the relationship between the quantity of dissolution copper and the aging. The trend varied regardless of aging or voltage, and the maximum was 7.9 mg/kg.

Fig 4.11 shows an example of the quantity of dissolution copper in the middle joint boxes of a same track, refueling section, and manufacturer. The difference in the trend was large in places and phases even under the same equipment conditions. In addition, the other cables showed the same trend.

The quantity of dissolution sulfur was 5.4 mg/kg on average and 62.2 mg/kg at maximum with 275-kV cables using synthetic oil, and the new synthetic oil was 5 mg/kg. Therefore,

sulfur compounds derived from petroleum at the time of production are also present in synthetic oil; however, its quantity is considerably small compared to that of mineral oil [15].

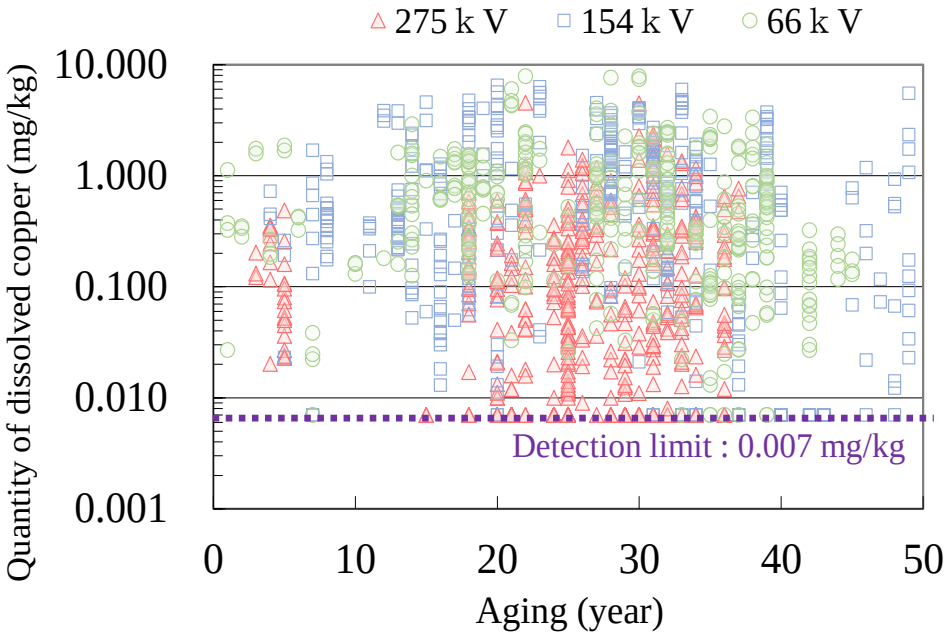

Fig 4.10 Relationship between the quantity of dissolution copper and the aging

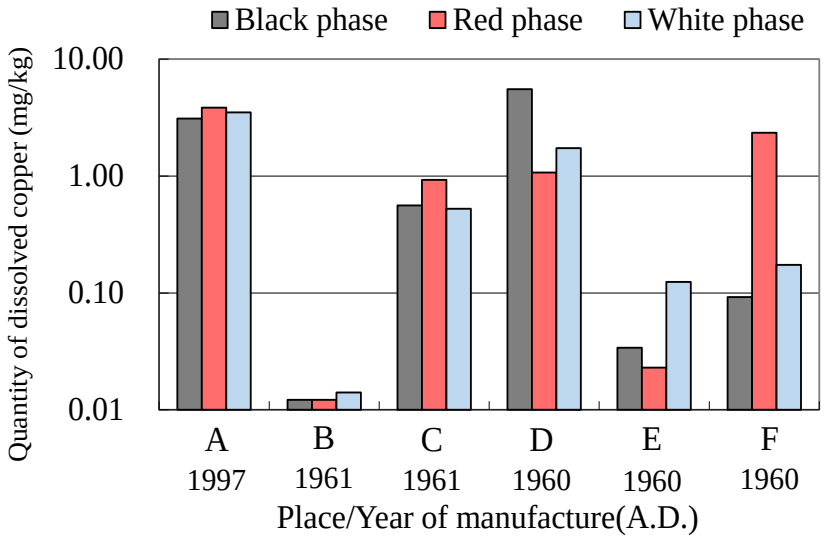

Fig 4.11 Quantity of dissolution copper at every place (same track, same refueling section, and same manufacturer)

(5) Discussion

Copper dissolves in the insulating oil of the OF cables; however, the dissolution trend is different in places even under the same equipment conditions. The data of the used cables shown in Fig 4.10 and 4.11 shows their trends.

It is possible that a part of sulfur is dissolved from the materials other than insulating oil in the OF cables, because the quantity of dissolution sulfur in a part of the used cables was more than that of the new synthetic oil. The quantity of the 66-kV cables containing mineral oil was an average of approximately 1200 mg/kg, which is clearly more than the synthetic oil. However, in the disassembled investigation of insulating paper of 66-kV cables, the electrical charging degradation did not particularly progress. Therefore, it is possible that the sulfur in oxidation sludge and copper sulfide is not derived from insulating oil. The origin of sulfur is examined in another section.

4.3.4 Dissolution trend of copper in insulating oil

(1) Introduction

The copper dissolution in the cable used was demonstrated; however, the origin of the copper was unknown. The origin of copper was considered to be the conductor and the copper pipe owing to the locality of the deposition area (cf. Fig 4.6). Therefore, the trend of copper to dissolve in insulating oil was confirmed through experiments.

(2) Methods

The dissolution trend of copper was confirmed by placing copper rods in insulating oil and heating. The insulating oil was a soft type of synthetic oil and mineral oil. In addition, the oxide film of the copper bar was checked for the influence of copper dissolution, because it is possible that the oxide film is formed on the surface of the copper bar due to the oxygen in the oil over time.

The samples were heated at 80 °C in a nitrogen atmosphere. Approximately 0.8 to 1.0 g of insulation oil in the samples was collected each arbitrary time. The quantity of dissolved copper was analyzed for the collected insulating oil. The analysis method was the same as the method of "4.3.2 Quantity of dissolved copper and sulfur in the used cable."

(3) Samples

The copper bars were acid cleaned and the oxide films were removed. Moreover, the copper bars covered with the oxide film were prepared by heating in the atmosphere. The heating condition was 8 h (thin film) and 7 days (thick film) at 105 °C. 390 g, 260 g, and 130 g of acid-cleaned copper bars were prepared. 130 g of copper bars covered with oxide film were prepared. Each copper bar was placed in each insulating oil of 200 mL.

(4) Results

Fig 4.12 shows the relationship between the quantity of copper bar (acid cleaning) and the quantity of dissolution copper. The dissolution quantity was 1 mg/kg or more in a short time and 29 mg/kg at maximum in synthetic oil. The quantity of synthetic oil tended to be more than that of mineral oil. The dissolution quantity showed a saturation trend with time. In addition, the dissolution rate of the small quantity of copper bars was slow, and the quantity of dissolution showing a saturation trend was also small.

Fig 4.13 shows the relationship between the surface oxide of a copper bar and the quantity of dissolution copper. The dissolution quantity showed a saturation trend with time. The dissolution rate was slower as the oxide film of the copper bars was thick, and the quantity of dissolution showing a saturation trend was also small.

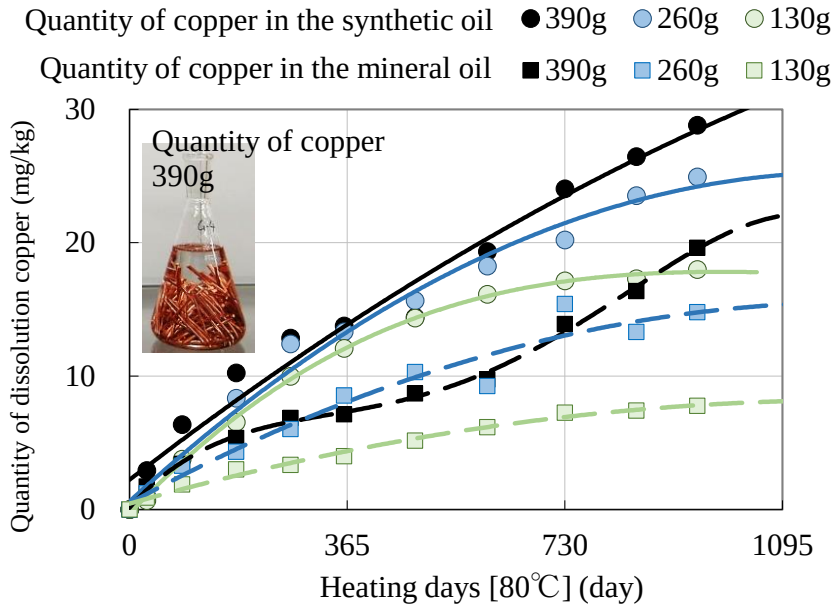

Fig 4.12 Relationship between the quantity of copper bar and the quantity of dissolution copper

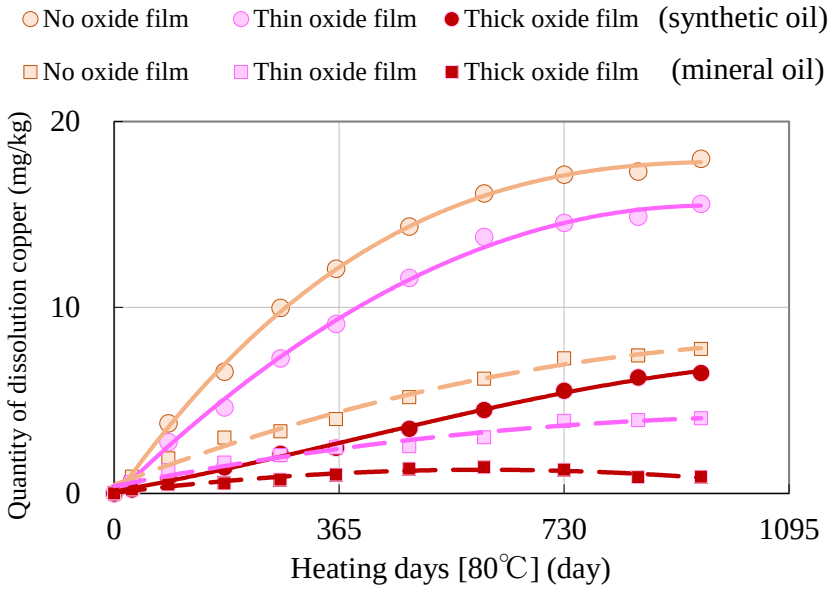

Fig 4.13 Relationship between the surface oxide of copper bar and the quantity of dissolution copper

(5) Discussion

Copper easily dissolves in insulating oil; however, the trend of the dissolution changes due to the type of the oil, quantity of the copper, and thickness of the oxide film. Therefore, the difference in material and environment is the difference in dissolution trend. This was the cause of the difference in dissolution trend under the same equipment conditions of the used cables. The structure, material, operating environment, and so on of the OF cables are more various. In particular, copper in synthetic oil is more soluble than mineral oil.

The acid-washed copper bars also showed a saturation trend with time. It is possible that an oxide film was formed due to heating and the oxygen in the oil, because the copper surface was discolored after heating.

95% of 66-kV used cables contain mineral oil; however, 275-kV used cables contain synthetic oil only (Fig 4.10). The quantity of the dissolution copper of 275-kV used cables were less than that of 66-kV used cables. This trend is opposite to experimental data. It is possible that electric charging degradation of 275-kV cables are easier than 66-kV cables, because an electric field related to the dielectrophoretic force is one factor causing degradation. Therefore, the reason for the reversed experimental value is that most of the dissolution quantity of the 275-kV cables was measured after decreasing due to the electric charging degradation.

4.3.5 Relationship between dissolved copper and the generation of oxidation sludge

(1) Catalytic effect of dissolved copper

a. Introduction

Dissolved copper promoted oxidative degradation of mineral oil as catalysts [15], and synthetic oil is also to be presumed to do the same. In STEP 2 of the electrical charging degradation process, dissolved copper aggregates and becomes a catalyst. As a result, oxidative degradation of insulating oil is promoted, and oxidation sludge is generated. Therefore, the phenomenon of STEP 2 was simulated by heating the synthetic oil containing high concentrations of dissolved copper. Thus, the generation of oxidation sludge and the oxidation degradation trend in insulating oil were confirmed by the simulation.

b. Samples

The sample was 10 mL of synthetic oil (soft type) containing 4, 6, 8, 10, 12, 14, and 16 mg/kg of dissolved copper. The copper-dissolved oil was prepared by heating the synthetic oil containing copper rods in a nitrogen atmosphere at 80 °C.

c. Method

The samples were heated in the atmosphere at 80 °C. Generation of oxidation sludge was visually confirmed at heating for 20, 60, and 110 days, and the insulating oil was measured by the ATR method of FTIR. Moreover, the absorbance height at 1710 cm^{-1}, which is the peak of carboxylic acid measured. The oxidation degradation trend of each sample was compared by the absorbance height. The FTIR used was a NEXUS670 (Thermo Fisher Scientific K.K., USA). The measurement conditions were a scan number of 32 times and a resolution of 4 cm^{-1}.

d. Results

Oxidation sludge was not generated. Fig 4.14 shows the relationship between the quantity of dissolution copper and the quantity of carboxylic acid in the oil. The carboxylic acid in the oil increased by heating. At each heating time, the quantity of dissolution copper increased in proportion to the quantity of carboxylic acid at each heating time.

e. Discussion

Dissolved copper promoted oxidative degradation of synthetic oil as a catalyst. Moreover, when the quantity of dissolution is considerable, the catalytic effect increases. However, oxidation sludge was not generated due to this simulation.

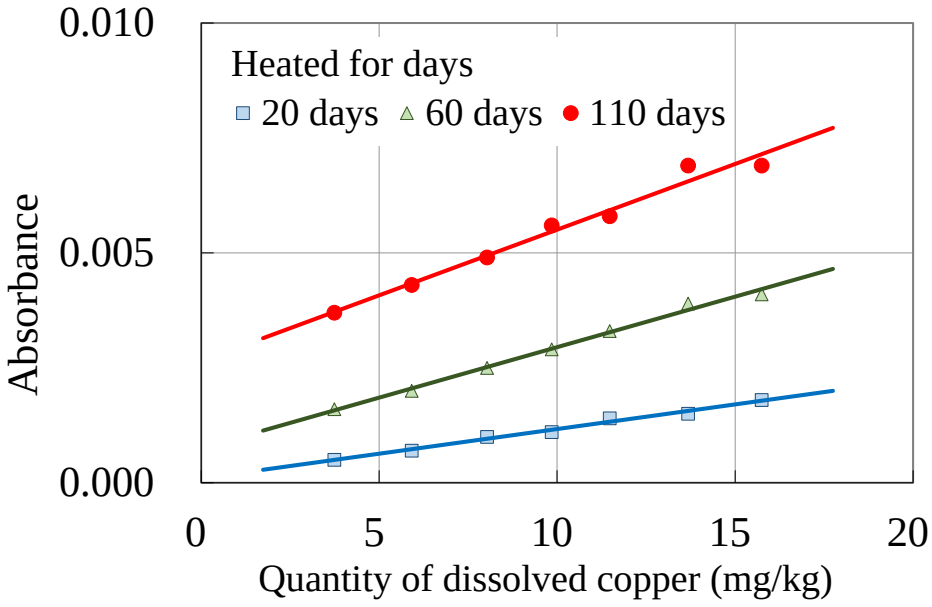

Fig 4.14 Relationship between the quantity of dissolution copper and the quantity of carboxylic acid in the oil

(2) Simulated generation of oxidation sludge by dielectrophoresis test

a. Introduction

Copper-dissolved oil of high concentration was placed in the high electric field region. As a result, the dissolved copper was confirmed to aggregate due to dielectrophoresis, and to generate oxidation sludge.

b. Samples

Table 4.2 shows the conditions of sample oil. Copper-dissolved oil was dissolved through heating copper rods in insulating oil at 80 °C in a vacuum atmosphere. In sample No. 3 and 4, sulfur powder was dissolved in insulating oil so that the quantity of sulfur in the oil was approximately 1,000 mg/kg. Thus, it was presumed that the sulfur binds with insulating oil instead of oxygen and oxidation sludge containing sulfur is generated, because the quantity of sulfur in the oil is more than the quantity of oxygen. As a result, oxidation sludge similar to the oxidation sludge of used cables is rapidly generated.

The sample oil was degassed before the start of the test, whereas the quantity of oxygen in the oil after degassing was approximately 800 mg/m^3. The sulfur powder used was Sulfur Powder of Practical Grade (Wako Pure Chemical Industries Corporation, Product code 195-04625, Japan).

c. Charging test methods

Fig 4.15 shows the test equipment and test conditions. The charge time was approximately one month. The generation tendency of oxidation sludge was periodically confirmed in the inside of the bottle via visual checking.

Table 4.2 Sample conditions

No.	Oil type	Quantity of dissolution copper (mg/kg)	Quantity of sulfur (mg/kg)	Sulfur powder	Electric charging
1	Synthetic oil	26.9	1.6	No	on
2	Mineral oil	9.3	299.4	No	on
3	Synthetic oil	19.9	945.6	In	on
4	Synthetic oil	19.9	945.6	In	off

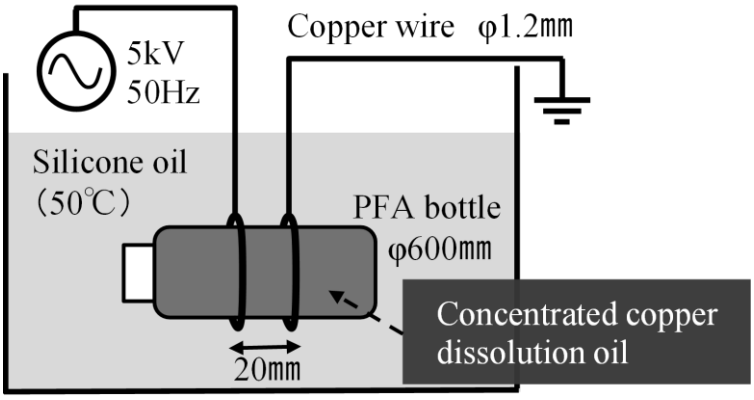

Fig 4.15 Test equipment and test conditions

d. Confirmation methods of oxidation sludge

Oxidation sludge analysis included two types of analyses: SEM-EDX and FTIR. The EDX used was an Edax Detecting Unit CD-S/S3400N (Ametek Ink., USA). The accelerating voltage was 15 kV. The oxidation sludge was collected with a metal needle and measured by the ATR method with FTIR. The FTIR spectrometer used was a Nicolet iS50 (Thermo Fisher Scientific K.K., USA). The measurement conditions were a scan number of 32 times and a resolution of 4 cm^{-1}.

e. Results

Fig 4.16 shows an example of the appearance of sample No. 3. In all four samples, deposits deposited at the bottom of the PFA bottle regardless of the charging. The deposits of sample No. 3 in which the sulfur powder was dissolved were able to be visually confirmed from approximately 4 days of charging, and the quantity was large. The deposits deposited on the whole side of the bottle, whereas it was especially aggregated along the main electrode.

Fig 4.17 shows the analysis results of the deposits using EDX. Copper was detected regardless of presence or absence of sulfur powder, whereas sulfur was detected more when sulfur powder was dissolved.

Fig 4.18 shows the analysis results of the deposits using FTIR. In all four samples, the peaks of hydrocarbon and carbonyl group were large. The peaks of sulfur oxide and thioketone were found in samples No. 3 and No. 4 in which sulfur powder was dissolved. In other words, these deposits were bound to the sulfur dissolved in the oil.

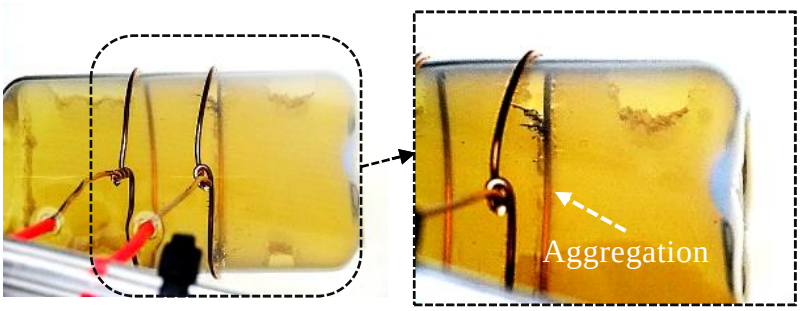

Fig 4.16 Image viewed from above the bottle

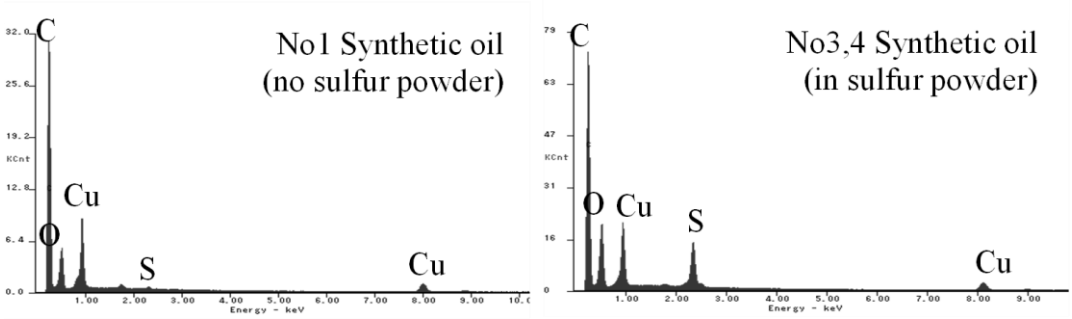

(a) No sulfur powder (b) In sulfur powder

Fig 4.17 Result of the elemental analysis of the deposits

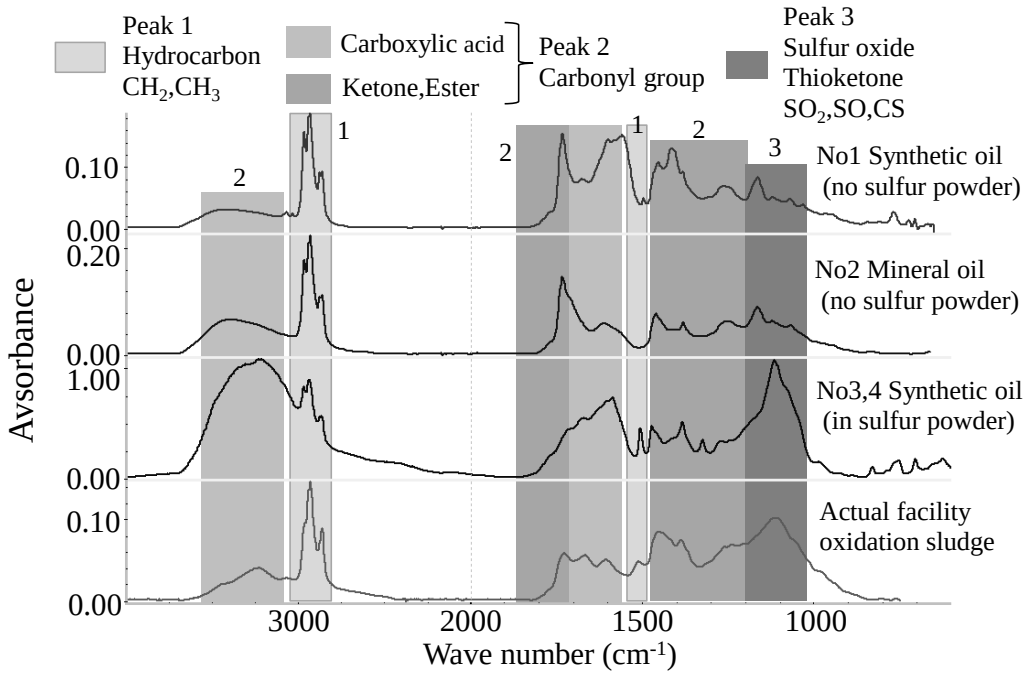

Fig 4.18 IR spectra of the deposits

f. Discussion

Organocopper compounds are deposited due to setting copper dissolution oil in a high electric field region. The compounds were determined to be the same as oxidation sludge in the used cables. The oxidation sludge is formed of hydrocarbon, carbonyl group, sulfur oxide, and copper. In other words, the oxidation sludge was deposited due to change via the oxidation reaction of the insulating oil, dissolved copper, oxygen, and sulfur. Moreover, the oxidation sludge is deposited in mineral oil as well.

In addition, it is possible that the dielectrophoretic force is acting on the oxidation sludge because of the aggregation near the main electrode. This possibility will be discussed in the next section.

(3) Dielectrophoresis of oxidation sludge

a. Introduction

To examine the causes why oxidation sludge aggregates due to dielectrophoresis, it is confirmed by simulation.

b. Samples

The samples were the oxidation sludge generated in the four samples shown in Table 4.2.

c. Confirmation methods

Fig 4.19 shows the test equipment. This method was the same as the dielectrophoresis test of copper powder in oil [16-17].

d. Results

Fig 4.20 shows the test results. The oxidation sludge was not above the electrode and it aggregated in the high electric field region near the electrode.

e. Discussion

Oxidation sludge aggregates in the high electric field region due to the dielectrophoretic force. This characteristic is the same as that of copper powder [16-17].

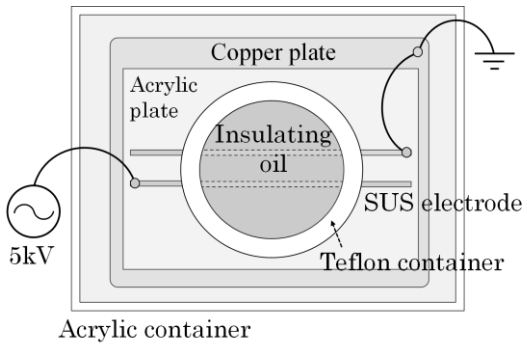

Fig 4.19 Method of the dielectrophoretic test

Fig 4.20 Result of the dielectrophoretic test

(4) Dissolution characteristics of copper compounds

a. Introduction

The form of dissolved copper in the used cable is a copper compound such as organocuprate or copper complex [18]. Moreover, the cause of the increase in the dielectric loss tangent (tan δ) of insulating oil is a copper complex dissolved in oil [3]. In other words, the characteristics of dissolved copper in insulating oil change because of the form of a copper compound. Therefore, the dissolution rate and the change in tan δ when dissolved were confirmed for each copper compound.

b. Samples

Table 4.3 shows sample conditions. The samples were prepared by dissolving an organic compound reagent and copper in insulating oil, and those prepared by dissolving an organocopper compound reagent. In addition, the organic compounds and the organocopper compounds were reagents presumed to change to copper complexes.

One sample was added for confirmation of the tan δ change. The sample is a reagent having a copper alkylbenzenesulfonate concentration of 5000 mg/kg in mineral oil. The measurement sample was attenuated with synthetic oil and adjusted to an appropriate concentration. The reagent used was CONOSTAN Oil Analysis Standards Cu 5000 mg/kg (SCP SCIENCE Corporate, Canada).

Table 4.3 Samples list

No.	Copper form	Reagent			Oil	copper
		Type	Manufacturer	wt%	(mL)	(g)
1	Solid copper	-	-	0	10	7.20
2		Aleic acid	Wako	1	10	7.20
3		8-Quinolinol	Wako	1	10	7.20
4		Benzothiazole	Wako	1	10	7.20
5		Acetylacetone	Wako	1	10	7.20
6		Thiophenecarboxylato	Wako	1	10	7.20
7	Reagent	Copper(II) Dimethyldithiocarbamate	Wako	1	100	0.90
8		Acetylacetone copper(II)	Tokyo Chemical Industry	1	100	0.89

c. Heating and analysis methods

The samples were heated in a nitrogen atmosphere at 80 °C. The quantity of dissolved copper and tan δ of the sample was measured at optional time during heating. The quantity of dissolved copper is the same as that in the measurement method shown in 4.3.3. tan δ was measured by heating at 80 °C and charging at 1 kV. The tan δ used was a DAC-STM-1 (SOKEN ELECTRIC Co, Ltd., Japan). The liquid electrode used was a DAC-OBE-2 (SOKEN ELECTRIC Co, Ltd., Japan).

d. Results

Fig 4.21 shows the change over time of the dissolution copper. Fig 4.22 shows the relationship between the quantity of dissolution copper and tan δ. tan δ of the samples in 4.3.3 was also measured, and the results were added to Fig 4.22. The samples were insulating oil collected from 1352 terminal and middle joint boxes of used cables. Dissolution rate was different for each sample. The relationship between the quantity of dissolved copper and tan δ was linear regardless of the types of the copper compounds. The inclination of the straight line was different for each copper compound.

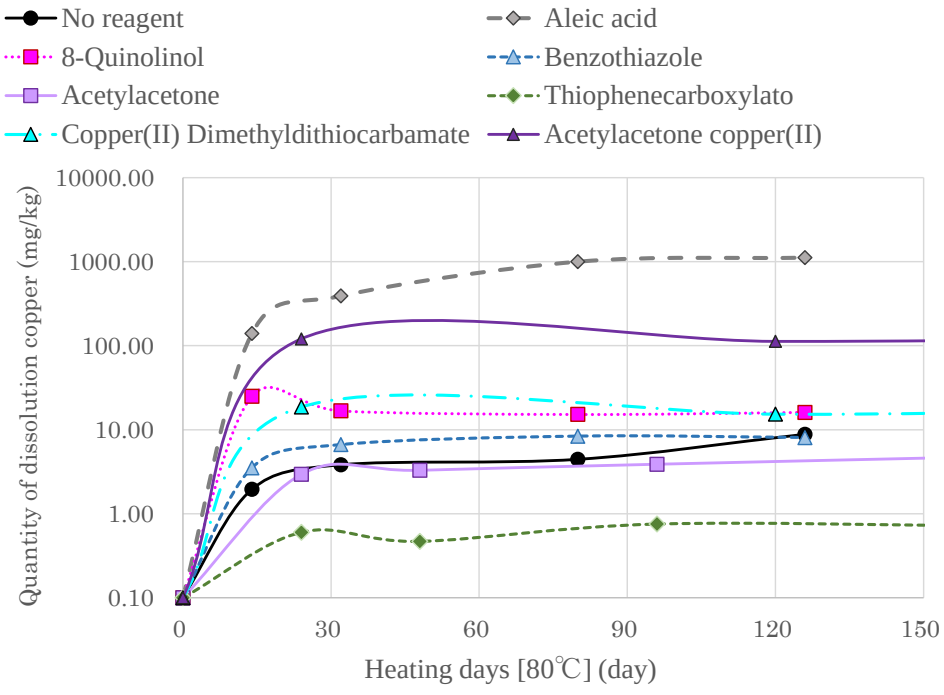

Fig 4.21 Change over time of the dissolution copper

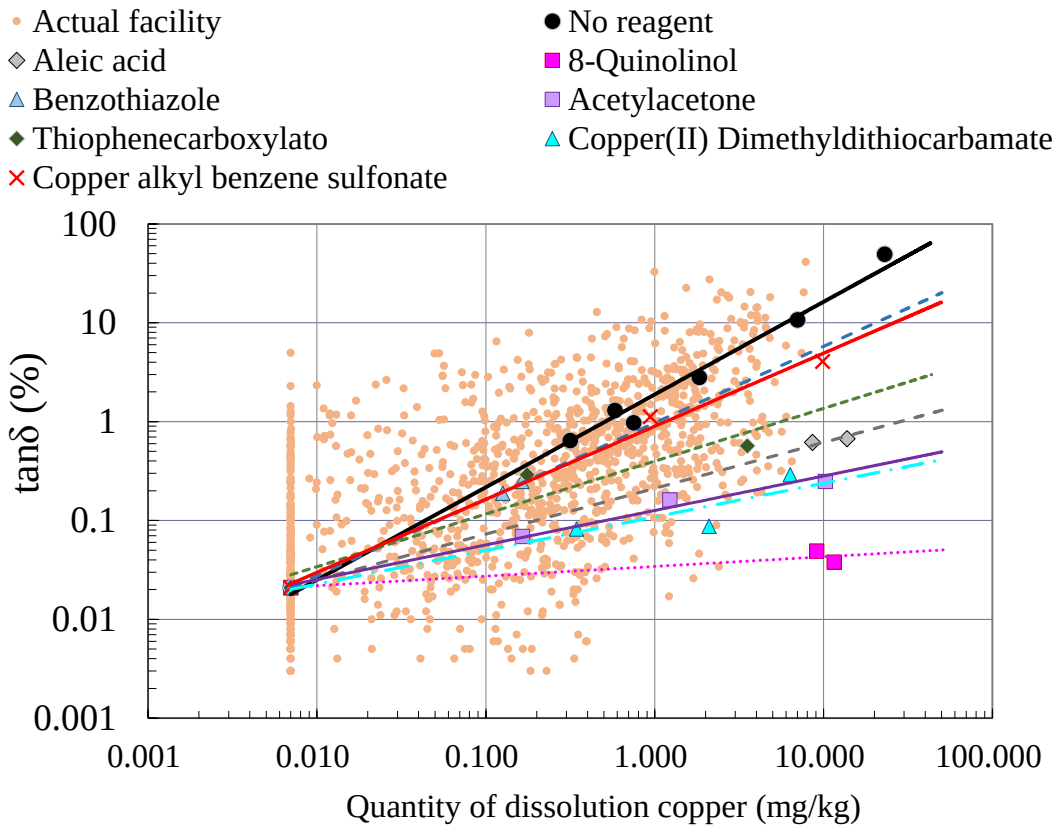

Fig 4.22 Relationship between the quantity of dissolution copper and tan δ

e. Discussion

Copper compounds such as organocuprate and copper complexes in oil are one of the causes of the increase in tan δ of insulating oil. The copper compounds are dissolved in different types and concentrations at each joint box because the plot of the actual facilities shown in Fig 4.22 varies widely and the inclination of the straight line was different for each copper compound. This cause will be elucidated in future studies.

4.3.6 Elution tendency of sulfur in insulating oil

(1) Introduction

It is possible that the origin of sulfur is not derived from insulating oil (shown in 4.3.3). The origin of sulfur was examined in another section. Therefore, the sulfur was presumed to elute from the material used in the cables.

Moreover, the quantity of the sulfur in the materials used was measured, and it was confirmed whether the sulfur in the materials was eluted in the insulating oil.

In addition, it was confirmed whether the same oxidation sludge as that in used cables was generated due to binding with the eluted sulfur.

(2) Confirmation of materials used

a. Construction of a joint box and materials used

Fig 4.23 shows the schematic diagram of a middle joint box and a semi stop. The materials containing sulfur are presumed to be insulating paper or carbon paper, which is pulp, and to be rubber such as seals on the semi stop or O-rings. The seals use rubber depending on manufacturer and age [1]. The rubber vulcanizing agent uses sulfur powder and sulfur compounds [19]. Therefore, it is possible that the vulcanized materials remaining in the rubber are eluted in the insulating oil. However, the qualitative analysis of the rubber is necessary because the types of the seals and O-rings was unknown.

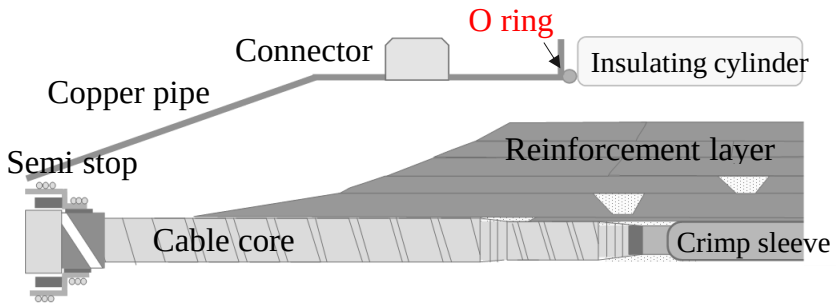

(a) Joint box

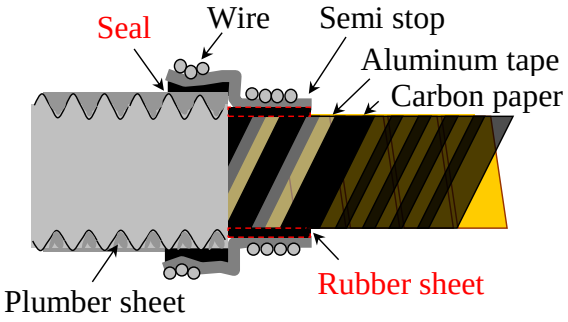

(b) Semi stop

Fig 4.23 Schematic diagram of middle joint box

b. Methods

The samples are O-rings, seals, and rubber sheets collected from used cables. The samples were qualitative analyzed using FTIR. The samples were measured by the ATR method with FTIR. The FTIR used was a Nicolet iS50 (Thermo Fisher Scientific K.K., USA). The measurement conditions were a scan number of 32 times, and a resolution of 4 cm^{-1}.

c. Results

Fig 4.24 shows the qualitative results. All three samples were NBR, whereas the used additives were different. There were peaks showing butadiene of around 976 cm^{-1} in all the three samples; however, the quantity of calcium carbonate, which was one of the fillers, was different. The main vulcanizing agent of NBR uses sulfur powder [19]. Therefore, it is possible that the sulfur powder remaining in the NBR is eluted in the insulating oil.

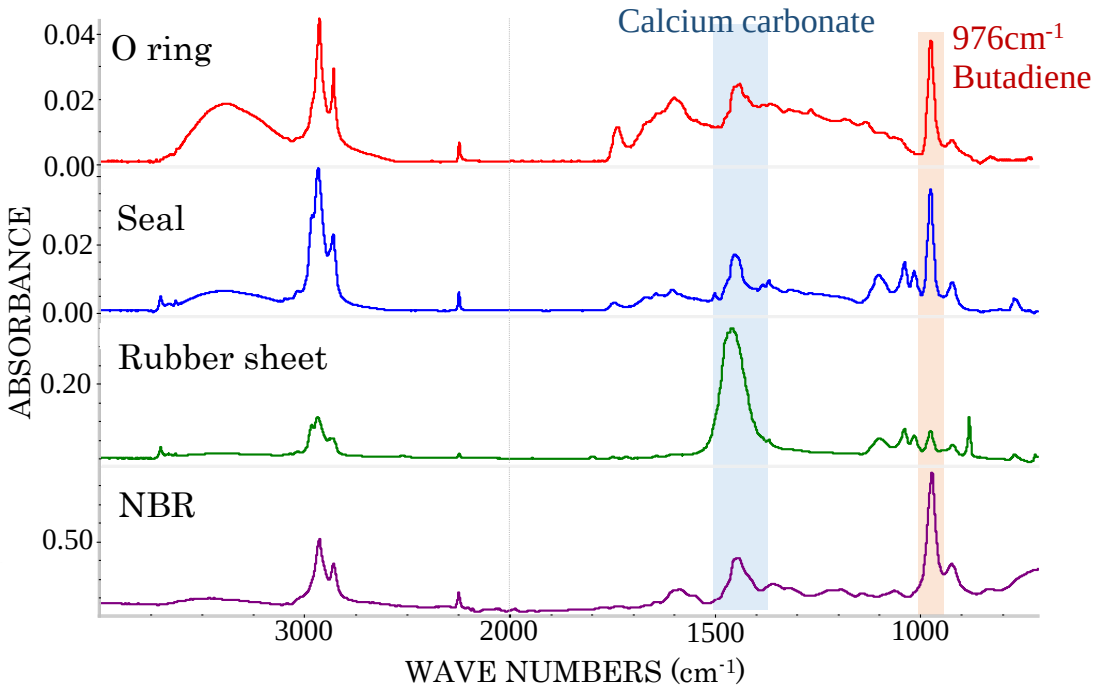

Fig 4.24 IR spectra and qualitative result of the rubber product in joint box

(3) Elution tendency of sulfur

a. Samples

Table 4.4 shows the tests and samples conditions. Only the new NBR sheet was pressurized, because O-rings and seals were pressurized from copper pipes and a semi stop. In other words, it is possible that the pressurization affects the elution of the sulfur.

Two of the new NBR sheets were sandwiched between aluminum plates and pressurized. The material standard of the NBR sheet was NBR-70-1 (Japanese Industrial Standard).

b. Methods

The sample was heated in a nitrogen atmosphere at 80 ° C. Approximately 0.8 to 1.0 g of insulation oil during heating was collected at optional time. The quantity of elements in the sample was quantitatively analyzed through the same measurement method shown in 4.3.3. The element to be analyzed was sulfur (S).

Table 4.4 Tests and sample conditions

Sample No	Conditions	Quantity of sample	Quantity of oil	Pressure
1	New NBR seat	200 × 400 mm 2 seat	300 mL	Yes
2	New NBR seat	200 × 400 mm 2 seat	300 mL	No
3	New O ring (Made by A company)	12 g	300 mL	No
4	Used seal (Made by A company)	12 g	300 mL	No
5	Used seal (Made by B company)	12 g	300 mL	No
6	New insulating paper	50 × 100 mm 1 seat	100 mL	No
7	New carbon paper	50 × 100 mm 1 seat	100 mL	No

c. Results

Fig 4.25 shows the change over time of the eluted sulfur. The new NBR sheets (No.1 and No.2) increased to 40 to 60 mg/kg in 5 days regardless of the presence or absence of pressure. However, the elution rate of sheet No.1 (no pressure) was slightly slow. The new O-ring (No.3) increased to 35 mg/kg in 7 days and 95 mg/kg in 27 days. The used seals (No.4 and No.5) increased to 4–8 mg/kg. The insulating paper (No.6) and carbon paper (No.7) did not increase.

d. Discussion

The sulfur in NBR is eluted into insulating oil, and in a short time of several days. It is possible that the elution rate varies according to the contact area between the NBR and the insulating oil. The contact area of No.1 sandwiched between aluminum plates was smaller than that of No.2, and its elution rate was slow. The sulfur is presumed to be not mainly a compound but a single substance because the main vulcanizing agent of NBR is sulfur powder. Insulating paper and carbon paper are not the origin.

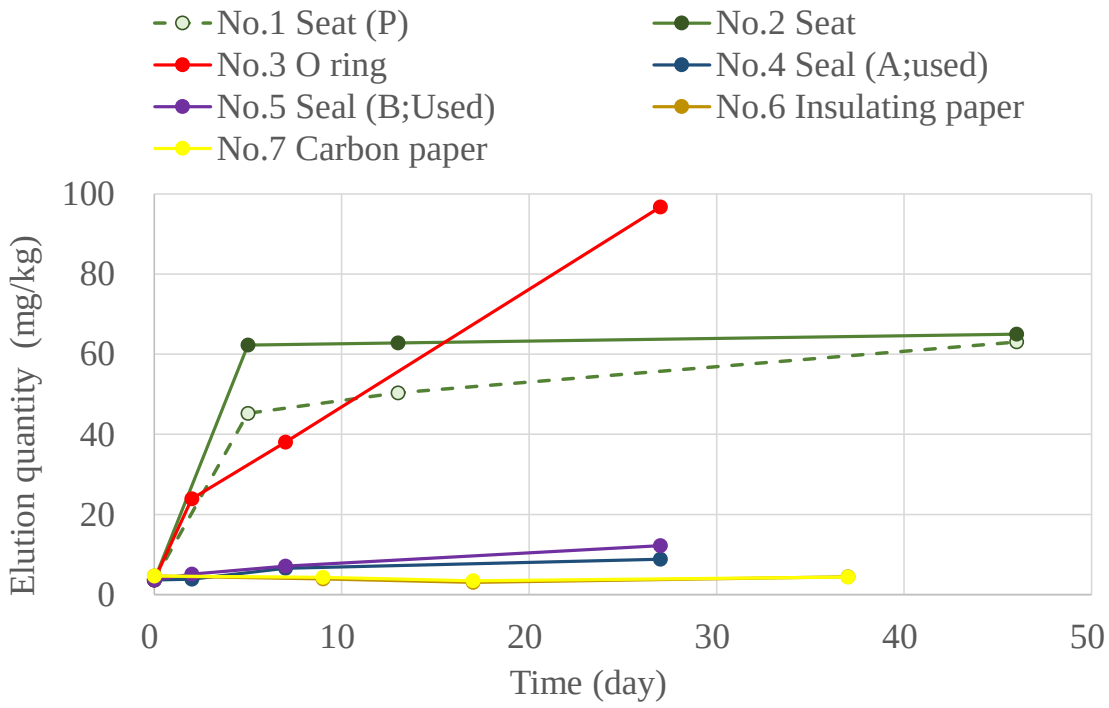

Fig 4.25 Change over time of eluted sulfur

(4) Generation of oxidation sludge

a. Samples

The insulating oil in which sulfur was eluted from NBR (Mixing No.1 and No.2 shown in Table 4.4) and in which acetylacetone copper was dissolved were mixed. The dissolved copper was 10.8 mg/kg and the dissolved sulfur was 38.1 mg/kg.

b. Generation methods

The generation methods were the same as the charging test methods shown in Fig 4.15. The charge time was approximately one month.

c. Confirmation methods

Oxidation sludge analysis using FTIR: The oxidation sludge was collected with a metal needle and measured by using the ATR method with FTIR. The FTIR spectrometer used was a Nicolet iS50 (Thermo Fisher Scientific K.K., USA). The measurement conditions were a scan number of 64 times and a resolution of 8 cm^{-1}.

d. Results

Fig 4.26 shows the IR spectra of the oxidation sludge generated by tests and the oxidation sludge collected from a used cable. The two IR spectra were nearly of the same shape.

e. Discussion

One of the origins of sulfur, which is the cause of electric charging degradation, is the O-rings and seals (NBR) in the joint boxes.

Sulfur, which is a vulcanizing agent remaining in the NBR, elutes in the insulating oil in a short time, and the eluted sulfur deposits the same oxidation sludge as the used cables. Therefore, this eluted sulfur is one of corrosive sulfur compounds.

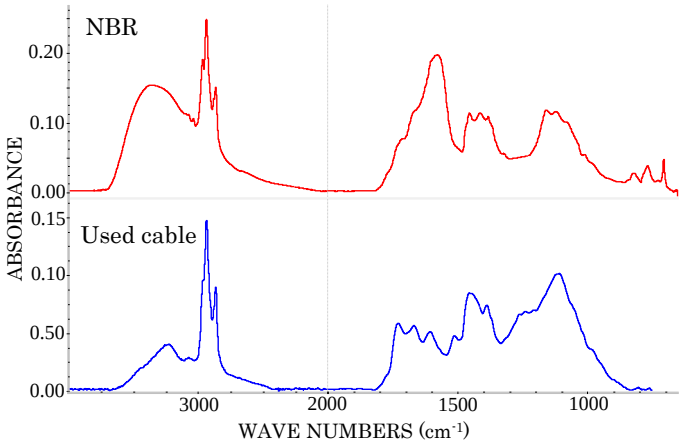

Fig 4.26 IR spectra of oxidation sludge

4.3.7 Electric charging degradation test

(1) Introduction

The electric charging degradation process is proved through a series of simulations. Therefore, the test circuit simulated an OF cable and its degradation process.

(2) Electric charging degradation test circuit

Fig 4.27 shows the test circuit. The simulation of STEP 1 of the electric charging degradation process (cf. Fig 4.7) diluted high-concentration copper-dissolved oil with insulating oil. In the simulation of STEP 2 (cf. Fig 4.7), the insulating oil was pressurized with nitrogen gas to flow in the circuit. In the simulation of aggregation by dielectrophoresis, the donut-shaped electrodes with different sizes at the top and bottom were used to create electric gradients.

Fig 4.28 and Fig 4.29 show the electrode composition. This electrode shape was referenced to the electrode shape and electric field distribution in the test in which the aggregation of copper sulfide was confirmed [20]. The position of the gap was the upside of the edge of the main electrode where the electric field strength was changing, because the dielectrophoretic force was generated within the gap in the insulating paper. In addition, in simulating the overlap of the gap portions in the used cables, the insulating paper was sandwiched between the electrodes so that the donut-shaped slits in the insulating paper overlapped. The counter electrode was a shape (condition 1 in Fig 4.28) in which the oil circulates outside the counter electrode and was a shape (condition 2 in Fig 4.29) in which the oil circulates through the center part of the counter electrode. The slits that are oil passages are added in the insulating paper, because the oil circulates from the main electrode to the gap and the center of the counter electrode.

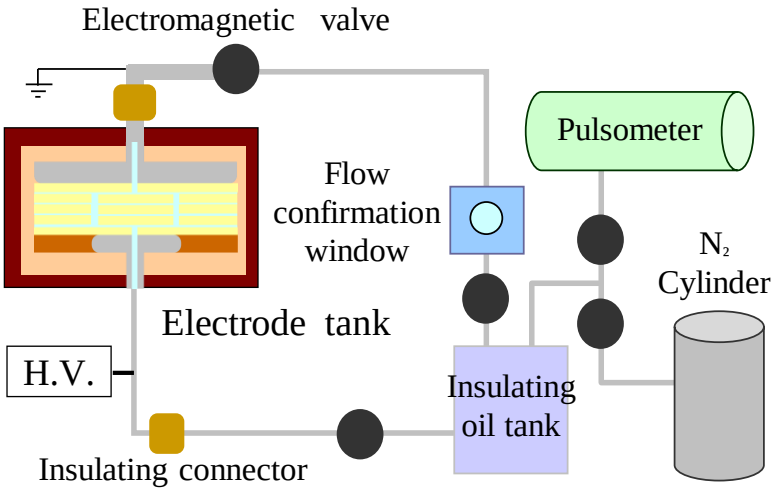

Fig 4.27 Electric charging degradation test circuit

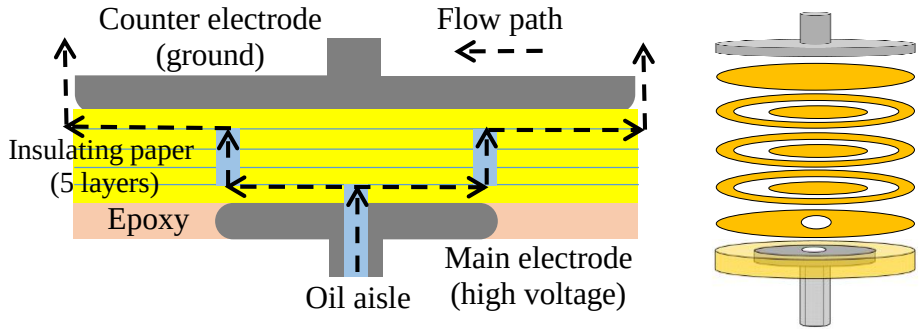

Fig 4.28 Electrode composition (condition 1)

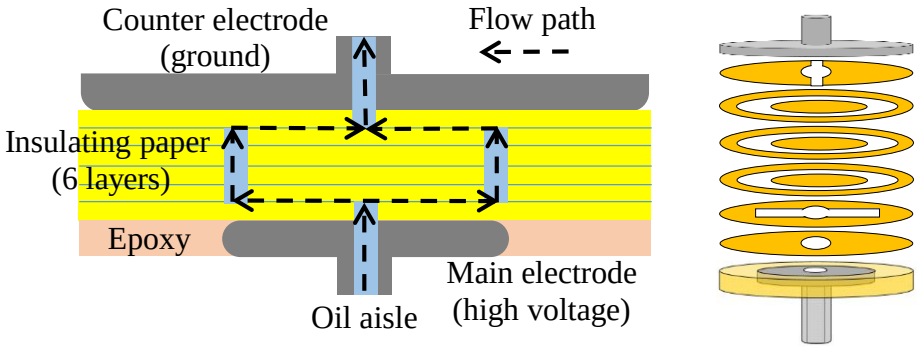

Fig 4.29 Electrode composition (condition 2)

(3) Methods

a. Electric charging

Table 4.4 shows the test conditions. The high-concentration copper-dissolved oil was attenuated by the reagent with synthetic oil and adjusted. The reagent had a copper alkylbenzenesulfonate concentration of 5000 mg/kg in mineral oil. When the concentration of mineral oil which is the base oil of the reagent is increased in sample oil, the test results indicate the degradation characteristics of mixed oil of synthetic oil and mineral oil. Therefore, the concentration ratio of mineral oil was adjusted to be about several percent relative to the synthetic oil, and the sample oil was almost in the situation of synthetic oil. As a result, the quantity of dissolved copper was approximately 200 mg/kg. The reagent used was CONOSTAN Oil Analysis Standards Cu 5000 mg/kg (SCP SCIENCE Corporate, Canada).

The charging was constant and impulse (Imp). Constant charging was applied so as to obtain AC 12 kV/mm (17 kVp/mm), which is the same electric field as that for the 275-kV OF cables. The Imp charging was assumed to be a switching surge. It is possible that one of the causes of the dielectric breakdown accident was the switching surge, because the cable was a connection line in the transformer substation. The electric field at the time of charging was approximately the maximum electric field (43.2 kVp/mm) when Imp charge

was superimposed on constant charging. Since the insulation strength (BSIL) of the switching impulse on 275-kV OF cables is 658 kV, the maximum electric field in the cable with a cable size of 2500 mm^2 is 43.2 kVp / mm [21].

Sample No. 1, which is five insulating papers, was always applied with AC 7.5 kV, and was applied 150 times in Imp 18.75 kV at a rate of 10 times/day. Sample No. 2 and No. 3, which are six insulating sheets, was always applied with AC 9 kV, and was applied 70 times in Imp 22.5 kV at a rate of 10 times/day. The circulation time of the insulating oil was 2 min (0.6 cc/min) at 6-h intervals, and the quantity of oil flow in the test circuit was 4.8 cc/day.

b. Partial discharge measurement

The partial discharge measuring device was connected to the electrode, and an oscilloscope and a data logger were connected to a partial discharge measuring instrument. The waveform of the partial discharge was checked with the oscilloscope at optional time. After confirming the generation of partial discharge, the voltage output from the partial discharge measuring device was measured. In addition, the voltage was correlated with the quantity of discharge intensity. The situation of the partial discharge, which is continuously generated, was observed with the data logger. The partial discharge measuring device used was a DAC-PD-3 (SOKEN ELECTRIC Co, Ltd., Japan). The oscilloscope used was a DLM2022 (Yokogawa Electric Corporation, Japan). The data logger used was a NR-1000 (Keyence Corporation, Japan).

Table 4.4 Electric charging degradation test conditions

No	Reagent	Electrode composition	Heating (°C)	Flow	Oil pressure (MPa)	Electric charging voltage	Copper (mg/kg)	Sulfur (mg/kg)	Charging time	Partial discharge measurement
1	ABS	condition 1	Electrode : 80	○	0.10	AC:7.5 kV (12 kV/mm) Imp:18.75 kV (30 kVp/mm)	202	207	AC:672(h) Imp:150(count)	(Unmeasured)
2	ABS	condition 2	Tank：80 Electrode : 80	○	0.01	AC:9 kV (12 kV/mm) Imp:22.5 kV (30 kVp/mm)	176	196	AC:1263(h) Imp:0(count)	Oscilloscope Data logger
3	ABS	condition 2	Electrode : 80	×	—	AC: 9kV (12 kV/mm) Imp:22.5 kV (30 kVp/mm)	180	211	AC:628(h) Imp:70(count)	Oscilloscope Data logger

c. Methods for analysis of insulating paper

After charging, the appearance of the insulating paper was observed with the microscope and a SEM. The electric charging degradation parts were analyzed via the same method as the qualitative analysis methods of the black parts shown in 4.2.2. The microscope used was a VHX2000 (Keyence Corporation, Japan). The scanning electron microscope used was a S3400N (Hitachi High-Technologies Corporation, Japan). The samples were nonevaporated. The observed images were BSE images at a low-vacuum mode of 30 Pa.

(4) Results

a. Breakdown and appearance

Dielectric breakdown occurred in sample No. 1 with the charge of 672 h. However, the generation of partial discharge before its breakdown was unknown because it was not measured. The charging of sample No. 2 and No. 3 was completed in 1263 h and 626 h due to time restrictions. No dielectric breakdown of the two samples occurred, whereas partial discharge was detected in sample No. 3.

Fig 4.30 shows the appearance of sample No. 1 with dielectric breakdown. The surface of the gap was discolored to dark brown, and the breakdown hole was in this discolored part.

Fig 4.31 shows the appearance of sample No. 3 in which partial discharge was detected. The surface of the gap was not more discolored than sample No. 1, but was discolored to dark brown in part.

Fig 4.32 shows the BSE image of the discolored part. The gap part was of higher white contrast than outside.

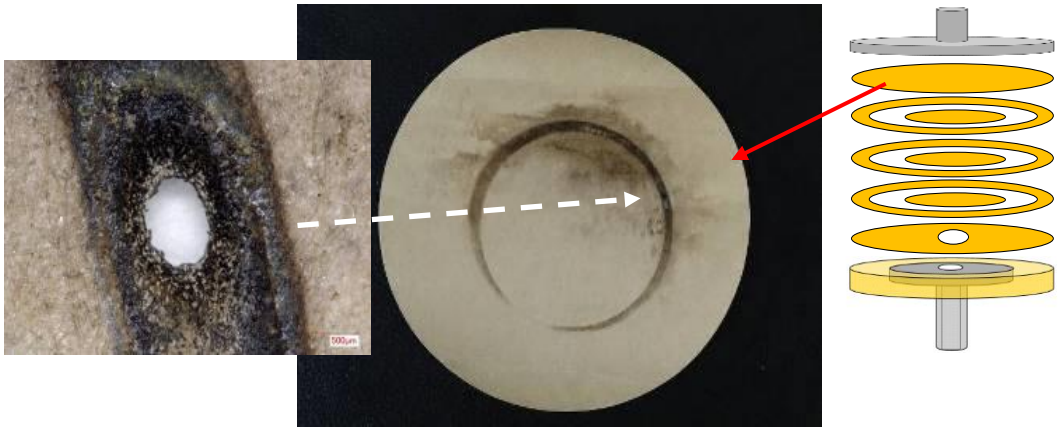

Fig 4.30 Appearance of sample No. 1

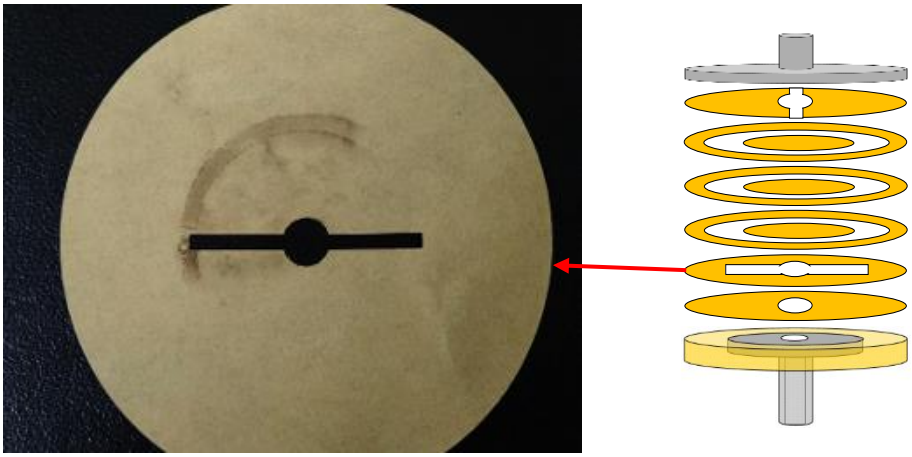

Fig 4.31 Appearance of sample No. 3

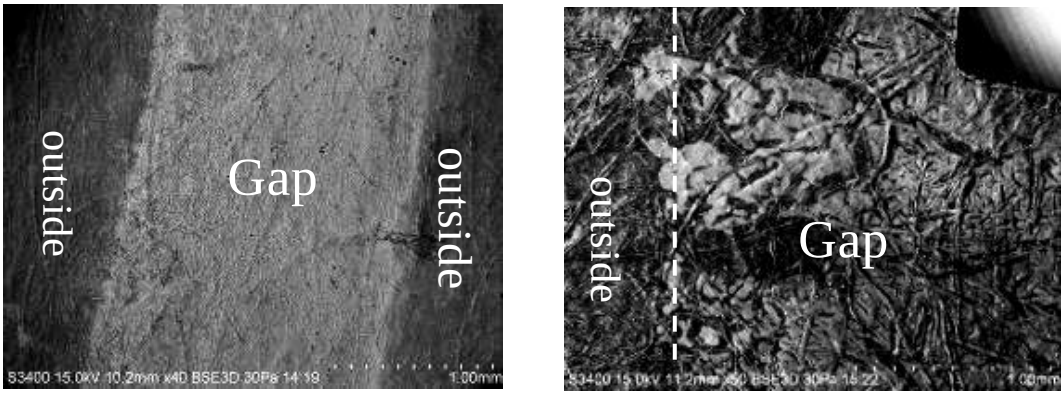

(a) Sample No.1 (b) Sample No.3

Fig 4.32 SEM image of the gap

b. Generation of oxidation sludge

Fig 4.33 shows the FTIR analysis result of deposits in the discolored part and the IR spectrum of oxidation sludge in the used cable. Fig 4.34 shows the results of elemental analysis of the deposits. Raman spectroscopy was not possible because of strong fluorescence. The absorption peaks of hydrocarbons, carbonyl groups, and sulfur oxides were found in the IR spectrum of the deposits. In addition, the spectrum was similar to that of the oxidation sludge of the cable used. The elements of the deposits detected were copper (Cu) and sulfur (S), whereas copper sulfide could not be confirmed.

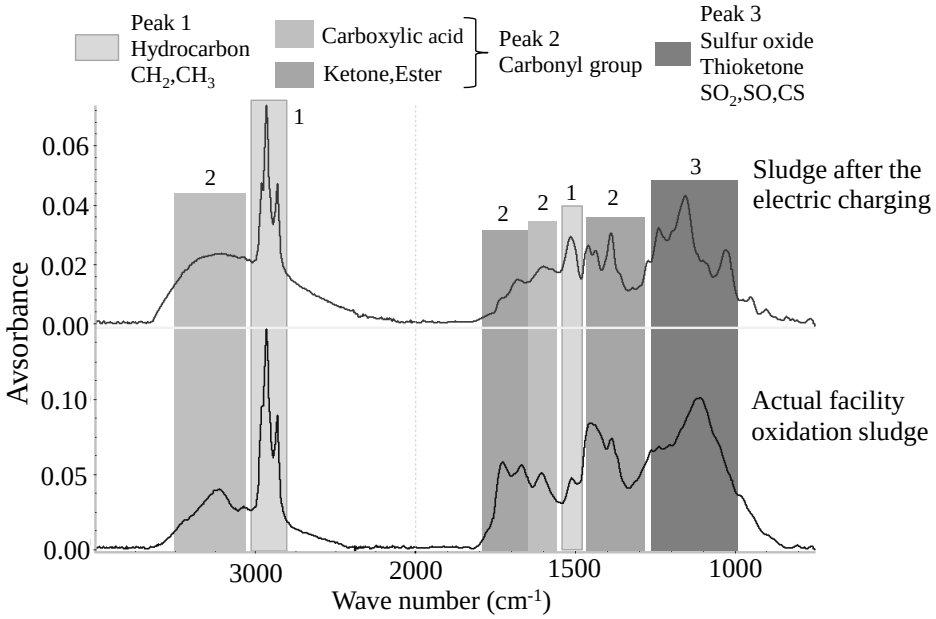

Fig 4.33 IR spectra of the sludge

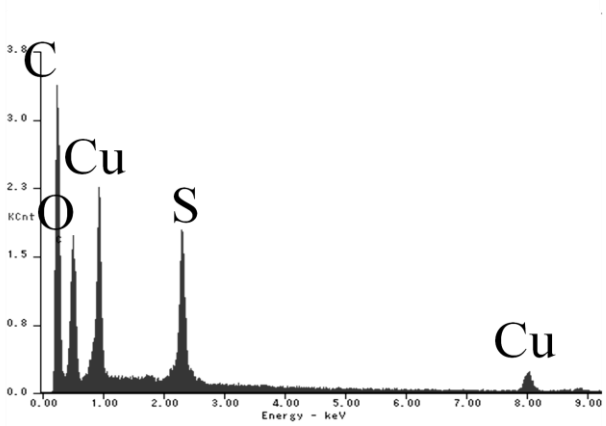

Fig 4.34 Result of the elemental analysis of the sludge

c. Partial discharge generation

Partial discharge was observed in the sample to which only AC charging was applied for 216 h. Fig 4.35 shows the change over time of the partial discharge obtained by the data logger after the partial discharge observation. The generation of the partial discharge was divided into intermittently generated time zones and continuously generated time zones (approximately 6 h). In addition, the discharge–charge amount in the continuously generated time zone was considerably large.

Fig 4.36 shows the partial discharge waveform when AC charging was applied for 579.5 h and Imp was applied 50 times. The discharge waveform was in the vicinity of the first and third quadrants and appeared almost in the same form within the positive or negative of the power supply voltage. The maximum partial discharge–charge amount was approximately 1,600 pC.

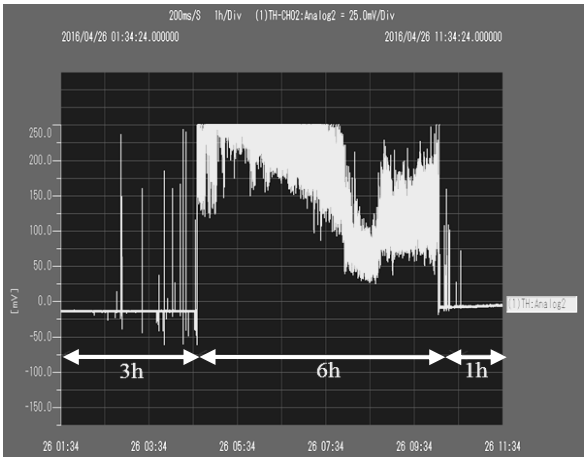

Fig 4.35 Change over time of partial discharge by a data logger [572 h–582 h]

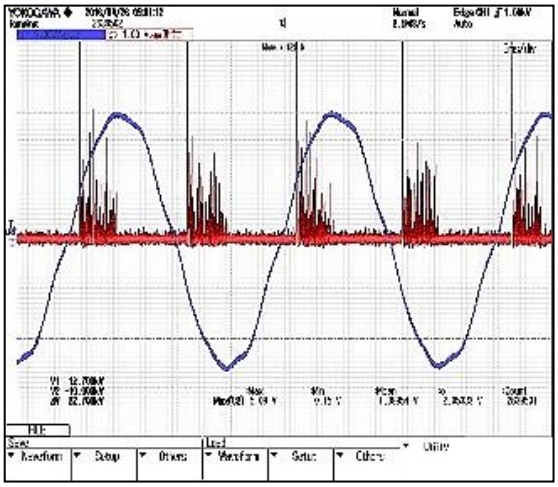

Fig 4.36 Partial discharge waveform when AC charging was applied for 579.5 h and Imp was applied 50 times

(5) Discussion

a. Breakdown and appearance

Elements heavier than the composition elements (carbon, oxygen) in the insulating paper were distributed on the gap as seen from the BSE image. In other words, the dark brown substances containing the heavy elements were deposited on the gap. It is possible that the deposits were the cause of dielectric breakdown because of the position of the breakdown hole.

b. Generation of oxidation sludge

The deposits were organocopper compounds very similar to the oxidation sludge in the used cables. Therefore, in the charging situation, the copper alkylbenzenesulfonate in the insulating oil was changed to organocopper compounds due to dielectrophoresis and the flow of oil, and was deposited on the gap. Dielectric breakdown occurred at the origin of the deposition. The results indicate that the electric charging degradation process was simulated through simulation tests.

The deposition amount of sample No. 2 was fewer than that of sample No. 1, because it is possible that oxidation sludge and oil were flowing out of the oil passage on the insulating paper. The deposition amount of sample No. 3 was also less than that of sample No. 1, because it is possible that dissolved copper is not supplied as there is no oil flow. In addition, dielectric breakdown did not occur due to the small amount of deposition.

c. Partial discharge generation

Oxidation sludge containing copper compounds aggregated locally due to electric charging degradation, and high electric field parts were made. Thus, it is presumed that partial discharge occurred because the oxidation sludge was deposited in the electric field direction. Moreover, it is possible that the generation of partial discharge was divided into intermittently generated time zones and continuously generated time zones. The generation trend of this partial discharge can be explored in a future study.

4.3.8 Conclusion

Copper sulfide was discovered on the black part on the insulating paper near the breakdown point of an OF cable by TEPCO. As a result, a five-step electric charging degradation process, which is the cause of this breakdown, was proposed. This proposed process was demonstrated through investigation of insulation oil in used cables and various simulation tests. As a result, STEP 1 to STEP 5 of this degradation process could be reproduced. The results indicate that the process, which leads to dielectric breakdown due to electric charging degradation, exists in OF cables under operating electric field and under pressure.

4.4 Electrical charging degradation of used cables

4.4.1 Introduction

To confirm whether electrical charging degradation occurs in a large number of OF cables, the black regions of used cables was investigated. The results indicated that it is possible for degradation to occur within any OF cable. The qualitative analysis of the black regions was performed via point analysis using SEM-EDX, FTIR, and Raman. The black parts were observed to occur in the form of lines and spots, perhaps indicating that electric charging degradation trends were not the same in different black shapes. Moreover, it is possible that the insulation performance varies owing to the differences in shape, which cannot be assessed completely by point analysis. However, it is in any case difficult to discuss these possibilities by point analysis. The one possible solution would be area analysis through elemental mapping with SEM-EDX, and plural point analysis with FTIR or Raman. This method is one of the best because the diffraction patterns of the black parts could not be measured via X-ray diffraction.

The difference in electric charging degradation trends and the relation with the decreasing electrical insulation by area or shape using this solution were discuss.

4.4.2 Analytical samples and methods

(1) Analytical samples

The analyzed samples were different shapes of black parts on insulating paper in aged OF cables. Table 4.5 shows the relevant data of the analytical samples. Selected samples were 275-kV joint boxes with BAB.

Each joint box was disassembled in order to reveal the black (deteriorated) parts on the insulating paper and obtain samples from them. Each sample was cut to a length of 10 cm. However, the insulating paper after disassembly contained insulating oil, which had to be removed prior to analysis. Therefore, the samples were naturally dried after immersion in acetone for approximately 10 minutes. In addition, non-solubility of the black part in acetone was confirmed by optical observation.

(2) External observation

The sites to perform analysis were selected by direct observation at 5–20 magnifications using an optical microscope. The selected places were observed at 20–100 magnifications with the same microscope, and then at 50–200 or even higher magnifications using an SEM. The microscope used was a VHX2000 (Keyence Corporation, Japan). The scanning electron microscope used was a S3400N (Hitachi High-Technologies Corporation, Japan). The samples were nonevaporated. The observed images were BSE images by a low-vacuum mode of 30 Pa.

Table 4.5 Relevant data of the analytical samples

Sample No.	Voltage	Joint Type	Aging	Insulating Oil	Black Part Location		
1	275 kV	Middle	37	BAB	Under Semistop	Cable Core	Outer Layer
2	275 kV	Terminal	28	BAB	Under Semistop	Cable Core	Middle Layer
3	275 kV	Terminal	28	BAB	Under Semistop	Cable Core	Most Inner Layer
4	275 kV	Terminal	30	BAB	Under Semistop	Cable Core	Most Inner Layer

(3) Copper sulfide analysis

Copper sulfide analysis included two types of analyses: elemental mapping with SEM-EDX and Raman analysis. In SEM-EDX elemental mapping, the mapped elements were copper, sulfur, carbon, and oxygen. The EDX used was an Edax Detecting Unit CD-S/S3400N (Ametek Ink., USA). The accelerating voltage was 15 kV.

Raman spectroscopy point analyses were performed on regions of weak fluorescence within the distribution of copper and sulfur. Raman analysis did not indicate strong fluorescence from the insulating paper and the oxidation sludge. Fig 4.2 shows the standard spectra of copper (I) sulfide (Cu2S) and copper (II) sulfide (CuS), which were used to determine copper (I) sulfide and copper (II) sulfide. The Raman spectroscope used was a Nicolet Almega XR (Thermo Fisher Scientific K.K., USA). The measurement conditions were a laser wavelength of 532 nm, and a laser output of 1%. Furthermore, the lens was operated at a distance of 100 magnifications, the exposure time was 30 seconds or more, and the scan number was 5 times or more.

(4) Oxidation sludge analysis

The oxidation sludge analysis also included two types of analyses. The black deposit sample was collected with a metal needle, placed on a diamond window, and measured by transmission method with FTIR. However, when sample collection was impossible due to the low deposition volume, or the small size of the black part on the insulating paper, the analysis was conducted using the ATR method. In addition, the absorbance difference spectrum of the black deposit sample and the insulating paper were obtained.

Fig 4.37 shows an example IR spectrum for oxidation sludge. The marked areas indicate the infrared absorption (IR) peaks, which correspond to three types molecular structures. The peaks near 2,900 cm^{-1} and 1,400 cm^{-1} (Peak 1 in Fig 4.37) correspond to hydrocarbons, those near 3,300 cm^{-1}, 1,700 cm^{-1}, and 1,300 cm^{-1} (Peak 2 in Fig 4.37) correspond to oxidation products, and the ones near 1,100 cm^{-1} (Peak 3 in Fig 4.37) to sulfur oxidation products. In addition, presence or absence of copper and sulfur was determined using the EDX. Oxidation sludge was determined by the presence or absence of the three IR peaks, copper, and sulfur.

The FTIR used was Nicolet Continuμm (Thermo Fisher Scientific K.K., USA). The measurement conditions were an MCT-A* detector, a scan number of 68 times, and a resolution of 8 cm^{-1}. EDX analytical conditions were the same as in the copper sulfide analysis.

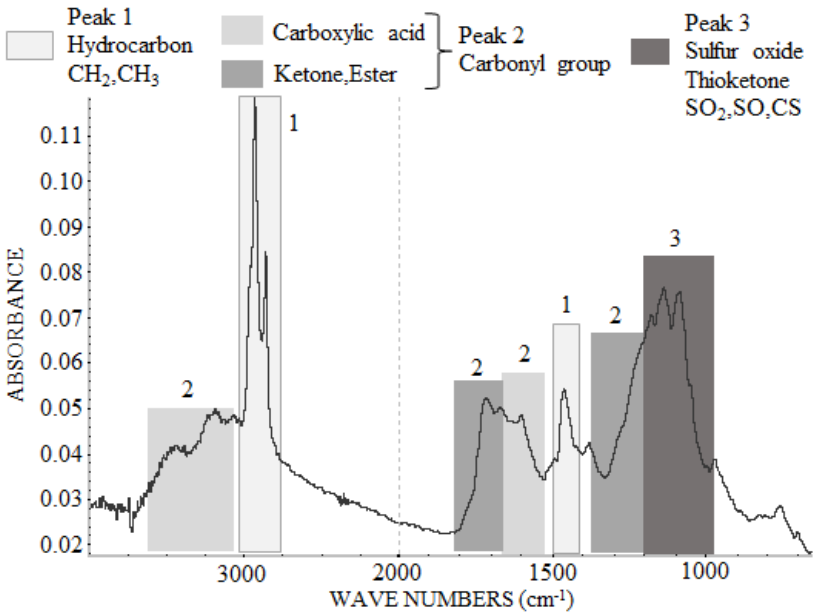

Fig 4.37 An example of the IR spectrum of oxidation sludge

(5) Wax analysis

Presence of wax was determined by dyeing the insulating paper with black parts with a dyeing aqueous solution of 0.03 wt% crystal violet (Wako Pure Chemical Industries Corporation, Product code 038-04862, Japan). In particular, the insulating paper was immersed in the dyeing solution at 40–60°C and dried naturally. Wax was considered present only in the non-dyed portion of the insulating paper.

(6) Discrimination of discharge mark

Black spots with cracks in the insulating paper were considered discharge marks by visual and optical microscopic observation. This discrimination was ensured when only carbon was detected in the EDX analysis.

4.4.3 Results

(1) Sample 1

Fig 4.38 shows the optical observation results of a black deposit around an oil gap. The insulating paper is cracked from the edge to the oil gap.

Fig 4.39 shows elemental distribution around the crack of the oil gap. Copper and sulfur are present in the entire oil gap and, in particular, around the crack. Only carbon appears in the thick cracked area (circle in Fig 4.39). Therefore, this crack was caused by discharge and was thus carbonized.

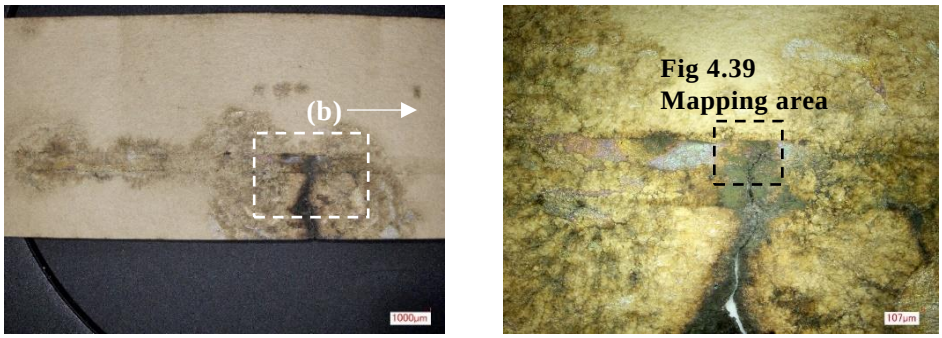

(a) x5 (b) x20

Fig 4.38 Optical observation of Sample 1

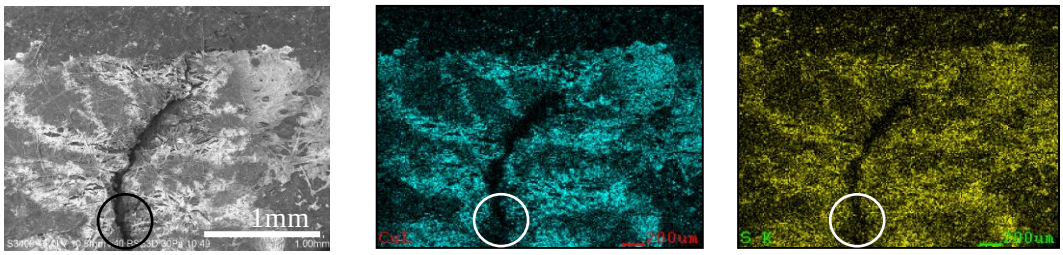

(a) SEM image (x40) (b) Copper (c) Sulfur

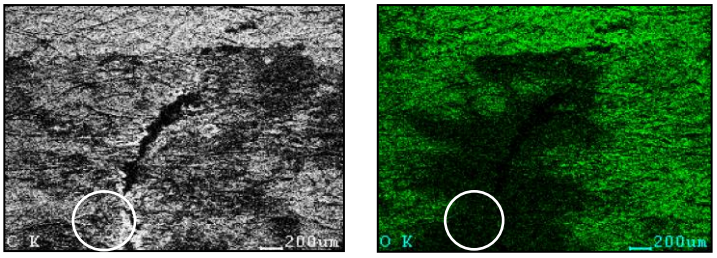

(d) Carbon (e) Oxygen

Fig 4.39. Element mapping around the oil gap crack

Fig 4.40 shows the FTIR analysis results. The areas between brackets indicate the analysis points. The IR spectra of all analysis points show oxidation sludge.

Fig 4.41 shows the Raman analysis results. The areas between brackets indicate analysis points. The Raman spectra of points (2) and (7) show copper (I) sulfide. In addition, the Raman spectra of all analysis points show a copper (II) sulfide peak near 480 cm^{-1}. The Raman spectrum of point (6) near the crack shows copper (II) sulfide and carbon.

Fig 4.42 shows the wax analysis results. The non-dyed portion is black part. However, it is not safe to consider that wax is present based only on this observation, because oxidation sludge is also a type of wax, and wax is not dyed regardless of the oil polymer produced by discharge. Therefore, the presence of oil polymer by discharge remains a possibility.

Fig 4.43 shows photographs of 14 consecutive sheets of paper aligned inside and outside the analysis sample. The crack appears in five consecutive paper sheets. The maximum length of the crack is 1 cm. The black part appears in 12 consecutive sheets of paper.

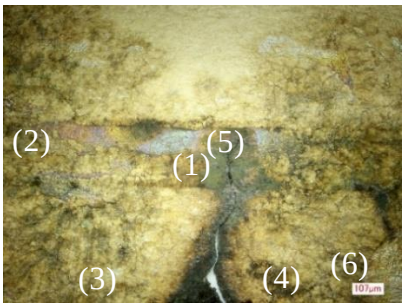

(a) Analysis point

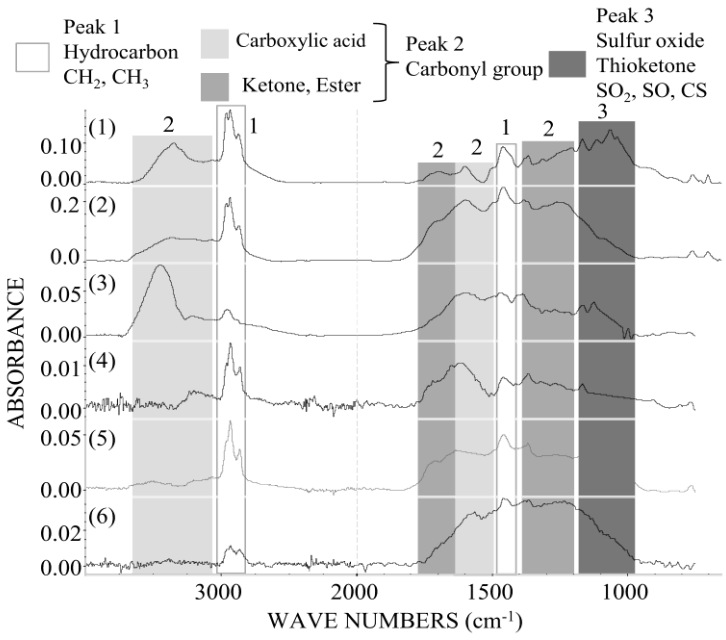

(b) FTIR spectra

Fig 4.40 FTIR analysis of six points

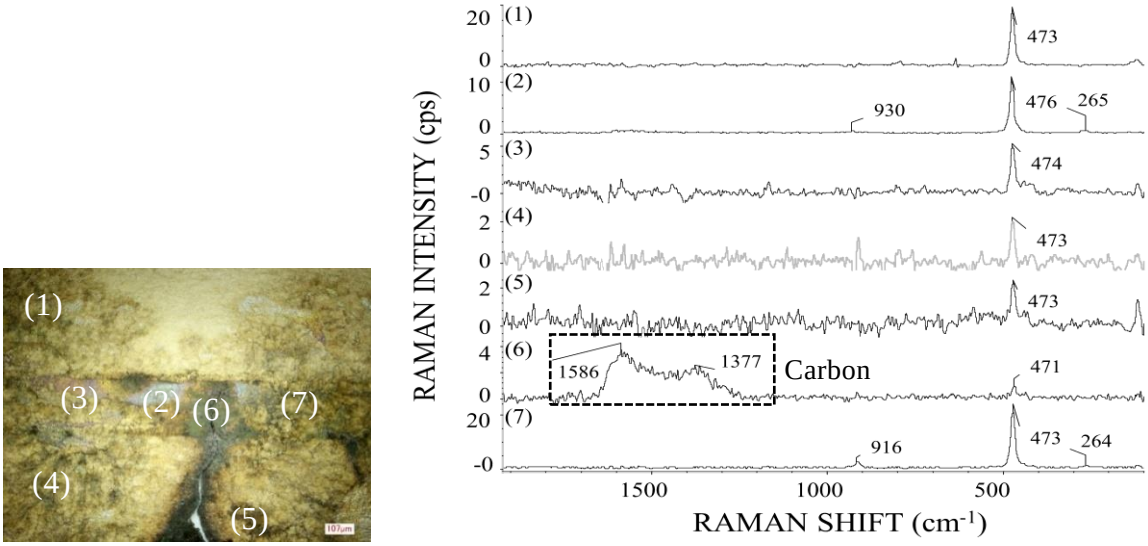

(a) Analysis point (b) Raman spectra

Fig 4.41 Raman analysis of seven points

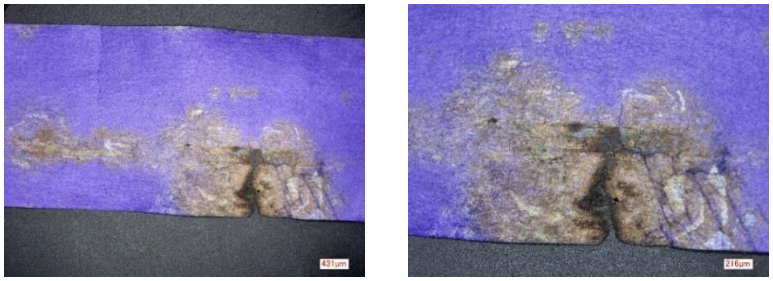

(a) x5 (b) x20

Fig 4.42 Results of wax analysis

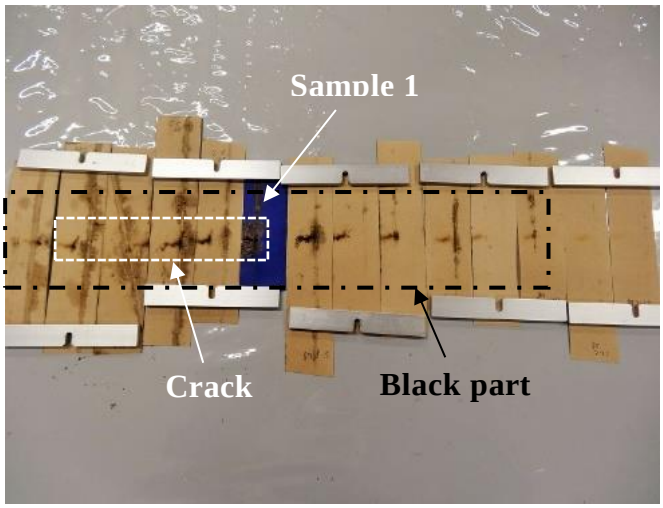

Fig 4.43 Photograph of 14 consecutive sheets of paper near the analysis sample

(2) Sample 2

Fig 4.44 shows the optical observation results of the sample-2 black part. The black part is distributed in spots on the entire insulating paper. Under magnification, deterioration (black) extends from the center outward.

Fig 4.45 shows the element mapping around the dark black part. Carbon and sulfur are distributed on the dark black part (circles in Fig 4.44 and 4.45). Copper is distributed in the thin black part around the dark black part.

Fig 4.46 shows the FTIR analysis results. The areas between brackets indicate analysis points. The IR spectra of all analysis points show oxidation sludge.

Fig 4.47 shows the Raman analysis results. The areas between brackets indicate analysis points. The Raman spectra of all analysis points show copper (II) sulfide peak near 480 cm^{-1}, and copper (I) sulfide peak near 280 cm^{-1}. In addition, the Raman spectrum of point (1) shows a carbon peak.

Fig 4.48 shows 500 magnifications of the thin black part (diamond shape in Fig 4.44b and point (4) in Fig 4.47) with SEM. Copper sulfide is deposited on the branches.

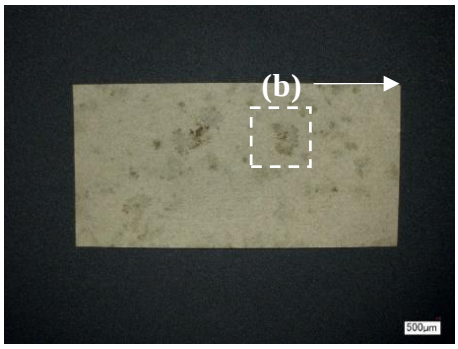

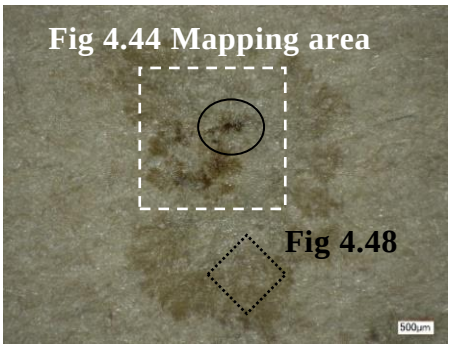

(a) x5 (b) x50

Fig 4.44 Optical observation of Sample 2

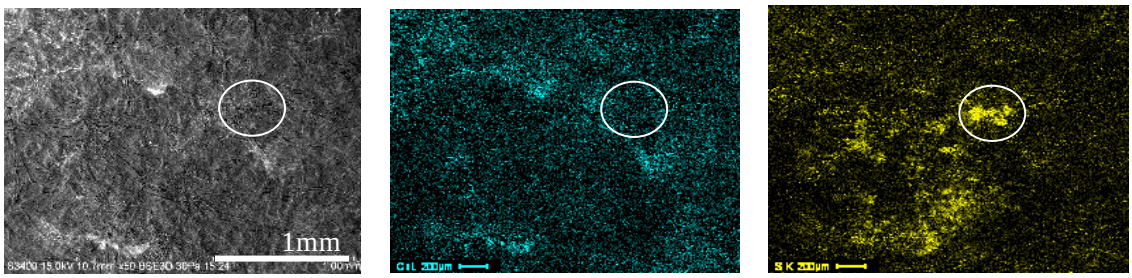

(a) SEM image (x50) (b) Copper (c) Sulfur

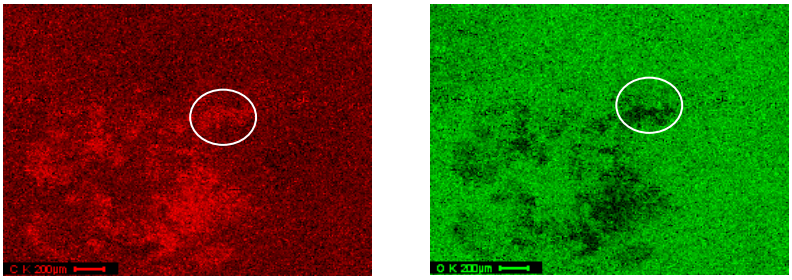

(d) Carbon (e) Oxygen

Fig 4.45 Element mapping of Sample 2

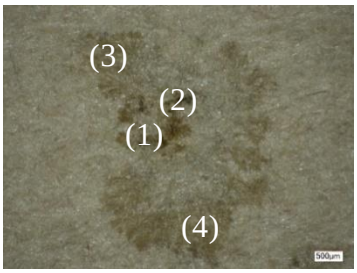

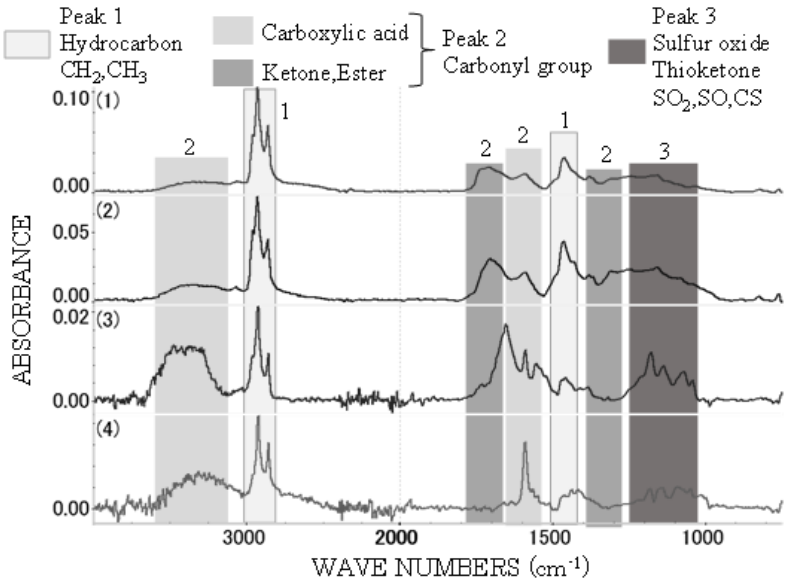

(a) Analysis point (b) FTIR spectra

Fig 4.46 FTIR analysis of four points

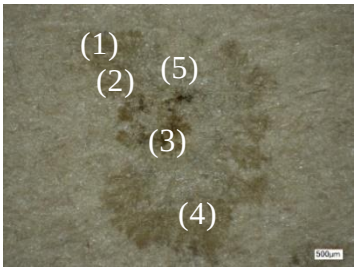

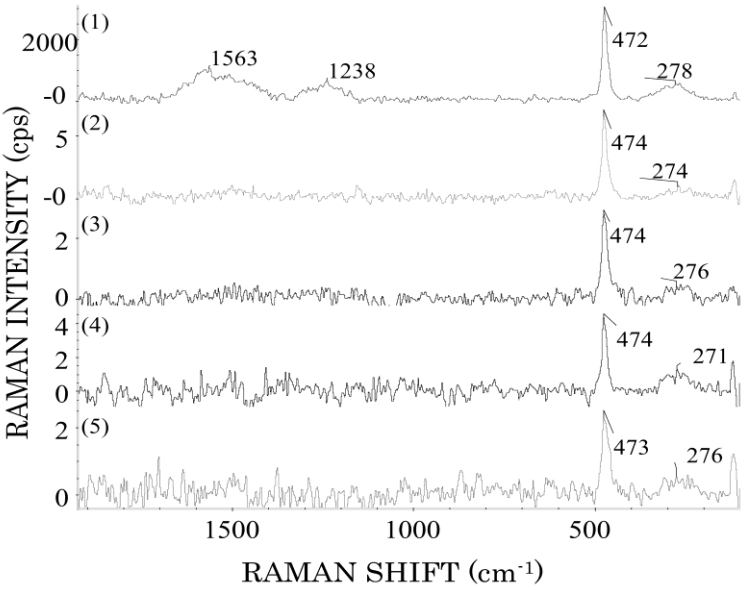

(a) Analysis point (b) Raman spectra

Fig 4.47 Raman analysis of five points

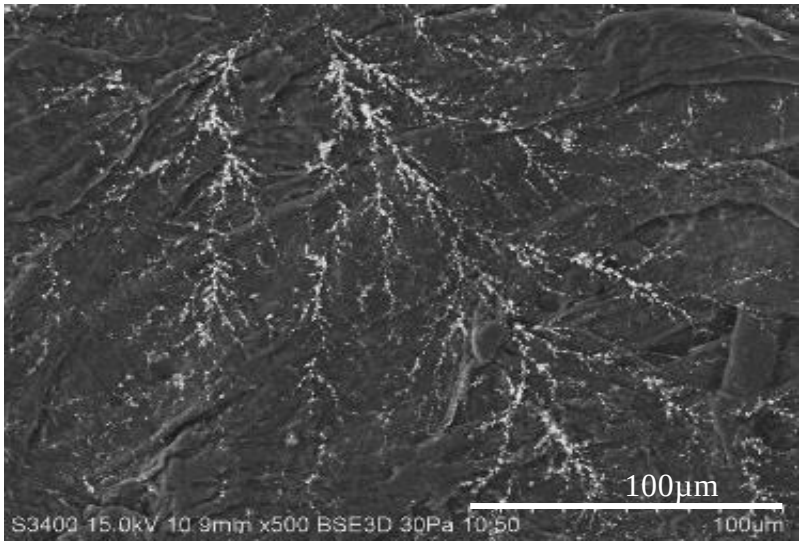

Fig 4.48 SEM image (×500) of the thin black part (diamond shape in Fig 4.44b and point (4) in Fig 4.47)

(3) Sample 3

Fig 4.49 shows the optical observation results of the sample-3 black part. The black part is distributed on an approximately straight line along the oil gap. Dark black parts are dotted inside the straight line.

Fig 4.50 shows the element mapping around a black dot. Copper and sulfur are distributed on the entire black part. Carbon is distributed on the black part center.

Fig 4.51 shows the results of FTIR and Raman analyses. In addition, measurements were obtained for only one part (arrow in Fig 4.49) because the black dot was small. The IR spectrum shows oxidation sludge. The Raman spectrum shows copper (I) sulfide and carbon.

Fig 4.52 shows SEM images of the black dot (square in Fig 4.50) at 500 and 2000 magnifications. Copper and sulfur are deposited on the branches and spread out from center of the black dot.

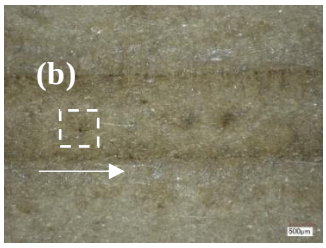

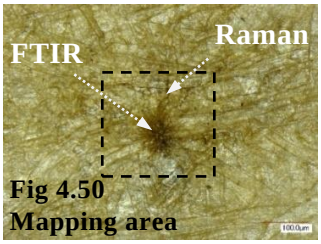

(a) x5 (b) x500

Fig 4.49 Optical observation of Sample 3

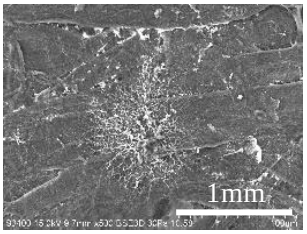

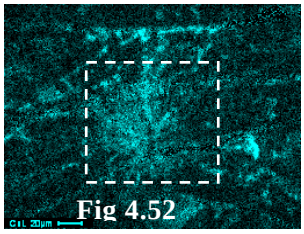

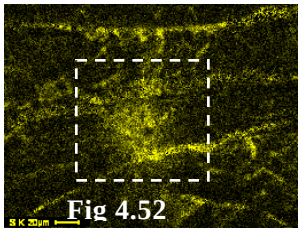

(a) SEM image (x500) (b) Copper (c) Sulfur

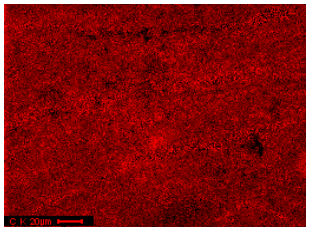

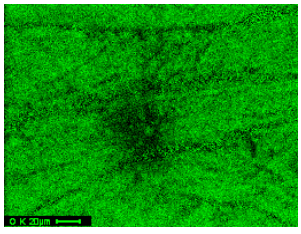

(d) Carbon (e) Oxygen

Fig 4.50 Element mapping of Sample 2

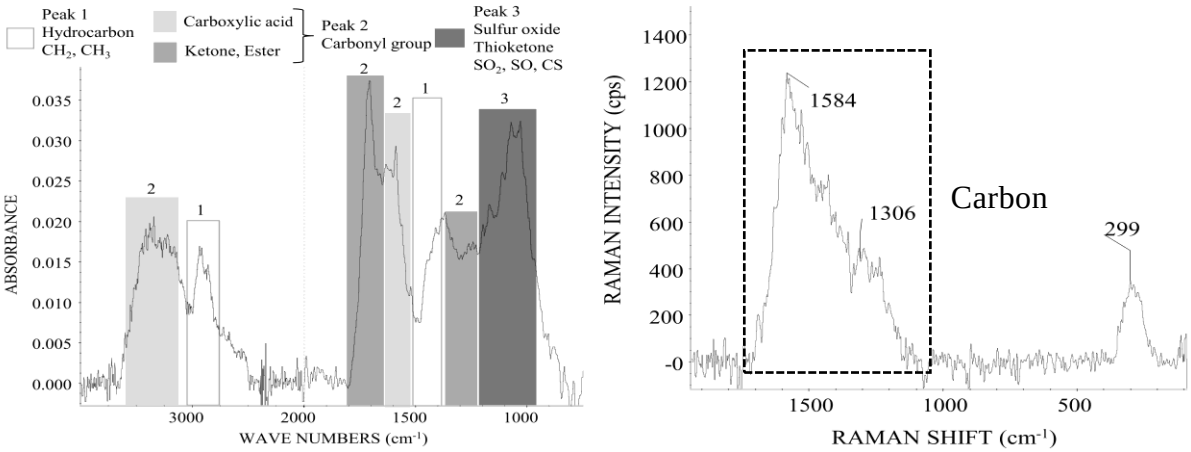

(a) FTIR spectrum (b) Raman spectrum

Fig 4.51 Result of the FTIR analysis and Raman analysis

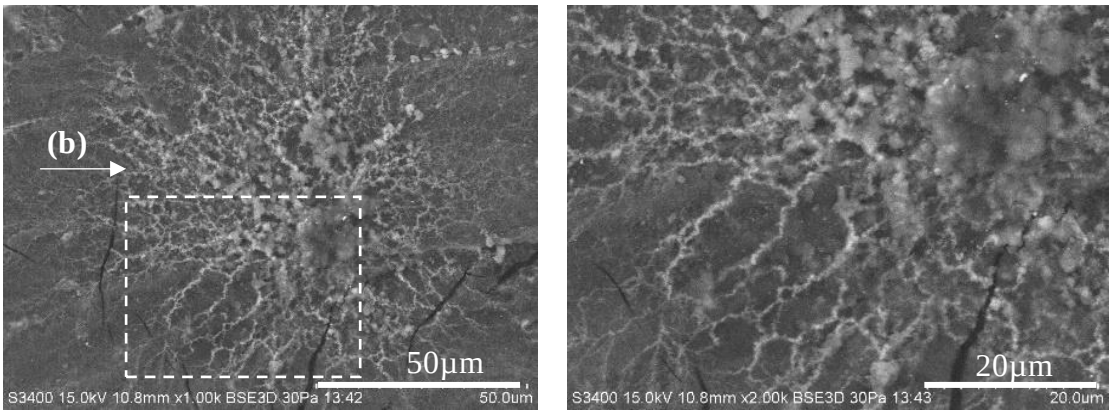

(a) x1000 (b) x2000

Fig 4.52 SEM image of the black dot (square in Fig 4.50)

(4) Sample 4

Fig 4.53 shows optical microscopic images of a black part, which is distributed like straight line along an oil gap. However, 500 magnification images reveal that the black part appears like straight line due to the arrangement of dot-shaped black spots.

Fig 4.54 shows element mapping around the dark black part. Carbon and sulfur are distributed on the dark black part (circles in Fig 4.53 and 4.54). Copper is distributed around the black part.

Fig 4.55 shows FTIR analysis results. The areas between brackets indicate analysis points. The IR spectra of all analysis points show oxidation sludge.

In addition, Raman analysis was not possible by strong fluorescence on entire black part.

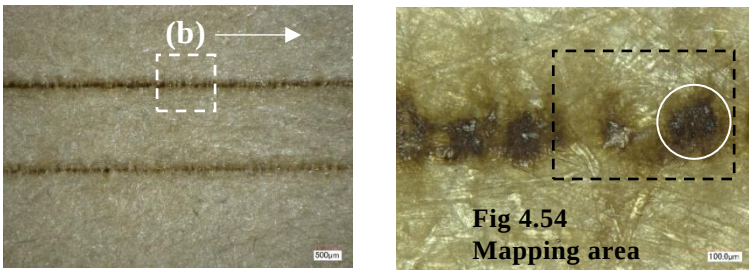

(a) x5 (b) x500

Fig 4.53 Optical observation of Sample 4

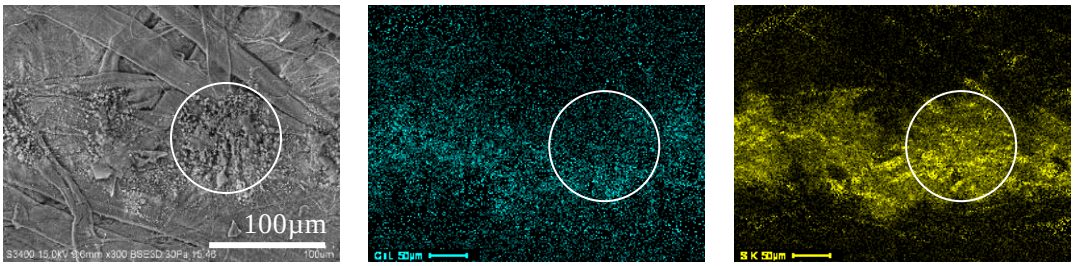

(a) SEM image (x300) (b) Copper (c) Sulfur

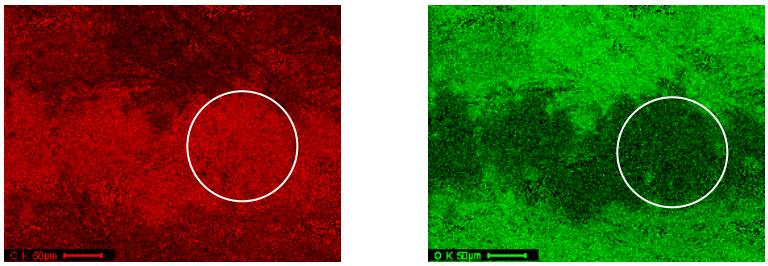

(d) Carbon (e) Oxygen

Fig 4.54 Element mapping of Sample 4

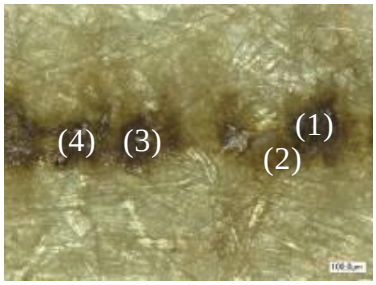

(a) Analysis point

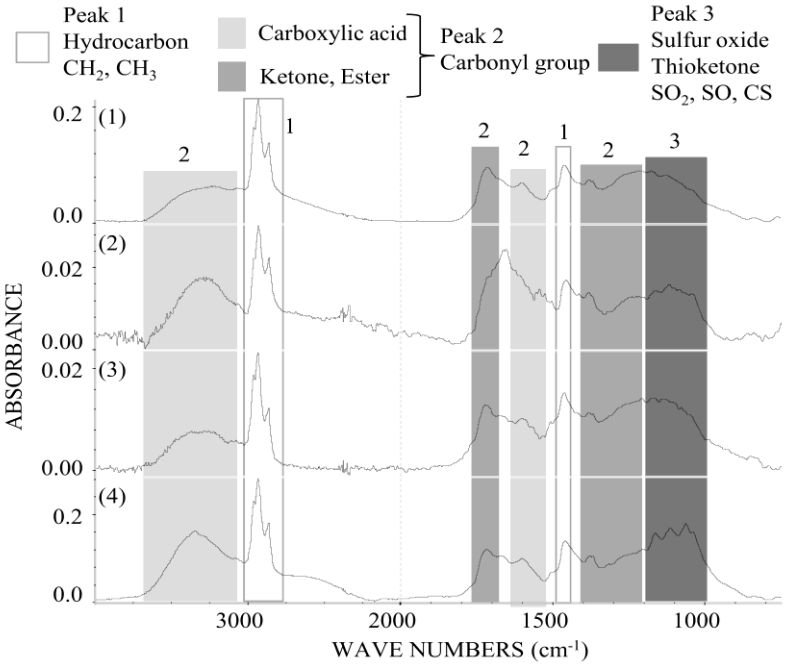

(b) FTIR spectra

Fig 4.55 FTIR analysis of four points

4.4.4 Discussion

(1) Physical properties of black part

The black deposits on the insulating paper correspond to oxidation sludge regardless of the shape. Copper sulfide is deposited as copper (I) sulfide, copper (II) sulfide, or both; sometimes, it is not deposited at all. Oxidation sludge is detected in the entire black parts of all four samples with different shapes. Copper sulfide (I) is detected in sample 1, copper sulfide (II) is detected in sample 3, and they both are detected in sample 2. Copper sulfide is not detected in sample 4. However, the composition of copper sulfide cannot be inferred from the analysis result.

Oxidation sludge sometimes contains little copper and a lot of sulfur. It is oxidation sludge in the dark black parts of samples 2 and 4 (circles in Fig 4.44 and 4.53). It is assumed that there is a bond between the insulating oil and sulfur, in addition to the bond with the dissolved copper. It is possible that sulfur in this surrounding is more than dissolved copper.

The black deposit on the insulating paper was determined to be the result of electric charging degradation regardless of its shape, and the previous attribution to "black part is carbonized trace" was mistaken [1]. This result will greatly affect maintenance of OF cable in the future.

(2) Generation process of copper sulfide

Oxidation sludge can be simulated experimentally, and the generation process can be elucidated. However, the generation process of copper sulfide is not sufficiently elucidated. Herein, the generation process of copper sulfide was found to involve two steps. First, oxidation sludge in the lower part of discharge path is decomposed by partial discharge. Then, copper and sulfur are bind by decomposition. Sample 1 (Fig 4.39) shows that copper and sulfur are distributed in large quantities along a crack by discharge. Therefore, copper and sulfur were deposited after the discharge. Samples 2 and 3 (Fig 4.48 and 4.52) show that copper sulfide was deposited in branch shape from the center of the black part to the outside. In addition, carbon is detected in some places. Moreover, the optical appearances of samples 2 and 3 are similar to the light emission pattern by discharge.

As a result, it is proposed that a partial discharge occurred in the black regions of samples 2 and 3. Moreover, presence or absence of partial discharge may be judged from the presence or absence of a branched black part. In the next section, partial discharge on oxidized sludge will be simulated.

(3) Insulation performance of black region

The insulation performance of the black region from the local scale to the whole cable core was examined based on the result of sample 1.

Fig 4.56 shows the state of electric charging degradation in the black part of sample 1.

The results indicate that electric charging degradation sites show low insulation performance. Discharge places are flocculated on the edge of the oil gap. Carbon is detected near the crack by Raman spectroscopy; the color in this area is jet black. Therefore, this jet-black area corresponds to carbon produced by discharge. In other words, the jet-black spot in the black part is a discharge site. These characteristics were also confirmed by electric charging tests simulating the electric charging degradation process (shown in 4.3.7). The partial discharge occurred under the operating electric field, when copper sulfide was aggregated in the electric field direction. Moreover, the degradation process, from the aggregation of copper compounds to dielectric breakdown (STEP 1-5 in Fig 4.7), was reproduced during the electric charging test.

Fig 4.57 shows the state of electric charging degradation from the outermost layer to the inside of the cable core with reference to Fig 4.43. First, partial discharge generates a crack, carbonization, and deposition copper sulfide. Moreover, insulation performance of black part promotes deterioration. The crack and the carbonization area have a maximum length of 12 mm and a maximum width of 3 mm. These correspond to eight sheets, that is, the thickness is 1.6 mm. In addition, copper sulfide is deposited along the crack. In other words, the combined width of these degradation portions is several millimeters and its thickness is 1 mm or greater. Then, partial discharge energy is strongly released in the direction of the paper edge and the outer layer. The crack is in the direction of the paper edge; there were five cracked papers toward the outer layer in sample 1. In addition, there are five sheets of carbonized paper toward outer layer and two sheets toward the inner layer in sample 1. Thus, Fig 4.57 shows important data for elucidating the dielectric breakdown process.

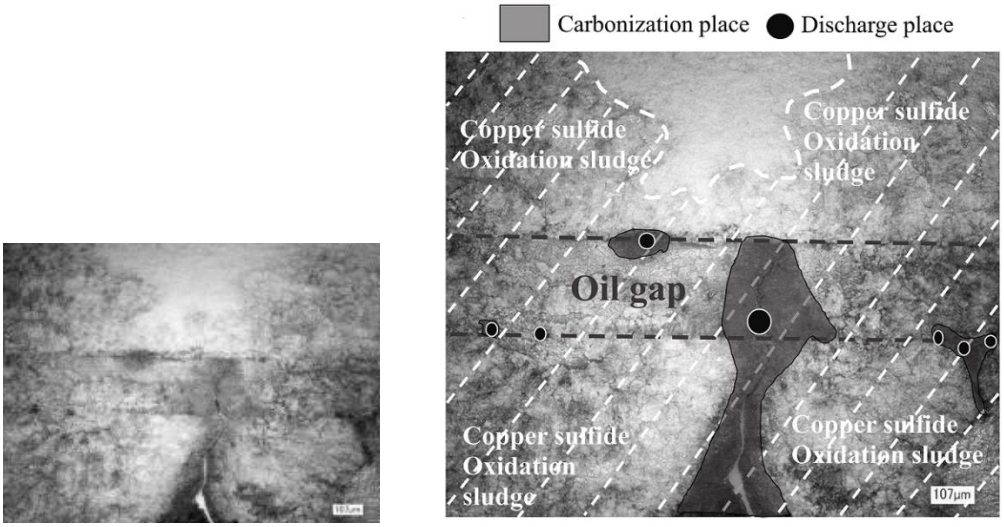

(a) Optical image (b) State of electric charging fegradation

Fig 4.56 State of electric charging degradation in the black part of Sample 1

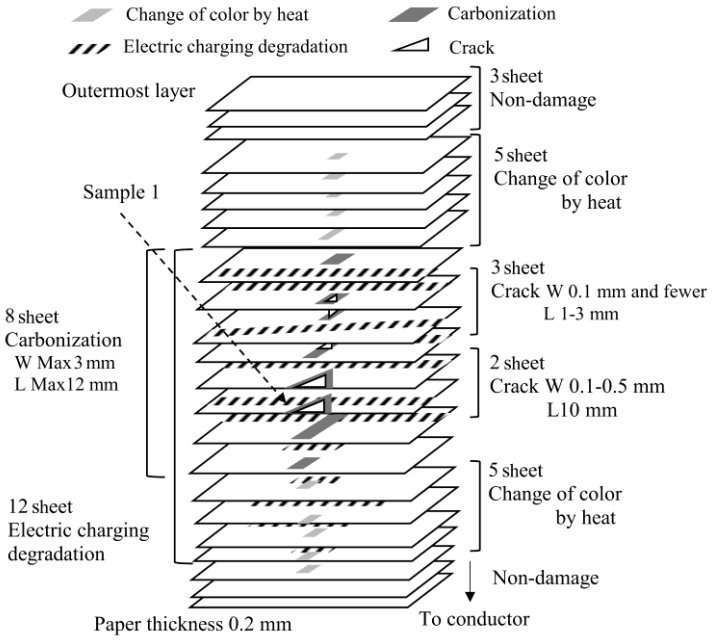

Fig 4.57 State of electric charging degradation from the outermost layer to the inside of the cable core with reference to Fig 4.43

4.4.5 Electric charging degradation situation in used cables

The degradation situation in used cables determined that the black deposits on insulating paper are due to electric charging degradation, regardless of their shape. Moreover, the electric charging degradation sites show low insulation performance due to starting point of partial discharge. In addition, copper sulfide, cracks, and carbonization are produced along the partial discharge path. Therefore, partial discharge of the electric charging degraded part accelerates degradation of insulation performance. This result was demonstrated on samples of aged OF cable, not experiments. In conclusion, in the present study, electric charging degradation was demonstrated to be a type of OF-cable degradation.

4.5 Development of degradation diagnosis by employing insulation oil analysis

4.5.1 Introduction

The quantity of dissolved copper increases in STEP 1 of the electric charging degradation process, decreases in STEP 2, and does not change after STEP 3, because the experimental results simulating each STEP of 4.3 indicated those characteristics. In other words, the progress of degradation (which STEP) can be estimated by the quantity trend of dissolved copper. In addition, oxidation sludge was generated by the deterioration of dissolved copper. Therefore, the quantity of oxidation sludge produced equals the decrease in the quantity of dissolved copper in STEP 2. As a result, the degradation stage can be diagnosed by the decrease in the quantity of dissolved copper.

However, there are two major problems. First, the aging of most OF cables is more than 20 years. In other words, the quantity of dissolved copper over the past 20 years is unknown, because the past quantity of dissolved copper cannot be measured at present. Therefore, methods for estimating the past quantity of dissolved copper are necessary.

Next, it is possible that the quantity of dissolved copper in the insulating oil decreases due to a cause other than the electric charging degradation. The cause is supply of oil, because the copper dissolution oil is diluted due to the transfer of oil. Therefore, methods for estimating the cause of the decrease are necessary.

4.5.2 Development of degradation diagnosis

(1) Methods for estimating the quantity of dissolved copper in the past

The relationship between the quantity of dissolved copper and tan δ of insulating oil was the logarithmic graph of Fig 4.22. Fig 4.58 shows the graph in which both axes in Fig 4.22 are integers. However, the quoted data was only the data on the copper that dissolved when copper rods were placed in oil. The relationship shows high linearity because of the high correlation function. As a result, the quantity of dissolved copper at any tan δ can be calculated due to this linearity. The quantity of dissolved copper can be calculated by equation (2). However, the copper compounds are dissolved in different types shown in Fig 4.22. As a result, the slope of this straight line is different for each joint, because the slope of this straight line is different for each copper compound.

$$Cu = (\tan\delta - \tan\delta_{new}) \times Cu_m / (\tan\delta_m - \tan\delta_{new}) \qquad (2)$$

Cu: Any quantity of dissolved copper

Cu_m: Measured value (quantity of dissolved copper)

tan δ: Any value tan δ_m: Measured value tan δ_{new}: New oil value

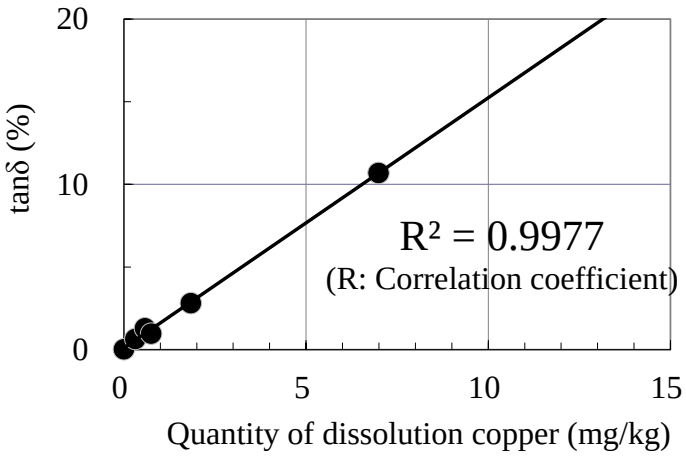

Fig 4.58 Relationship of the quantity of dissolution copper and tan δ

(2) Determination of the cause of increase and decrease in the quantity of dissolved copper

a. Introduction

Various chemical reactions occur due to copper dissolution and the generation of oxidation sludge. As a result, it is possible that decomposition gas is generated due to the chemical reactions. However, the gas does not generate because of the supply of oil, because no chemical reactions occur. In other words, the decrease in the quantity of dissolved copper due to this degradation can be determined from the decomposition gas. Therefore, the tendency of the decomposition gas at the time of degradation was investigated.

b. Methods

The dissolution of copper and the generation of oxidation sludge were reproduced by simulation tests. The test circuit and methods are the same as the test methods described in 4.3.5 (2). The insulating oil used was synthetic oil (soft type). The insulation oil was degassed at the beginning of the test. The quantity of oxygen in the oil after degassing was 800 mg/kg.

Table 4.6 shows the sample in the PFA bottle and the test conditions. Sample No. 3–5 were copper-dissolved oils with previously dissolved copper rods. The sulfur powder used was Sulfur, Powder of Practical Grade (Wako Pure Chemical Industries Corporation, Product code 195-04625, Japan).

After the test, the insulation oil samples were analyzed for gas in oil. The measurement gases were hydrogen, carbon monoxide, methane, ethylene, ethane, acetylene, and the total quantity of combustibility gas (TCG). The automatic analyzer for in-oil gas used was a SGOA-10A-12T (SANMI CORPORATION).

Table 4.6 Samples in PFA bottles and test conditions

Sample number		1	2	3	4	5
Imitation		Copper dissolution		Generation of oxidation sludge		
Oil type		Synthetic oil	Mineral oil	Synthetic oil	Mineral oil	Synthetic oil
Reagent		Copper tape	Copper tape	-	-	-
Sulfur powder	[mg/kg]	-	-	-	-	945.6
Heating temperature	[°C]	50	50	50	50	50
Heating time	[month]	2	2	1	1	1
Charge		-	-	5 kV, 50 Hz	5 kV, 50 Hz	5 kV, 50 Hz
Quantity of dissolution copper [mg/kg]	Before the test	0.0	0.0	26.9	9.3	19.9
	After the test	0.4	0.5	8.6	1.6	4.8

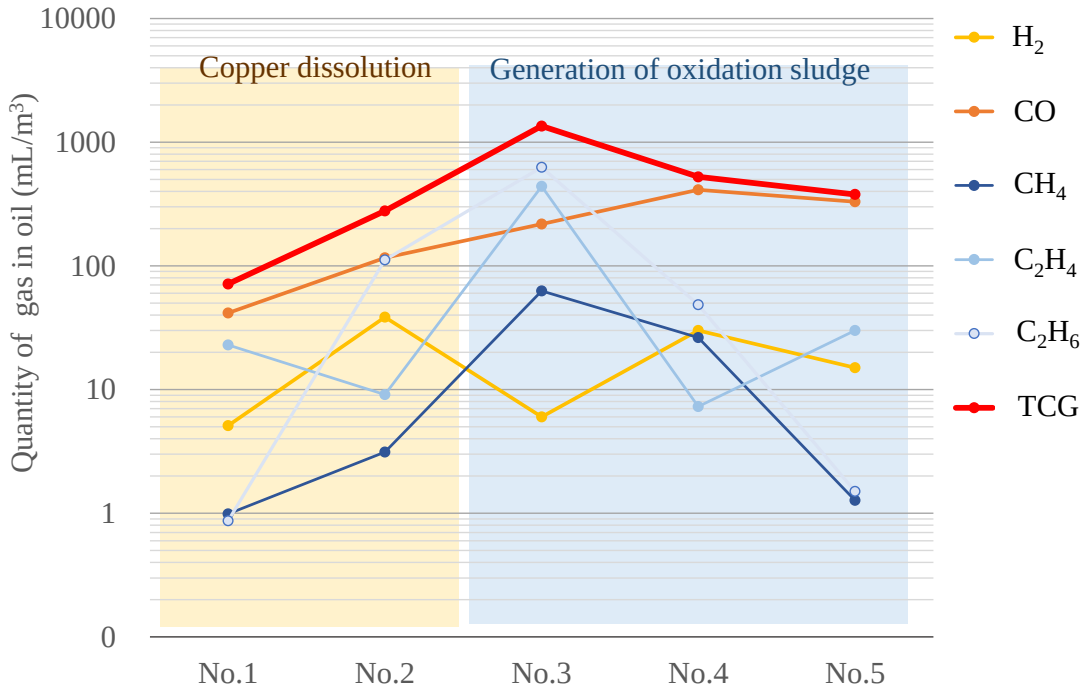

Fig 4.59 Result of the analysis of gas in oil

c. Results

The dissolution of copper and the generation of oxidation sludge were confirmed.

Fig 4.59 shows the measurement results of the quantity of gas generated in oil. Carbon monoxide was detected in considerable quantities in all samples. Hydrogen was detected in all samples, but the amount was different. Hydrocarbons were detected in all samples, but the amounts were quite different. As a result, TCG was detected in considerable quantities in all samples. No acetylene was detected.

d. Discussion

The cause of the decrease in the quantity of dissolved copper and the degree of degradation can be estimated by the quantity of TCG, because TCG is generated through the generation of oxidation sludge.

(3) Aggregation power of oxidation sludge

a. Characteristic of aggregation

Oxidation sludge aggregates in the high electric field region due to the dielectrophoretic force as shown in Fig 4.20. Copper compounds in oil changing to oxidized sludge are dissolved in different types and concentrations at each joint box, as shown in 4.3.5 (4). In other words, it is possible that the characteristics of agglutination are different because of the differences in the type and proportion of copper compounds. Such differences can be used for degradation diagnosis. Therefore, the aggregation characteristics of copper compounds were investigated.

b. Methods

Table 4.7 shows the sample conditions. The samples of copper-dissolved oil were dissolved copper to 10 mg/kg or more via the conditions shown in Table 4.7. Sample No. 1 and 2 were heated by placing the copper rods in insulating oil. No. 3 and 4 were heated by placing the copper compound reagents in insulating oil. No. 5 were heated by placing the copper rods and reagents in insulating oil. At the time of preparing the sample, the quantity of dissolved copper and tan δ were measured for each concentration. The measurement methods were the same as the measurement methods of dissolved copper quantity and tan δ described earlier.

Oxidation sludge was generated with this copper-dissolved oil, and the methods were the same as in 4.3.5 (2). The oxidation sludge was tested by dielectrophoresis, and the methods are the same as in 4.3.5 (3). The characteristics of aggregation were investigated through the measurement time when aggregation by visual observation was confirmed.

The quantity of dissolved copper and the tan δ of the insulating oil in used cables were measured. The samples were the insulation oil in 48 used joints disassembled by TEPCO. In addition, the results of disassembly investigation were provided by TEPCO. The characteristics of aggregation in the used cables were compared and investigated through the quantity of dissolved copper, tan δ, and generation region of oxidation sludge. Table 4.8 provides the definitions of generation regions.

Table 4.7 Sample conditions

Sample No.	Oil type	Reagent	Conditions for dissolution	
			Atmosphere	Temperature [°C]
1	Synthetic oil	Copper rod	Vacuum	60
2	Mineral oil	Copper rod	Vacuum	60
3	Synthetic oil	AACu, Sulfur powder	Air	60
4	Synthetic oil	AACu	Vacuum	60
5	Synthetic oil	8-Quinolinone	Vacuum	60

Table 4.8 Definition of oxidation sludge generation regions

Generation area	Reinforcement insulation layer	Cable core
Wide	All over	All from inner layer to outer layer
Narrow	Partially	Part of oil gap of inner and outer layers

c. Results

Fig 4.60 shows the relationship between the quantity of dissolution copper and tan δ. In addition, the aggregation time of oxidation sludge obtained by the dielectrophoresis test is shown in Fig 4.60. The aggregation time of Sample No. 4 was approximate because the exact time was unmeasured.

When the ratio of tan δ to the quantity of dissolved copper (tan δ/Cu) that indicates the slope of the straight line is large, the aggregation time of oxidation sludge was several tens of seconds. When tan δ/Cu was small, the time was hundreds of seconds.

Fig 4.61 shows the relationship between the quantity of dissolution copper, tan δ, and the oxidation sludge generation region. The region of generation of 11 joints was a wide region. The minimum of these tan δ/Cu values was 0.95. The straight line shown in Fig 4.61 shows the ratio of 0.95. However, the ratio of joints in the green shaded area shown in Fig 4.61 was more than 0.95, whereas the generation region was a narrow region. The maximum quantity of dissolved copper in each joint calculated using equation (2) shown in 4.5.2 (1) was less than 0.1 mg/kg.

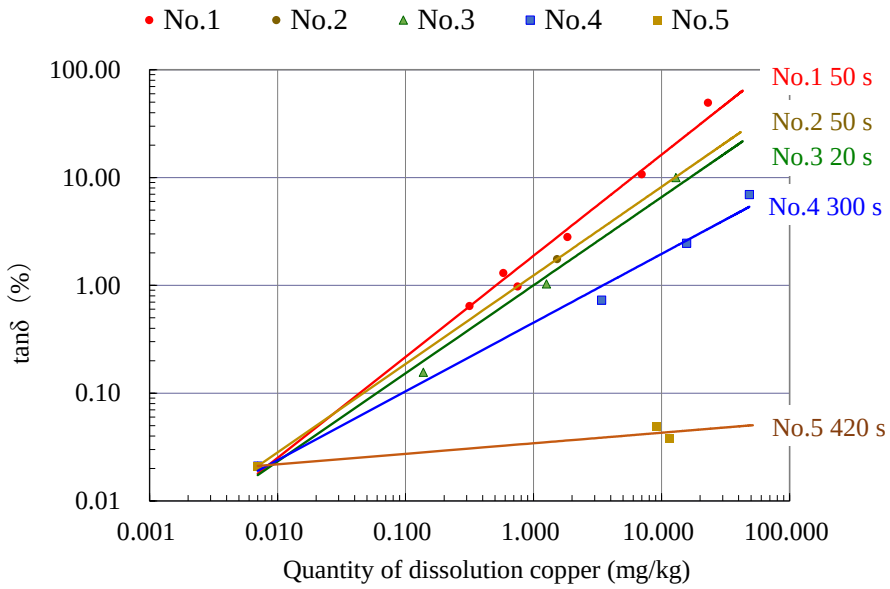

Fig 4.60 Relationship between the quantity of dissolution copper, tan δ, and aggregation time

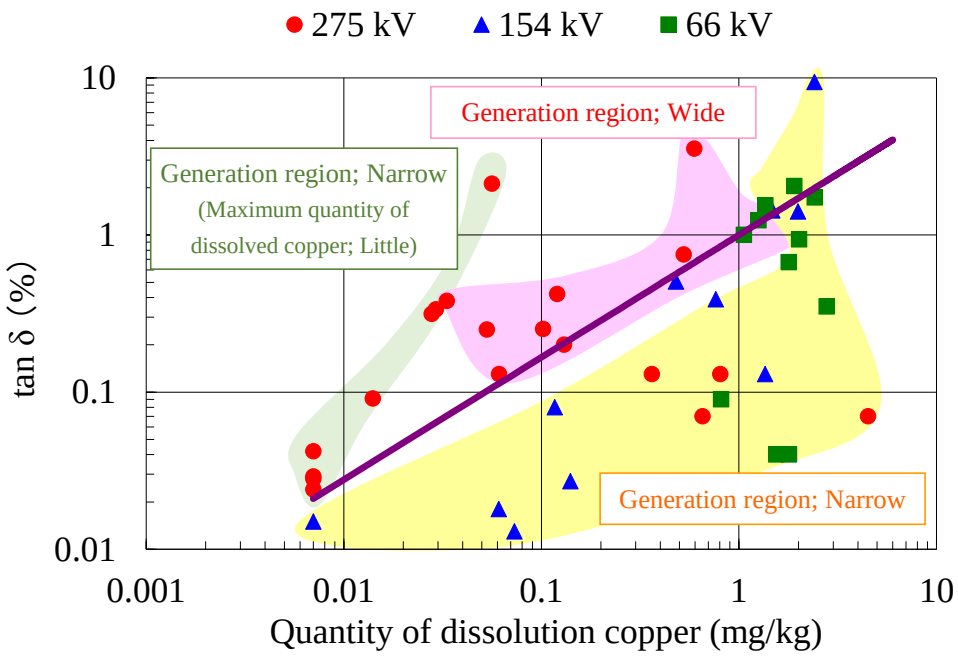

Fig 4.61 Relationship between the quantity of dissolution copper, tan δ, and oxidation sludge generation region

d. Discussion

Under the same electric field, the oxidation sludge generated when tan δ/Cu is high receives a large dielectrophoretic force, because the agglomeration time is short according to the test results. In addition, the dielectrophoretic force is shown by equation (1) in 4.3.2 [22]. Under the same electric field, the intensity of the force is determined by the radius and the relative permittivity of a particle. In fact, the radius and the relative permittivity of the particles of oxidation sludge are different at each connection, because the copper compounds, which changed to oxidized sludge and dissolved in oil, are dissolved in different types and concentrations at each joint box. In other words, even under a weak electric field, the oxidation sludge generated when tan δ/Cu is high receives a large dielectrophoretic force and aggregates. In conclusion, when tan δ/Cu is high, electric charge degradation occurs in a wide region within the joint including a weak electric field region. The results indicate that tan δ/Cu becomes a determining factor in estimating the region of degradation.

(4) Relationship between the degradation position in the used cables and the quantity of TCG

a. Quantity of TCG at each degradation position

The quantity of TCG increases due to electric charge degradation as shown in Fig 4.59. However, detecting the abnormality inside the joint by acetylene or hydrogen gas in oil is difficult, because the gas diffusion to the outside of insulating paper is very gentle [23]. In other words, when the electric charge degradation occurs inside a joint, the quantity of TCG containing hydrogen is less degraded than when it is outside. As a result, it is possible that degradation diagnosis performed by using the quantity of TCG cannot be detected completely the degradation inside the joint. Therefore, the relationship between the degradation position and TCG was compared with the results of disassembly investigation and the quantity of TCG before the investigation.

b. Electric charging degradation position

Fig 4.62 shows the electric charging degradation positions. Near the semi stop (Near Semi) and the reinforcement layer edge were set as the outside because of the direct contact with the insulating oil in the joint box (blue line in Fig 4.49). The rest were set as the inside because it was surrounded with the cable core and the reinforcement layer (red line in Fig 4.49).

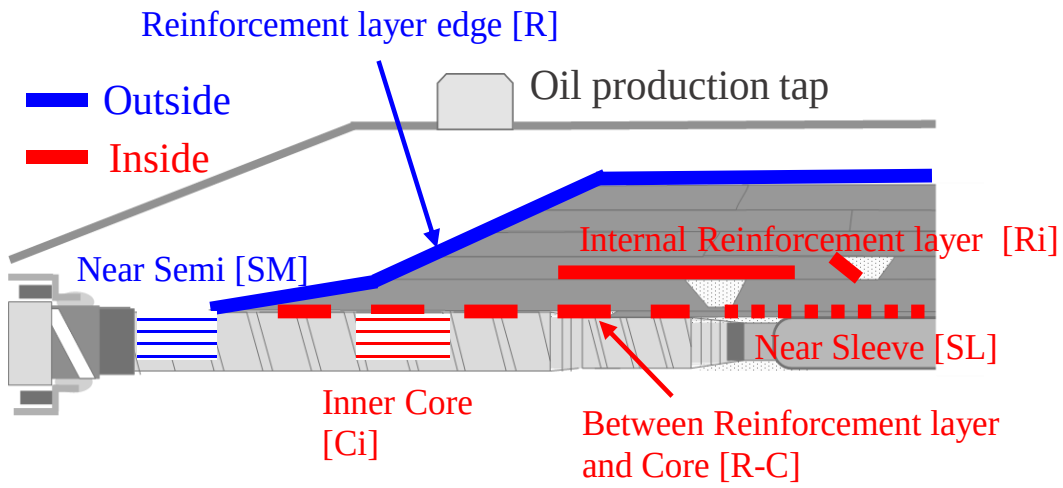

Fig 4.62 Electric charging degradation positions

c. Methods

The samples were ten joints of 275-kV OF cables that were disassembled.

First, two joints whose disassembly rank is “a” were investigated. This disassembling rank is specified in Vol. 70 of Electric Technology Research Association in Japan [1]. The electric charging degradation positions of the two joints were inside and outside. The detailed degradation position was confirmed based on Fig 4.63. The quantity of dissolved copper in insulating oil, tan δ, and TCG were measured by taking oil before disassembly. Past tan δ and TCG provided previous inspection data. Moreover, tan δ/Cu and the past maximum quantity and decrease quantity of dissolved copper were calculated from those data, trends, and equation (2) shown in 4.5.2 (1). In addition, the maximum quantity of TCG and decrease time at the time of decreasing tan δ were confirmed by the trend and past data.

Each characteristic value of the remaining eight joints was confirmed using the same methods.

The results of disassembly investigation were provided by TEPCO.

d. Results

Fig 4.63 shows the electric charging degradation positions of the two joints of rank “a” and the characteristic values of the insulating oils in the two joints. The degradation positions of joint A was a wide region; the positions were three outer layers in the cable core near the semi, the rising part of the reinforcing layer, and near the sleeve. Moreover, discharge marks with holes in insulating paper were in the electric charging degradation region. Therefore, the degradation position was an inside region. The degradation positions of joint B was an outside region; the positions were mainly the outer three layers in the cable core near the semi. Moreover, discharge marks with holes in insulating paper were in the electric charging degradation region, and the degradation situation was a local region. The quantity of TCG in joint A whose degradation position was an inside region was smaller than that in joint B, whereas the tan δ/Cu of joint A was higher than that of joint B. The maximum quantity of dissolved copper in the past at joint B was significant.

Table 4.9 shows the electric charging degradation positions of the ten joints and the characteristic values of the insulating oils in the ten joints. When tan δ/Cu is 1.0 or more and the decrease quantity of dissolved copper is 1 mg/kg or more, the electric charging degradation positions were inside and outside. The discharge marks were in the degradation region inside of the joints. However, the quantity of TCG in the joints tended to be smaller than in the joints with tan δ/Cu values less than 0.5 and the joints with the same disassembling rank. When tan δ/Cu is approximately 0.5, the degradation position is also inside the joint, whereas the discharge mark was only near semi outside of the joint. J3 with a short decrease time had a disassembly rank “b” even with the same quantity of

dissolved copper as a joint with disassembly rank “a.” The decrease quantity and decrease time of J7 with a low tan δ/Cu was significant.

TCG: 194 mg/kg, Ratio [tan δ/Cu]: 2.63,
Quantity of dissolution copper
Past the maximum value: 2.39 mg/kg　　Decrease quantity: 1.4 mg/kg

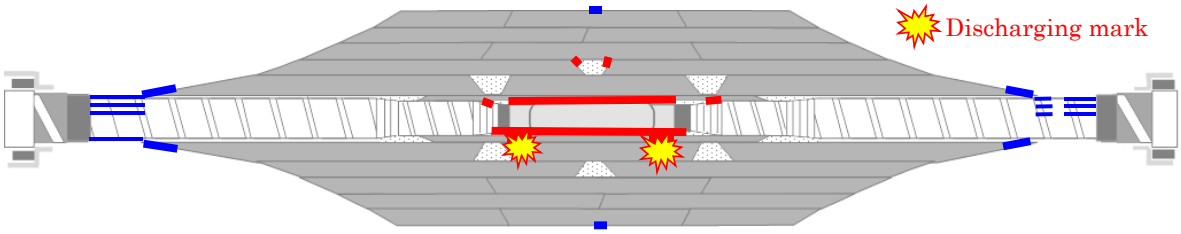

(a) Joint A (Position: Inside）

TCG: 341 mg/kg, Ratio [tan δ/Cu]: 0.12,
Quantity of dissolution copper
Past the maximum value: 24.8 mg/kg　　Decrease quantity: 23.5 mg/kg

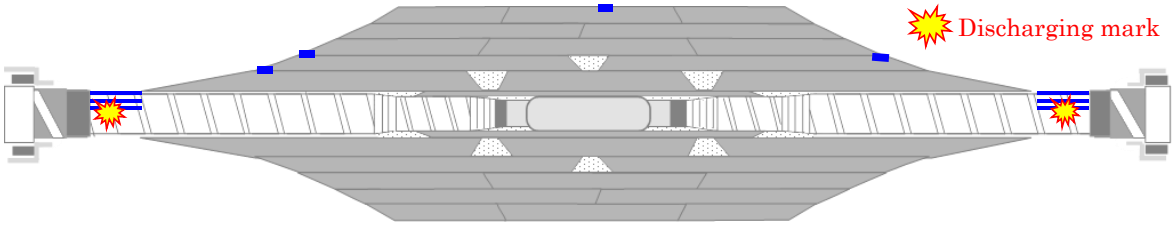

(b) Joint B (Position: Outside)

Fig 4.63 Comparison of the joints with different electric charging degradation positions

Table 4.9 Relationship between the degradation position and the insulation oil characteristics for used joints

No	Disassembly rank	Electric charging degradation position		Discharging mark position	TCG	Ratio	Quantity of dissolution copper		Decrease time
		Outside	Inside		[mL/m^3]	[tanδ/Cu]	Past the maximum value [mg/kg]	Decrease quantity [mg/kg]	[year]
J1	c	SM･R	-	-	36	3.0	0.4	0.4	22.0
JA	a	SM	SL	SL	194	2.6	2.4	1.4	14.5
J2	a	SM･R	Ri R-C	R-C	175	1.3	2.7	1.7	17.0
J3	b	R	SL	-	135	1.0	3.7	3.5	9.8
J4	b	SM･H	Ri R-C SL	-	431	0.5	7.0	5.7	15.5
J5	a	SM･R	R-C	SM	347	0.4	8.1	7.1	10.5
J6	b	SM･R	-	-	340	0.3	8.2	7.4	12.0
JB	a	SM･R	-	SM	341	0.1	24.8	23.5	13.0
J7	a	SM･R	R-C SL	-	304	0.1	20.8	19.2	22.5
J8	b	SM･R	-	-	78	0.1	0.8	0.4	11.0

e. Discussion

Oxidation sludge and copper sulfide are generated from dissolved copper. Moreover, when the decrease quantity of dissolved copper is more, the generation quantity of oxidation sludge and copper sulfide increases. In addition, when the decrease time of dissolved copper is longer, the generation time of oxidation sludge and copper sulfide is longer. Therefore, when the decrease quantity is more and the decrease time is longer, electric charging degradation progresses. The results indicate that decrease quantity and decrease time become determining factors that can be estimated the region of the degradation. However, even though the quantity of dissolved copper is less, the dissolved copper aggregates more due to the dielectrophoretic force when tan δ/Cu is high, and the degradation occurs inside the joint. Moreover, the TCG generated inside the joint is difficult to diffuse to the outside [23]. In other words, it is possible that the quantity of dissolved copper and the TCG change are small even though deterioration is progressing. It is therefore necessary that the criterion for degradation diagnosis at a high tan δ/Cu is set lower than when tan δ/Cu is low.

The degradation region is mainly outside of the joint when tan δ/Cu is low, because strong dielectrophoretic forces are required. The regions with strong dielectrophoretic forces are near the semi according to the electric field analysis results shown in 4.3.2, whereas the regions coincide with the tendency of the degradation positions shown in Table 4.9. The results indicate again that the electric field analysis results are correct.

(5) Devising degradation diagnostic methods

The degradation diagnostic methods were devised based on the relationship of electric charging degradation, trend of quantity of dissolved copper, tan δ, and quantity of TCG.

Fig 4.64 shows the characteristic values used for the diagnostic methods. The quantity of dissolved copper in the past and its trend are calculated by tan δ and equation (2) shown in 4.5.2. In addition, the cause of the decrease in the quantity of dissolved copper is able to be judged by the quantity of TCG. In fact, when the quantity of TCG at the time of decrease is large, electric charging degradation is judged to be a cause of the decrease.

Fig 4.64 shows the outline of degradation diagnostic methods. The degradation step is determined by the trend graph shape of tan δ; the degradation step is represented by the steps of the electric charging degradation process shown in Fig 4.7. The decision rank indicating the degree of degradation is D when the decision is STEP 0 or STEP 1, because oxidation sludge and copper sulfide are not deposited yet.

In STEPs 2–5, the decision rank is determined based on the number of decision items exceeding the reference value. However, the reference value differs depending on the value of tan δ/Cu ([a]). The division of tan δ/Cu was set to three levels with reference to Fig 4.61 and Table 4.9. However, it is possible that the division will be modified based on the results of disassembly investigation in the future. It is desirable that the reference value is set through each data of the insulating oil in used cables and the results of disassembly investigation. The reference value is not able to be disclosed in this study because of the knowhow.

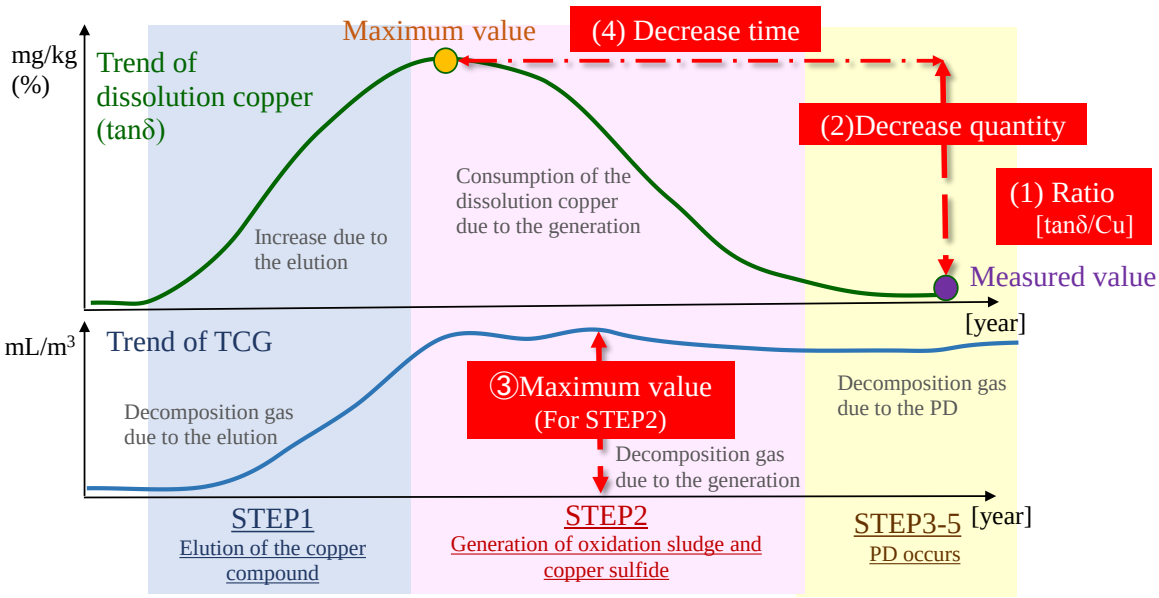

Fig 4.64 Characteristic values for degradation diagnosis

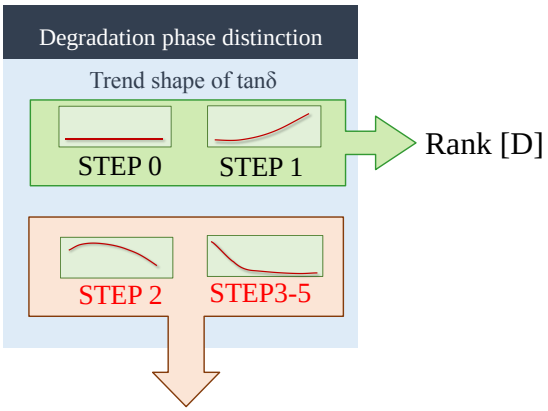

Decision item and value				Decision Rank	
[a] Ratio	[b] TCG	[c] Decrease quantity	[d] Decrease time	Hit number (Item [b, c, d])	Rank
≧0.9	A mL/m^3	D mg/kg	G year	3	A
0.4-0.9	B mL/m^3	E mg/kg	H year	2	B
0.9≧	C mL/m^3	F mg/kg	Q year	1	C

Fig 4.65 Overview of a degradation diagnosis method

4.5.3 Confirmation of diagnosis accuracy

(1) Methods

The diagnostic accuracy was confirmed using the coincidence ratio between the disassembly rank of used joints and the degradation diagnostic rank. In addition, the disassembly rank was classified into four ranks (a, b, c, and d) due to the generation status of black parts, whereas the cause of the generation in this discrimination method was carbonization instead of electric charging degradation [1]. Herein, the word of "carbonization" using in this discrimination method was replaced everything with the word of "electric charging degradation."

The reference values for degradation diagnosis were determined based on Fig 4.10, Table 4.9, and past data of inspection (TCG, tan δ).

(2) Results

Table 4.10 shows the confirmation results, and Table 4.11 shows the breakdown of the disassembly rank of the compared joints. The data of "Criterion of Electr. Technol. Res. Vol. 70. No. 1" were cited from the reference [1]. The quoted data were the result of comparing between the results of abnormality diagnosis by using insulating oil analysis, which is a conventional method, and disassembly rank data of the joints. This developed diagnostic method was confirmed to be considerably more accurate than the conventional method.

Table 4.10 Result of matching with disassembly investigation results

Diagnosis method	Number of diagnosis	Hitting percentage		Overestimation		Underestimate	
		%	number	%	number	%	number
Criterion of Electr. Technol. Res, Vol. 70, No1	312	61 %	190	26 %	81	13 %	41
This diagnosis method	24	96 %	23	0 %	0	4 %	1

Table 4.11 Breakdown of the disassembly rank of joints compared

Disassembly rank	a	b	c	d	Total
Number	7	7	9	1	24

4.5.4 Electric charging degradation diagnosis by insulation oil analysis

The degradation diagnosis method targeting electric charging degradation by employing insulation oil analysis was developed; the quantity of dissolved copper in oil, tan δ of oil, and TCG are the analysis items. The degradation stage (STEP 1-5) is diagnosed from the trend of quantity of dissolved copper and tan δ. The degree of degradation is determined in four stages (ABCD) using tan δ/Cu, the quantity of decrease in dissolved copper and the decrease time, and TCG. Moreover, the quantity of dissolved copper in the past can be calculated from tan δ. The degree of degradation of these four stages is correlated with the disassembly rank shown in the reference [1]. However, the definition of the black part in the reference [1] replaces carbonization with electric charging degradation.

The diagnostic accuracy of this developed method was confirmed to be higher than that of the conventional abnormality diagnosis method by employing insulation oil analysis. The results indicate that this developed method is a possible diagnostic method correlated with the electric charging degradation process. In addition, this diagnostic method can be easily introduced, because the measurement of this diagnostic method only added the measurement of quantity of dissolved copper to the conventional method.

This developed method is a diagnostic method that can be expected to be widely used in the future owing to the above two points. However, it is possible that it will be necessary to review the reference value in the future, because the accuracy check data are few.

4.6 Conclusion

In recent years, the dielectric breakdown accidents of OF cables of 275 kV, 154 kV have occurred in TEPCO. After that, the black parts on the insulating paper were confirmed through the disassembly investigation of the broken down cables. Subsequently, copper sulfide was discovered on the black parts by TEPCO. As a result, the cause of the accidents was considered to be electric charging degradation due to copper sulfide, and the degradation process was devised. It is therefore necessary to study the process and origin of this copper sulfide deposition on insulating paper in OF cables for the purpose of accident prevention.

Therefore, in the present paper, it is revealed that the devised degradation process was demonstrated through each simulation test. Moreover, it is revealed that the black parts on the insulating paper are deposits of copper compounds due to electric charging degradation regardless of shape. In addition, the degradation parts become the starting point of the partial discharge and adversely affect the insulation performance. In the simulation tests, copper eluted as compounds or complexes from the conductor to the insulating oil, and then oxidation sludge was deposited by dielectrophoresis of the dissolved copper. In the charging test, partial discharges occurred on the electric charging degradation part and finally dielectric breakdown occurred. The charge test condition was the same as that for the OF cable under the electric field and pressure. Moreover, it was thought that the degradation of OF cables does not occur under these conditions. Finally, it was confirmed that the deposition of copper sulfide on insulating paper, cracks, and carbonization were generated along the partial discharge path at the electric charging degradation part in the aged cables. In other words, the electric charging degradation of OF cables is demonstrated to be degradation leading to dielectric breakdown.

A conventional abnormality diagnosis method using insulation oil analysis was not able to capture electric charging degradation. Therefore, in the present paper, a degradation diagnosis method by employing insulation oil analysis that is able to capture the degradation was devised. In this diagnostic method, the degradation tendency is determined in four levels: the trend of dissolved copper quantity and tan δ, tan δ/Cu, decrease time and quantity of dissolved copper quantity, and TCG. In addition, this developed method was confirmed to be more accurate than the conventional diagnosis method.

Further studies are needed to elucidate the process from the occurrence of partial discharge to dielectric breakdown, because a series of data from partial discharge to dielectric breakdown cannot be measured. Moreover, in the developed degradation diagnostic method, it is possible that it will be necessary to review the reference value in the future, because the accuracy check data are few. However, in the present paper, a new natural degradation phenomenon related to the OF cables was elucidated, and a new

degradation diagnosis method by using insulating oil analysis was developed. In other words, it is expected that this present paper will be an important achievement for the elucidation of natural degradation of OF cables and the maintenance of OF cables in the future.

REFERENCES

[1] Electric Technology Research Association, “Maintenance methods for underground transmission cable systems,” Electr. Technol. Res, Vol. 70, No1, 2014.

[2] S. Nsukawa, H. Amanai, and K. Fukuda, “Investigation of the oldest 154 kV Oil-filled cable in japan,” National convention, IEE Japan, No. 7-197, 2009.

[3] Y. Tanimura, T. Doi, and M. Nishiuchi, “Investigation of Aged Oil-filled Cable,” Annual Conference of Power and Energy Society, IEE Japan, No. 255, 2010.

[4] Y. tanimura, T. shiro, T. Iida, Y. aihara, Y. Morishita, and T. Nagano, “Investigation of Aged Oil-filled Cable Joint,” Annual Conference of Power and Energy Society, IEE Japan, No. 422, 2012.

[5] F. Scatiggio, V. Tumiatti, R. Maina, M. Tumiatti, M. Pompili, and R. Bartnikas, “Corrosive Sulfur Induced Failures in Oil-Fi1led Electrical Power Transformers and Shunt Reactors,” IEEE Trans. Power Delivery, Vol. 24, NO. 3, pp. 1240-1248, 2009.

[6] CIGRE WG A2-32, “Copper sulphide in transformer insulation,” Final Report, Brochure 378, 2009.

[7] H. Kawarai, Y. Fujita, J. Tanimura, N. Yamada, and E. Nagao, “Deve1opment of quantitative evaluation of copper sulfide deposition on insulating paper,” IEEE, 2008 Annual Report Conference on Electrical Insulation Dielectric Phenomena.

[8] T. Amimoto, E. Nagao, J. Tanimura, S. Toyama, Y. Fujita, H. Kawarai, and N. Yamada, “Identification of affecting factors of copper sulfide deposition on insulating paper in oil,” IEEE Trans. Dielectr. Electr. Insul, Vol. 16, pp. 265-272, 2009.

[9] T. Amimoto, N. Hosokawa, E. Nagao, J. Tanimura, and S. Toyama, “Concentration dependence of corrosive sulfur on copper-sulfide deposition on insulating paper used for power transformer insulation,” IEEE Trans. Dielectr. Electr. Insul, Vol. 16, pp. 1489-1495, 2009.

[10] H. Kawarai, Y. Uehara, K. Mizuno, S. Tyama, and E. Nagao, N. Hosokawa, T. Amimoto, “Influences of oxygen and 2,6-di-tert-butyl-p-cresol on copper sulfide deposition on insulating paper in oil-immersed transformer insulation,” IEEE Trans. Dielectr. Electr. Insul, Vol. 19, pp. 1884-1890, 2012.

[11] K. Mizuno, R. Nishiura, F. Kato, and M. Hikita, “Elucidation of formation mechanism of by-products of copper sulfide deposition on insulating paper in oil-immersed transformer,” IEEE Trans. Dielectr Electr. Insul, Vol. 21, pp. 1376-1383, 2014.

[12] T. Ono, “Report in the activity of the sub-committee of investigation on corrosive sulfur problems in transformers,” 33rd Technical Meeting on Insulating Oil Section, JPI.

[13] N. Nakade, T. Matsui, S. Sugimoto, J. Haneda, and S. Nagahara, “Existence of Electric

Charging Degradation Mechanism by Copper Compounds such as Copper Sulfide under Operation Electric Field in Oil Filled Cables," IEEJ Transactions on Power and Energy, Vol. 137 No. 5, pp. 405-414, 2017.

[14]The Japan Petroleum Institute, "Electric Insulating Oil Handbook", Kodansha ltd., pp. 15, pp. 121, 1987.

[15]N. Mashimo, Y. Aihara, A. Toya, Y. Murata, S. Katakai, and S. Narisada, "Study of Metal Particles Behavior in Insulation Oil under Nonuniform Electric Field (Part 1)," National convention, IEE Japan, No. 2-001, 2004.

[16]N. Mashimo, Y. Aihara, A. Toya, Y. Murata, S. Katakai, and S. Narisada, "Study of Metal Particles Behavior in Insulation Oil under Nonuniform Electric Field (Part 2)," National convention, IEE Japan, No. 2-002, 2004.

[17]J. Kawai, M. Nakade, and T. Matsui, "About copper dissolution to electrical oil cable in electric charging degradation mechanism by the copper compounds such as copper sulfide (2)," National convention, IEE Japan, No. 7-151, 2016.

[18]The Society of Rubber Science and Technology, Japan, "Handbook of Rubber Industry," Soc. Rub. Sci. Technol., Japan, 4th ed., 1994.

[19]J. Kawai, M. Nakade, and T. Matsui, "Electric charging degradation mechanism by the copper compounds such as copper sulfide in oil filled cable (3)," Annual Conference of Power and Energy Society, IEE Japan, No. 326, 2015.

[20]Electric Technology Research Association, "Rationalization of insulation design," Electr. Technol. Res, Vol. 44, No. 3, pp- 238, 1988.

[21]The Institute of Electrostatics Japan, "Electrostatics Handbook," Ohmsha, pp. 307 , 1998

[22]M. Inoue, T. Shiro, T. Iida, T. Tsutsumi, K. Akita, and Y. Sakaguchi, "Study of partial discharge deterioration characteristic for oil gap of OF cable," IEEJ Transactions on Power and Energy, Vol. 133 No. 8, PP. 672-677, 2013.

Chapter 5 Conclusions

5.1 Conclusions

In this paper, the degradation process of insulating materials for underground power transmission cables was clarified from the chemical point of view. Moreover, degradation diagnostic methods were developed based on the clarified degradation process. These clarified degradation processes and the developed degradation diagnostic methods were summarized.

In Chapter 1, this study background, the purpose of this study, and the structure of this paper were described.

In Chapter 2, the thermal oxidative degradation characteristics of XLPE and EPR, which are the insulation materials in CV cables were elucidated, and degradation diagnostic methods based on these characteristics were developed.

The thermal oxidative degradation of XLPE depended on the carbonyl groups, which are the oxidation products of the degradation. The degradation characteristics until the lifetime were confirmed to be a volume resistivity that does not change and linearly increasing carbonyl groups. The degradation characteristics of EPR until the lifetime were confirmed to be a volume resistivity that does not change and linearly decreasing OIT and IOT. In addition, the characteristics were confirmed to be not influenced by temperature or manufacturer.

Lifetime diagnostic methods were developed based on the results. The diagnosis method of XLPE exploited the linear increase of carbonyl group. In EPR, the already proposed lifetime diagnosis method based on the OIT had problems concerning accuracy and usability. Therefore, a lifetime diagnosis method that uses the IOT and based on the same principle as the OIT method was developed. The degradation tendency of used cables was investigated by these diagnostic methods. The possibility of dielectric breakdowns in the XLPE of 66-kV CV cables is low in the current usage scenario because the results of the diagnosis of cables indicated lifetimes of 100 years or more. However, the dielectric breakdown due to thermal oxidation degradation was confirmed to occur in 6-kV CV cables. The EPRs of the 66-kV cables were confirmed to have the lifetime of 20 years at the shortest.

In conclusion, in the present study, thermal oxidative degradation was confirmed to be one of the breakdown factors of CV cables. There are few examples of dielectric breakdown due to thermal oxidative degradation; however, it is possible that the dielectric breakdown increases when used cables become older. As a result, it is expected that the developed lifetime diagnosis method would become more important in the future.

In Chapter 3, ions that are one of the causes of water tree degradation in CV cable insulation were the focus points. First, qualitative analysis methods of ions in water trees were developed to be able to qualitatively analyze monatomic ions and polyatomic ions, because there was no effective method to analyze these ions. Using the methods, the types of electrolytes and ions were elucidated to be closely related with origin contamination. In addition, the types and distribution areas of ion in water trees were elucidated to affect the development speed, shape, breakdown origin, and insulation performance. The hazardousness assessment methods for water trees were established based on the results. In these methods, the hazards based on the electrical characteristics and development speed were determined from the types and distribution areas of electrolytes.

Water tree degradation is a major cause of degradation of CV cables, and there are other degradation diagnostic methods that are already being practically used. Moreover, the direct hazardousness of water trees was mainly evaluated in this work in terms of water tree length, whereas ions that influence the electrical characteristics and development speed of the water trees were not included in the hazardousness assessment. Therefore, it is expected in the future that the developed methods will be useful methods of water tree analysis. However, further studies are needed that consider the tree length and the curvature radius of the tip of a tree as well.

In Chapter 4, the effect of the characteristics of electric charging degradation on the insulating paper, which is an OF cable insulating material, were elucidated, and a degradation diagnosis method that uses insulation oil analysis that captures the degradation was developed.

First, the black parts on the insulating paper were confirmed through the disassembly investigation of used cable joints. After that, copper sulfide was discovered on the black parts by TEPCO. As a result, the cause of the accidents was considered to be electric charging degradation due to copper sulfide, and the degradation process was devised. In this study, the devised degradation process was demonstrated through simulation test. Moreover, it was revealed that the black parts on the insulating paper are deposits of copper compounds due to electric charging degradation regardless of their shape. In addition, it was revealed that the degradation parts become the starting point of partial discharge and cause insulation performance degradation.

A conventional abnormality diagnosis method by employing insulation oil analysis was not able to capture electric charging degradation. Therefore, in the present study, a degradation diagnosis method by employing insulation oil analysis that is able to capture the degradation was devised. In this diagnostic method, the degradation tendency is determined in four levels through the trend of dissolved copper quantity and tan δ, tan δ/Cu, decrease time and quantity of dissolved copper, and TCG. In fact, it was confirmed that the diagnostic accuracy of this developed method is higher than that of the conventional

diagnosis method.

In the present paper, a new natural degradation phenomenon associated with OF cables was elucidated, and a new degradation diagnosis method that employs insulating oil analysis was developed. In other words, it is expected that this present paper will be an important achievement for the elucidation of natural degradation of OF cables in the future and ensure improved maintenance of OF cables. However, further studies are needed to elucidate the process from partial discharge occurrence to dielectric breakdown. Moreover, in the developed degradation diagnostic method, it is possible that reviewing the reference value in the future will be necessary.

5.2 Future prospects

A major area of concern regarding CV and OF cables of 66 kV or more are long-term degradation and natural degradation due to aging. However, long-term and natural degradation other than that due to water trees have hardly been studied because there was hardly any insulation breakdown accident. Therefore, the degradation of each insulating material of CV and OF cables have not been discussed from a chemical point of view.

In this study, the long-term and natural degradation of the insulating materials was elucidated from the chemical point of view, and new degradation diagnostic methods were developed. The degradation phenomena are thermal oxidative degradation and water tree degradation of CV cables, and electric charging degradation of OF cables.

Many dielectric breakdowns due to water tree degradation have occurred, whereas dielectric breakdown due to thermal oxidative degradation was confirmed for the first time in this study for a 6-kV CV cable. The electric charging degradation of OF cables is a new degradation phenomenon demonstrated through this study. In recent years, dielectric breakdown accidents due to this degradation have occurred. In addition, the cause of the fire accident in the Niiza cable tunnel in 2016 was the dielectric breakdown of the OF cable, and one of the breakdown causes was this degradation. Therefore, it is possible that dielectric breakdown due to thermal oxidative degradation and electric charging degradation increases, with more underground transmission cables aging further in the future. In that situation, it is expected that the results of this study will be an important reference for equipment maintenance considering long-term and natural degradation of underground transmission cables. Moreover, the importance of discussing degradation from a chemical point of view has been demonstrated through this study.

Acknowledgment

I would like to express my gratitude to Prof. Masatake Kawada, Graduate School of Technology, Industrial and Social Sciences, Tokushima University, who gave me the opportunity to write this thesis, valuable suggestions, and continuing encouragement. I would like to express my gratitude to Prof. Masaki Hashizume, the chairperson, and Prof. Masahide Hojo, a member of the doctoral dissertation committee. I received a lot of valuable advice from them.

This paper summarizes the results of research that I was involved in the degradation of underground power transmission cables for about 20 years. This research was executed with R&D Department TEPCO Research Institute and Tokyo Densetsu Service Corporation (TDS). I would like to express my gratitude to Dr. Masahiko Nakade, senior chief engineer of TEPCO Research Institute, who has been executed research with me for about 20 years and gave me guidance and suggestions.

I would like to thank to Hitoshi Tomogane, Takafumi Hirose, Yoshinori Fujimura, Masaki Hatanaka, Manabu Fujita, Mitsuhiro Watabe, Kenji Umekawa, Kenichi Nagata, Takeo Matsui, TEPCO Power Grid, Incorporated, who was valuable supports and helpful discussion throughout this research. In addition, I would like to thank Shigeki Nagahara, Jyunya Haneda, Hayato Koyama, and those involved with TDS for their great cooperation at the time of practical implementation of the research.

I would like to sincerely thank Yukihiko Namiki, technical advisor of TDS until 2011, who had guided the know-how of chemical analytical techniques. My present chemical analysis techniques are based on his guidance.

Finally, I would like to express my gratitude to my family, my wife Takami, my son Jin and my daughter Sumi for their support and encouragement.

List of Publications

Original papers on this thesis

a. Transactions and Journals

[1] M. Nakade, M. Hatanaka, K. Kunii, H. Tomokane, and S. Sugimoto, "Life Estimation of XLPE Cables in consideration of Oxidative Degradation," T.IEE Japan, Vol. 122-B, No. 1, pp. 90-95, 2002.

[2] M. Hatanaka, M. Nakade, T. Hirose, S. Sugimoto, and Y. Namiki, "Service Life Estimation Technique of Oxidized XLPE Cables," T.IEE Japan, Vol. 123-B, No. 12, pp. 1593-1597, 2003.

[3] S. Sugimoto, Y. Fujimura, S. Nagahara, M. Nakade, and M. Watabe, "Analysis of Ion in Water tree by Micro–FTIR, and Evaluation of Harmfulness of Water Tree," T.IEE Japan, Vol. 131-B, No. 1, pp. 52-57, 2011.

[4] M. Nakade, T. Matsui, S. Sugimoto, J. Haneda, and S. Nagahara, "Existence of Electric Charging Degradation Mechanism by Copper Compounds such as Copper Sulfide under Operation Electric Field in Oil Filled Cables," T.IEE Japan, Vol. 137-B, No. 5, pp. 405-414, 2017.

[5] S. Sugimoto, and M. Nakade, "Copper Compound Deposition for Decreasing Electrical Insulation in Aged Oil–filled Cables," IEEE Trans. Dielectr. Electr. Insul, Vol. 25, Issue. 5, pp. 1660-1667, 2018.

b. International Conferences

[1] S. Sugimoto, Y. Fujimura, S. Nagahara, M. Watabe, and M. Nakade, "Development of 66 kV Class XLPE Cable Degradation Diagnosis Technology," Proceedings of the 2010 International Conference on Condition Monitoring and Diagnosis, IEE Japan, B 2-2, 2010, Tokyo, Japan.

c. Domestic Conferences

[1] S. Sugimoto, Y. Fujimura, M. Nakade, and M. Fujita, "Analysis technique of ion in water tree that uses μ–FTIR," Annual Conference of Power and Energy Society, IEE Japan, No. 117, 2007.

[2] M. Fujita, M. Nakade, S. Sugimoto, and Y. Fujimura, "Ion analysis in water–tree of the actual cable line by μ–FTIR," National convention, IEE Japan, No. 7-202, 2009.

[3] S. Sugimoto, Y. Fujimura, S. Nagahara, M. Nakade, and M. Fujita, “Analysis of ion in water tree by Micro–FTIR, and evaluation of harmfulness of water tree (2),” Annual Conference of Power and Energy Society, IEE Japan, No. 425, 2012.

[4] S. Sugimoto, Y. Fujimura, S. Nagahara, M. Nakade, and K. Nagata, “Dielectric breakdown of XLPE cable by thermal oxidative degradation and degradation diagnosis,” National convention, IEE Japan, No. 7-139, 2013.

[5] M. Nakade, T. Matsui, J. Kawai, S. Sugimoto, S. Nagahara, and J. Haneda, “Electric charging degradation mechanism by the copper compounds such as copper sulfide in oil filled cable (1),” Annual Conference of Power and Energy Society, IEE Japan, No. 324, 2015.

[6] S. Sugimoto, S. Nagahara, J. Haneda, M. Nakade, and T. Matsui, “Electric charging degradation mechanism by the copper compounds such as copper sulfide in oil filled cable (2),” Annual Conference of Power and Energy Society, IEE Japan, No. 325, 2015.

[7] S. Sugimoto, J. Haneda, S. Nagahara, H. Koyama, M. Nakade, and T. Matsui, “About copper dissolution to electrical oil cable in electric charging degradation mechanism by the copper compounds such as copper sulfide (1),” National convention, IEE Japan, No. 7-150, 2016.

[8] S. Sugimoto, J. Haneda, S. Nagahara, M. Nakade, and T. Matsui, “Electric charging degradation mechanism in oil filled cable under the operating electric field (1) – Generation of an oxidation sludge –,” Annual Conference of Power and Energy Society, IEE Japan, No. 307, 2016.

[9] J. Haneda, S. Sugimoto, S. Nagahara, M. Nakade, and T. Matsui, “Electric charging degradation mechanism in oil filled cable under the operating electric field (2) – The dissolution promotion technique of the copper and the special quality of the copper compound dissolved –,” Annual Conference of Power and Energy Society, IEE Japan, No. 308, 2016.

[10] T. Matsui, M. Nakade, J. Haneda, S. Sugimoto, and S. Nagahara, “Electric charging degradation mechanism in oil filled cable under the operating electric field (3) – Generation of partial discharge –,” Annual Conference of Power and Energy Society, IEE Japan, No. 309, 2016.

[11] T. Matsui, M. Nakade, S. Sugimoto, J. Haneda, S. Nagahara, and H. Koyama, “Characteristic of insulating oil by electric charge degradation of the oil filled cable (1) – Relation between electric charge degradation mechanism and the quantity of dissolved copper, tan δ –,” National convention, IEE Japan, No. 7-172, 2017.

[12] J. Haneda, S. Sugimoto, S. Nagahara, H. Koyama, M. Nakade, and T. Matsui, “Characteristic of the insulating oil by electric charging degradation of the Oil filled cable (2) – Generation of gas by dissolution of copper and generation of oxidation sludge –,” National convention, IEE Japan, No. 7-173, 2017.

[13]S. Sugimoto, J. Haneda, S. Nagahara, H. Koyama, M. Nakade, and T. Matsui, “Characteristic of the insulating oil by electric charging degradation of the Oil filled cable (3) – Electric charging degradation diagnosis method by the insulating oil analysis – ,” National convention, IEE Japan, No. 7-174, 2017.
[14]S. Sugimoto, S. Nagahara, M. Nakade, and T. Matsui, “Lifetime Estimation Method by Initial Oxidation Temperature of Tape Lapped Joint for XLPE Cable,” Annual Conference of Power and Energy Society, IEE Japan, No. 263, 2017.
[15]M. Nakade, T. Matsui, S. Sugimoto, and S. Nagahara, “Lifetime Estimation of EPR Tape for Tape Lapped Joint and Lifetime Investigation of actual facilities,” Annual Conference of Power and Energy Society, IEE Japan, No. 264, 2017.
[16]S. Sugimoto, J. Haneda, S. Nagahara, H. Koyama, M. Nakade, and T. Nakamura, “Improvement of Electric Charging Degradation Diagnosis Method of Oil Filled Cable by Insulation Oil Analysis,” National convention, IEE Japan, No. 7-135, 2018.
[17]T. Nakamura, M. Nakade, S. Sugimoto, J. Haneda, S. Nagahara, and H. Koyama, “Specification of an occurrence point of the sulfur ingredient included in Oil Filled Cables,” National convention, IEE Japan, No. 7-137, 2018.

List of Patents on this thesis (in Japanese)

[1] M. Hatanaka, M. Nakade, T. Hirose, S. Sugimoto, and Y. Namiki, “Insulation degradation lifetime diagnosis methods of cables,” Patent registration number 3970199, Jun. 2007.
[2] M. Fujita, M. Nakade, Y. Fujimura, and S. Sugimoto, “Ion analysis methods in a water tree,” Patent registration number 4956322, Mar. 2012.
[3] M. Nakade, T. Matsui, S. Sugimoto, S. Nagahara, and J. Haneda, “Estimation methods of copper sulfide production condition in oil-filled cables by insulation oil analysis, and diagnostic methods of risk,” Application number 145433, Jul 2015.
[4] M. Nakade, T. Matsui, S. Sugimoto, S. Nagahara, and J. Haneda, “Estimation methods of organocopper compounds and copper sulfide production condition in oil-filled cables by insulation oil analysis, and diagnostic methods of risk of abnormal occurrence in oil-filled cables,” Application number 017098, Feb. 2017.
[5] M. Nakade, T. Matsui, S. Sugimoto, and S. Nagahara, “Remaining lifetime diagnosis method of insulating tape,” Application number 169314, Sep. 2017.

Awards on this study results

[1] “2013 IEE Japan Excellent Paper Presentation Award,” IEE Japan, 2013, “Dielectric breakdown of XLPE cable by thermal oxidative degradation and degradation diagnosis,” National convention, IEE Japan, No. 7-139, 2013.

[2] “The 65th Electrical Science and Engineering Encouragement Award,” The Promotion Foundation for Electrical Science and Engineering, 2017, “Elucidation of electric charging degradation mechanism under operating electric field in OF cable.”